Development of a PNN Pincer Ligand and Its Iron and Cobalt Complexes for Selective Catalytic Amide Synthesis

By

Nirvana Almada

A Thesis Submitted in Partial Fulfilment of the Requirements for the Degree of Master of Science in Chemistry

Middle Tennessee State University

August 2023

Thesis Committee:

Dr. Keying Ding, Chair

Dr. Adrienne Friedli

Dr. Charles Chusuei

ACKNOWLEDGMENTS

I would like to thank my research advisor and committee chair, Dr. Keying Ding, for her generous support during my duration at Middle Tennessee State University as an intern, student, and researcher. Her enthusiastic attitude and drive to expand research inspired my enrollment at this university and desire to broaden my skills in becoming a more renowned researcher. With her support I have achieved great challenges in my academic and professional life and have gained abilities I will carry with me through future endeavors.

I would like to thank Dr. Andrienne Friedli, for her coordination in the REU program and allowing the extension of my acceptance to attend MTSU as an intern. Without her I would have never been a part of this University to the extent in which I have. I would like to thank Dr. Charles Chusuei for his knowledge and quickness in guiding me through the master's program enrollment process. Thank you to all three committee member for the support through this academic process and supporting my success in earning my Masters of Science in Chemistry.

Thank you to Dr. Oleksandr Hietsoi for his exceptional knowledge and support with the X-ray crystallography experiments and analyses.

I would like to give a special thank you to Dr. Erik Wasinger who ignited my passion and curiosity for chemistry during my first chemistry course at Chico State University and for seeing something in me early on that I did not see in myself.

Lastly, I would like to thank my family for supporting my academic journey no matter where it has led me in life.

ABSTRACT

The formation of amide bonds from carboxylic acids and amines has been the commercially available route for decades, enabling the synthesis of various compounds used in industries ranging from pharmaceuticals to polyurethanes. However, these conventional methods of synthesis have significant sustainability challenges, as they generate copious amounts of waste, produce harmful by-products, and rely on the use of toxic chemicals. Given the increasing demand for amide-containing compounds and the environmental drawbacks associated with traditional synthesis routes, researchers have been prompted to explore more sustainable approaches to amide bond formation, aligning with the principles of Green Chemistry. [1], [2], [3]

In this paper, we report the design and synthesis of cobalt (II) and iron (II) complexes with a new type of PNN pincer ligand to facilitate selective amide formation during an alcohol and amine coupling reaction. We propose two new pincer ligands, $^{Ph}PN^{H}N$ and $^{iPr}PN^{H}N$, that are designed to allow for modes of metal-ligand cooperativity (MLC) in order to expand on the versatility of their chemical functions. The metal complexes provide an opportunity for a fundamental understanding of the key mechanistic steps in selective amide formation in addition to structure-reactivity relationships to improve future catalyst design. With the support of single crystal X-ray crystallography, ^{31}P NMR, ^{1}H NMR, elemental analysis, and high-resolution mass spectrometry we report the successful synthesis of a new type of $^{Ph}PN^{H}N$ pincer ligand and two new organometallic complexes.

TABLE OF CONTENTS

LIST OF FIGURES

LIST OF SCHEMES

LIST OF TABLES

LIST OF REPORTS

CHAPTER I

INTRODUCTION

1.1. The Importance of Amide Bonds and Their Applications

The discovery of the amide bond dates back several decades and is a fundamental component of several chemical industries. In the pharmaceutical industry, amide formation is one of the most widely utilized reactions. Approximately 25% of all synthesized pharmaceuticals contain at least one amide bond. Amide bonds can be found in commonly used over-the-counter medications such as ibuprofen and melatonin, as well as prescribed antibiotics like penicillin and amoxicillin. These bonds play a vital role in peptide synthesis, enabling the coupling of two amino acids or peptides to form longer chains. This is particularly important in the development of therapeutic peptides and protein-based drugs. [2], [4]

Moreover, the petroleum industry relies on amides for the synthesis of polyurethanes, which are highly versatile polymers known as poly(urethane amide). Polyurethanes find applications in various industries, including construction, automotive, and textiles, due to their unique mechanical and thermal properties. The incorporation of amide bonds into the polymer backbone enhances the material's stability, strength, and flexibility. [5]

Additionally, amide-based herbicides are extensively employed in the agricultural sector worldwide to control unwanted plant growth and increase crop yields. These herbicides

inhibit specific enzyme systems in plants, effectively suppressing their growth and providing selective weed control in various agricultural settings. [3]

The wide range of applications and industries that rely on amide bonds underscores their significance in diverse fields. From pharmaceuticals to polymers and herbicides, amides play a vital role in various processes, making them a subject of intense research and development. The understanding and utilization of amide synthesis have greatly contributed to advancements in these industries and continue to be an area of active exploration.

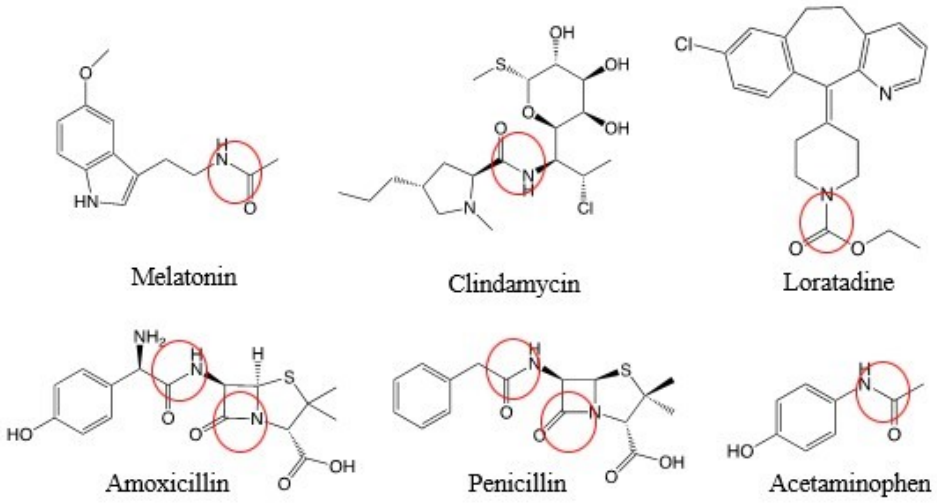

Figure 1.1: Commonly used pharmaceuticals containing an amide bond(s).

1.2. Classical Methods of Amide Synthesis

The amide bond has long been synthesized in various industries using conventional reactions such as condensation and amidation between an amine and a carboxylic acid under different reaction conditions. [1]

1.2.1. DCC/HOBT Method

The DCC (dicyclohexylcarbodiimide)/HOBT (1-hydroxybenzotriazole) method is a classic and widely used approach for amide bond formation. The reaction proceeds as follows:

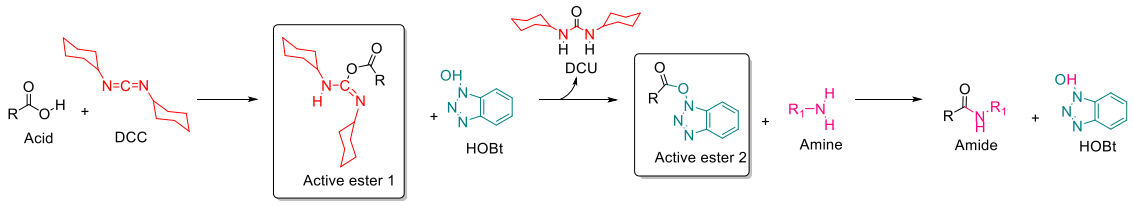

Scheme 1.1: Mechanistic overview of DCC coupling reaction of a carboxylic acid.

i. Activation: DCC acts as a coupling reagent that activates the carboxylic acid by converting it into an O-acylisourea intermediate. This activation step involves the reaction between DCC and the carboxylic acid to form a dicyclohexylurea byproduct and the O-acylisourea.

ii. Coupling: The O-acylisourea intermediate then reacts with the amine to form the amide bond. This step involves the nucleophilic attack of the amine on the carbonyl carbon of the O-acylisourea, leading to the formation of the desired amide product.

HOBT is typically added as a catalyst in this reaction to enhance the efficiency and selectivity of the process. It acts by preventing undesired side reactions, such as the formation of urea derivatives.

1.2.2. Peptide Coupling Reagents

Peptide coupling reagents are commonly used in amide synthesis, particularly in peptide chemistry. They facilitate the formation of amide bonds by activating the carboxylic acid and promoting the coupling reaction with the amine. The general mechanism using (1-[bis(dimethylamino)methylene]-1H-1,2,3-triazolo[4,5-b]pyridinium 3-oxid hexafluorophosphate) (HATU) proceeds as follows:

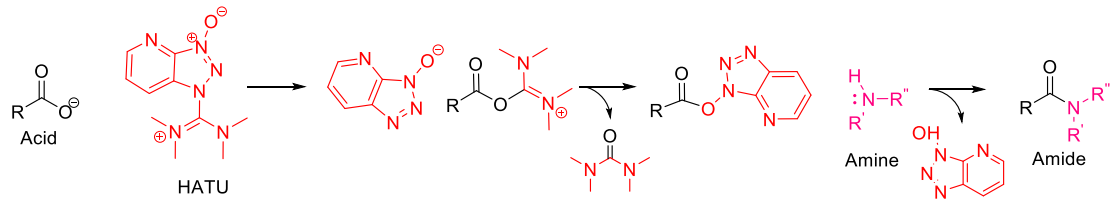

Scheme 1.2:: Reaction overview of peptide coupling reaction of a carboxylic acid

i. Activation: HATU reacts with the carboxylic acid to form an acyl azide intermediate. This activation step involves the formation of an O-acylurea intermediate, followed by conversion to the acyl azide upon reaction with HATU.

ii. Coupling: The acyl azide intermediate then reacts with the amine to yield the desired amide product. This step involves the nucleophilic attack of the amine on the acyl azide, leading to the formation of the amide bond.

A base, such as DIEA (diisopropylethylamine), is typically added to neutralize the acid byproduct and facilitate the reaction.

1.2.3. Transition Metal-Catalyzed Methods:

a) Palladium-Catalyzed Methods:

Palladium catalysts have been extensively studied for their ability to facilitate amide bond formation through C-N bond activation. For example, Szostak group recently reported a catalytic Buchwald–Hartwig coupling involving prevalent esters and amides. This approach selectively cleaves the C(acyl)–X (X = O, N) bond, enabling efficient access to aryl amide functionality through a cross-coupling strategy. The reactions are facilitated by readily available and well-defined Pd–PEPPSI type precatalysts, exhibiting remarkable versatility. [6]

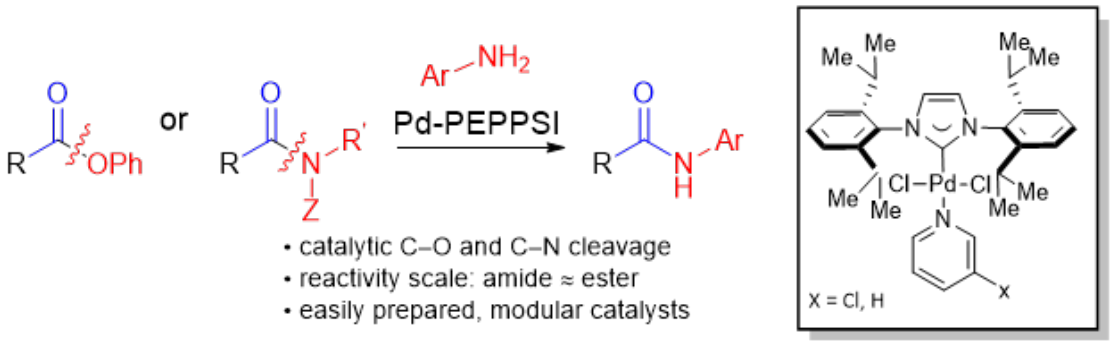

Scheme 1.3: C-(acyl)-Buchwald-Hartwig amination of common esters and amides.

b) Copper-Catalyzed Methods:

Copper catalysts are commonly employed in Ullmann-type reactions for amide bond formation. In 1906, Irma Goldberg developed the first example of the Cu-catalyzed arylation of benzamide and salicylamide. These reactions involve the coupling of aryl

halides, such as aryl bromides or aryl chlorides, with primary amide to synthesize secondary amides. [7]

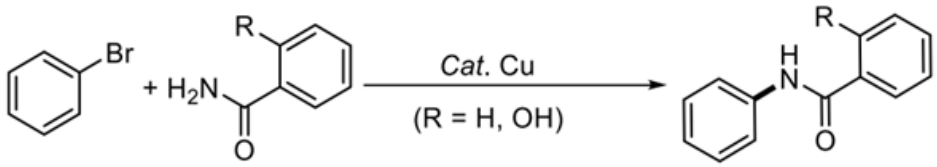

Scheme 1.4: Ulmann-Goldberg reaction scheme.

These conventional amide synthesis methods utilizing palladium and copper catalysts have proven to be valuable tools in organic synthesis, enabling the efficient and selective formation of amide bonds. Their mechanisms have been extensively studied and optimized to provide reliable synthetic routes for amide synthesis.

1.3 Limitations of Conventional Amide Synthetic Methods

1.3.1. Limited Substrate Compatibility

One of the drawbacks of conventional amide synthesis methods is limited substrate compatibility. These methods often work well with simple carboxylic acids and primary amines. However, when more complex or sterically hindered substrates are involved, the reaction efficiency can decrease significantly. Bulky or electron-deficient groups present in the starting materials can hinder the reaction progress or lead to undesired side reactions, resulting in low yields or incomplete conversions.

1.3.2. Harsh Reaction Conditions

Certain conventional amide synthesis methods require harsh reaction conditions. For example, the DCC/HOBT method often necessitates the use of organic solvents such as

dichloromethane or dimethylformamide and requires low temperatures. Similarly, some transition metal-catalyzed methods may require high temperatures, high pressures, or the use of toxic or expensive catalysts. These harsh reaction conditions can limit the scalability and practicality of the synthesis, especially for large-scale industrial applications.

1.3.3. Side Reactions

Conventional amide synthesis methods can be prone to side reactions, leading to the formation of undesired byproducts. For instance, the DCC/HOBT method can result in the formation of dicyclohexylurea, a common byproduct that requires additional purification steps to obtain the desired amide product. Similarly, transition metal-catalyzed methods can be susceptible to side reactions, such as over-oxidation or protodepalladation, which can reduce the yield and selectivity of the desired amide bond formation.

1.3.4. Protection and Deprotection Steps

In certain cases, conventional amide synthesis methods may require additional protection and deprotection steps. Protecting groups are used to shield functional groups that might react undesirably during the amide bond formation. These extra steps can add complexity, time, and cost to the synthesis process and may require the use of additional reagents and purification steps.

1.3.5. Environmental Impact

Some conventional amide synthesis methods involve the use of toxic or environmentally harmful reagents, solvents, or catalysts. These substances can have negative impacts on

human health and the environment, posing challenges in terms of safety and sustainability. Additionally, the generation of waste byproducts during the synthesis process can further contribute to environmental concerns.

1.4. Turning to Green Chemistry

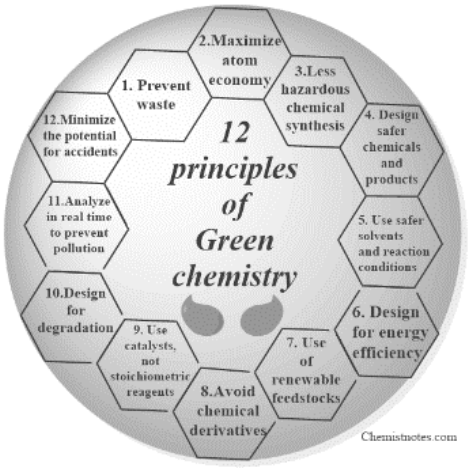

Figure 1.2: Principles of Green Chemistry

Sustainability is an increasingly prominent topic of conversation, driven by the challenges we face as a society in combating self-induced climate change. This necessitates significant adjustments to our lifestyles and practices. Such adjustments can vary greatly depending on whether we consider individual actions or those of industries. When discussing everyday impacts, some individuals focus on recycling or using public transportation instead of vehicles. However, within the field of chemistry, scientists are working to integrate the principles of green chemistry into their synthetic designs and practices. These principles serve as a foundation for scientists to minimize the environmental impact of their work.

The principles of Green Chemistry encompass various key aspects, including prevention, atom economy, the use of less hazardous chemicals for synthesis, and the design of energy-efficient pathways. By embracing these principles, scientists are driving innovation in the chemical industry, providing sustainable guidelines for the field of chemistry. They have inspired scientists to undertake the task of redesigning synthetic pathways and developing chemicals and materials that are more environmentally friendly and sustainable.

To address the drawbacks brought by conventional amide synthetic methods, researchers are continually exploring and developing alternative amide synthesis methods to enhance the efficiency, versatility, and sustainability of amide bond formation in various applications. In 2007, the ACS GCI identified amide formation with efficient and sustainable atom economy as one of the top challenges to overcome in the realm of green chemistry. The impact of the ACS GCI's green chemistry initiative on amide synthesis has been significant. It has prompted researchers to explore innovative synthetic methods and develop more sustainable approaches to amide bond formation. Several strategies and advancements have emerged as a result:

1.4.1. Catalytic Methods

The development of catalytic methods for amide synthesis has been a major focus of green chemistry initiatives. Transition metal catalysts, such as palladium, copper, and nickel, have been widely investigated for their ability to promote amide bond formation with high efficiency and selectivity. These catalytic approaches often offer improved

atom economy by minimizing the use of stoichiometric reagents and reducing waste generation.

1.4.2. Coupling Reagents

Efforts have been made to identify and optimize coupling reagents with improved atom economy. For example, the use of coupling reagents like carbodiimides and phosphonium salts can enhance the atom efficiency of amide formation reactions. These reagents facilitate the direct coupling of carboxylic acids and amines, eliminating the need for intermediate activation steps and reducing waste.

1.4.3. Solvent-Free or Aqueous Conditions

Green chemistry initiatives have emphasized the development of solvent-free or aqueous conditions for amide synthesis. These approaches minimize the use of organic solvents, which often pose environmental and health hazards. Water, as a green solvent, has been explored as a medium for amide bond formation reactions, offering several advantages such as reduced waste generation, enhanced atom economy, and improved safety.

1.4.4. Renewable Feedstocks

Another focus area of green chemistry in amide synthesis is the utilization of renewable feedstocks. By incorporating biomass-derived or bio-based starting materials, such as renewable acids and amino acids, the environmental impact of amide synthesis can be reduced. This approach aligns with the principles of sustainability and contributes to a more circular and bioeconomy-driven chemical industry.

These green chemistry initiatives and advancements have not only addressed the challenges identified by the ACS GCI but also paved the way for more sustainable and environmentally friendly amide synthesis methods. They have led to the development of greener synthetic routes that prioritize atom efficiency, minimize waste, reduce the use of hazardous reagents, and promote the use of renewable resources, thereby contributing to the overall sustainability of the chemical industry.

1.5. Amine Alcohol Dehydrogenative Couplings to Amide

Research progress on amine alcohol dehydrogenative couplings to amide products has gained significant attention in recent years. This synthetic approach offers an alternative and sustainable method for amide bond formation by utilizing amine and alcohol substrates without the need for external oxidants or preactivation steps (Scheme 1.5). This route offers numerous advantages, including the mitigation of environmental concerns associated with waste generation and the promotion of atom economy, as the reaction byproducts consist of hydrogen gas and water, both of which are environmentally benign. Furthermore, by carefully engineering the catalyst, researchers can strive to eliminate the reliance on heavy metals, thus further enhancing the sustainability of the process. Given the significant influence of amides in various industries, the endeavor to develop a more sustainable synthetic pathway has garnered considerable attention in the past decade.

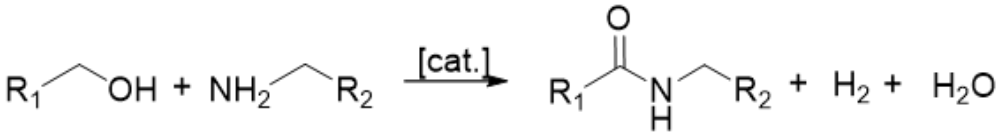

Scheme 1.5: General reaction for amine alcohol dehydrogenative coupling.

The pioneering work conducted by the Milstein group involved the development of a Ru pincer catalyst (Figure 1.3) that enables direct amidation via dehydrogenative coupling of primary alcohols and amines. Their catalyst design aimed to minimize waste production by avoiding the use of coupling reagents or corrosive acidic and basic media, while also considering atom economy. They successfully synthesized amides from primary amines and alcohols, with hydrogen gas being the sole byproduct. Their proposed mechanism involved the dehydrogenation of hemiaminal intermediates formed through the reaction of an in-situ aldehyde intermediate with the amine. Although the Milstein work made significant contributions to sustainable chemistry and the redesign of the catalytic amide pathway, the organometallic complexes still relied on the use of heavy metals. However, their achievements laid the foundation for subsequent projects, wherein other scientists and research groups aimed to develop more sustainable catalysts for this coupling reaction. [8]

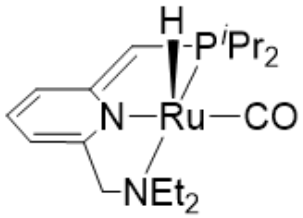

Figure 1.3: Milstein's ruthenium (Ru) catalyst for amide formation.

Building upon the work of Milstein's lab, several other groups, including Stahl, Bernskoetter, Beller, and even Milstein's own lab, worked on synthesizing environmentally friendly catalysts. They successfully developed various metal-organic complexes, employing base transition metals as alternatives to heavy metals. While these advancements propelled the field forward, it is important to note that this area of organic chemistry is still relatively new, offering ample opportunities for further exploration. Specifically, improving selectivity remains a challenge, as current catalysts often yield a combination of amide and imine products. Moreover, expanding the substrate scope of these catalysts would enhance their versatility for synthesizing a broader range of amide bonds. [9], [10], [11], [12], [13], [14]

Overall, the research conducted by these groups represents a significant advancement in the pursuit of sustainable and efficient catalytic amide synthesis. Continued efforts in this field hold the promise of developing more environmentally friendly catalysts, with enhanced selectivity and expanded substrate scopes, ultimately contributing to the greening of the amide synthesis process.

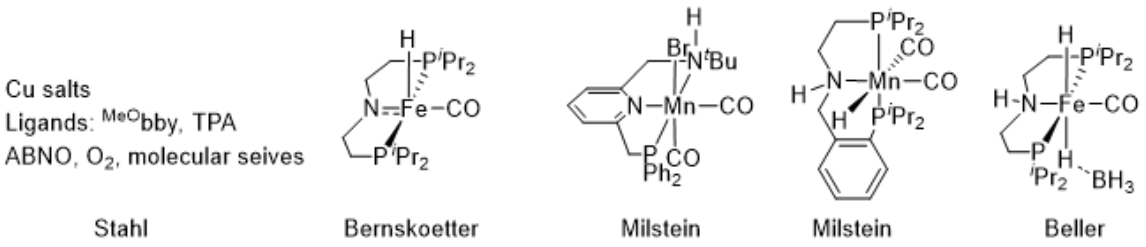

Figure 1.4: Base transition metal catalysts for amide formation.

1.6. Development of Pincer-Type Ligand for Catalytic Amide Formation

Ligand development plays a crucial role in transition metal catalysis by influencing the reactivity, selectivity, and stability of the catalytic systems. Ligands serve as coordinating entities that bind to the metal center and modulate its electronic and steric properties, thereby controlling the outcome of catalytic reactions. In our lab, our research has primarily focused on the exploration of earth-abundant transition metal catalysis and the concurrent development of ligands tailored for these catalytic systems.

1.6.1. Pincer-Type Ligand

Recently, our group proposed a pincer-type ligand used for amide formation. A pincer-type ligand, also known as a scorpionate ligand, is a class of ligands that exhibit a tridentate coordination mode. These ligands possess a donor atom framework that resembles a scorpion's pincers, hence the name. Typically, pincer ligands feature three coordinating atoms that surround and bind to a central metal atom, creating a stable coordination complex. The coordinating atoms are usually arranged in a linear or nearly linear fashion. Common donor atoms in pincer ligands include nitrogen, phosphorus, and sulfur. The distinctive characteristic of pincer ligands is their ability to provide multiple coordination sites for the metal center. This results in strong metal-ligand bonding and enhanced stability of the resulting metal complex. The rigid and chelating nature of pincer ligands also prevents the dissociation of the metal during catalytic reactions, leading to improved catalytic activity and selectivity. Pincer ligands find extensive applications in various fields, such as catalysis, organometallic chemistry, and materials

science. Their versatility, stability, and unique coordination properties make them valuable tools for designing efficient catalysts and functional materials. [15]

1.6.2. Proposed Pincer-Type Ligands

Our proposed ligand, known as PNN pincer ligand, contains three coordination sites: one originating from phosphorus, one from pyridine N donor and the third one from the amide nitrogen between the pyridine ring and the phosphorus donor.

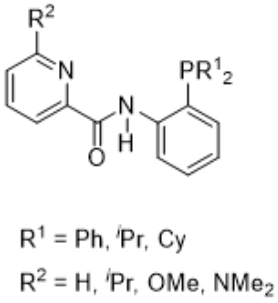

Figure 1.5: Proposed PNN pincer ligands.

This ligand has been meticulously designed with specific structural features to serve its unique purpose. It consists of a pyridine arm with an amide linked to a phosphophenyl ring, allowing for potential attachment of different R groups on both the pyridine and phosphophenyl rings, thus enabling tunability of the ligand and diverse functionality (Figure 1.5). The ligand's design incorporates several distinctive characteristics, promoting multiple modes of metal-ligand cooperativity and enabling the tunability of the electronic structure of the metal center for selective amide formation.

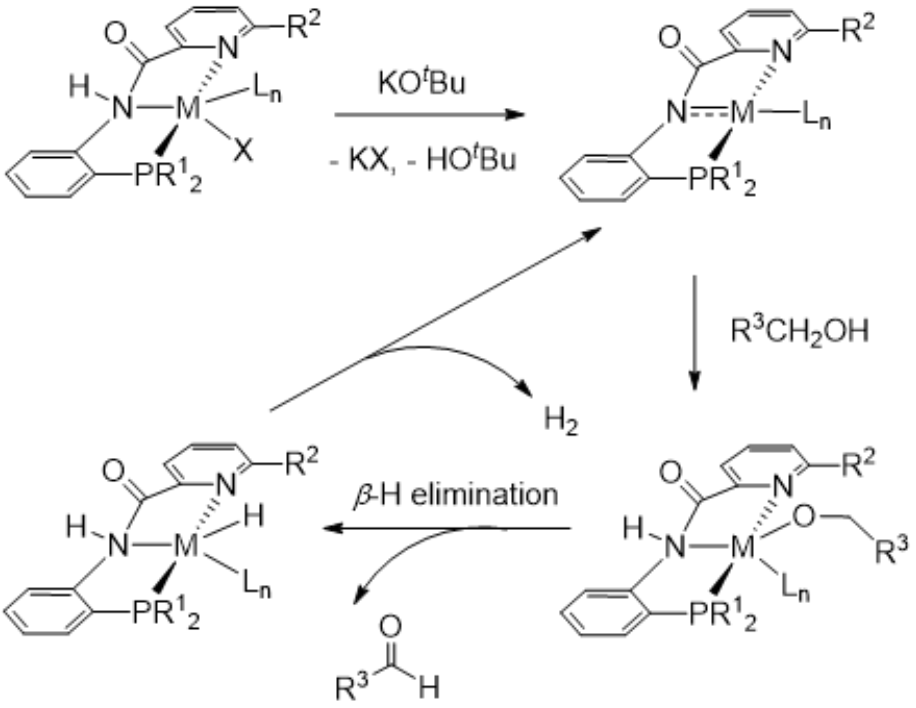

Scheme 1.6: Alcohol activation by MLC over the M−N bond.

Feature 1. Alcohol activation through metal-ligand cooperativity

This feature capitalizes on the ligand's central amide nitrogen donor, which facilitates the activation of alcohols via metal-ligand cooperativity (Scheme 1.6). The ligand enables the reversible transfer of a proton to the amide nitrogen and a hydride to the metal center. This process activates the alcohol and can be reversed, allowing the ligand to return to its original state and releasing hydrogen gas. The cooperative interaction between the metal and the ligand enhances the reactivity of the alcohol substrate.

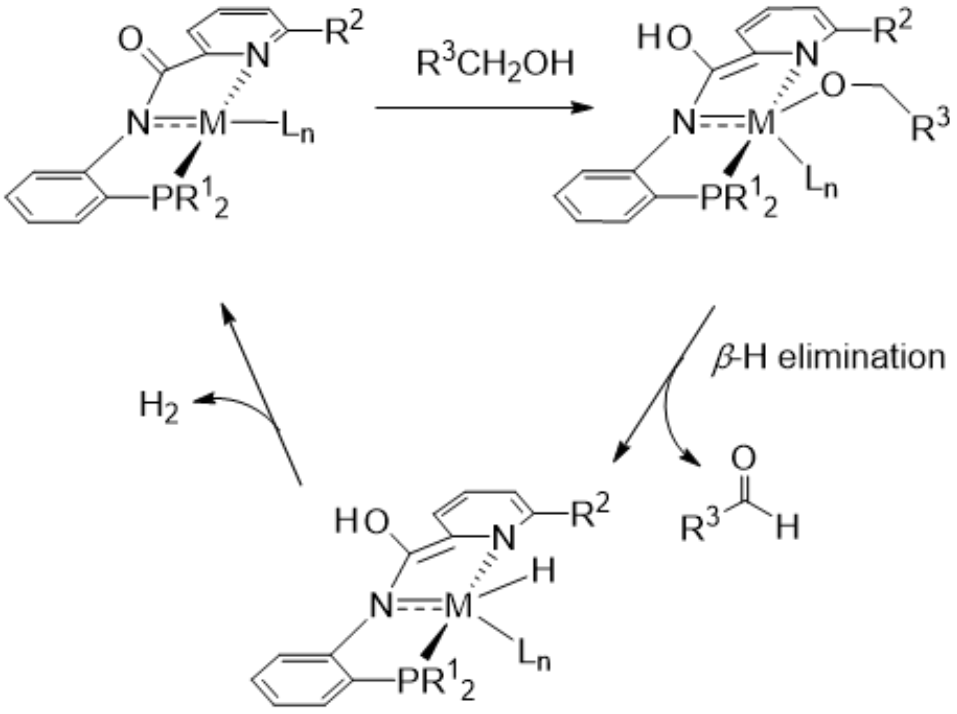

Scheme 1.7: Dynamic dearomatization-aromatization events for alcohol activation from the −C=O group.

Feature 2. Activation of alcohol from the carbonyl group through dynamic dearomatization-aromatization

This feature exploits the presence of a carbonyl group in the ligand design, coupled with a pyridine side arm. The oxygen of the carbonyl group may receive a proton from the alcohol substrate, inducing de-aromatization of the pyridine ring. Subsequent aromatization restores the ligand to its original state, with the only by-product being H+ (Scheme 1.7). This process leads to the in-situ formation of an aldehyde, which is a crucial step for selective amide formation.

Feature 3. Tuning of the metal center's electronic profile by an external Lewis acid

The ligand incorporates a carbonyl group, which can adjust the electronic properties of the metal center when coordinated to an external Lewis acid, such as a boron compound. This coordination event renders the metal center more electrophilic, favoring the binding of an aldehyde, which is essential for amide formation. By introducing a Lewis acid, the ligand allows for fine-tuning of the metal center's reactivity and selectivity (Scheme 1.8).

Scheme 1.8: Electronic profile of the metal center tuned by the external Lewis acid.

Feature 4. Possible modulation of the metal-ligand cooperativity (MLC) mode through ligand structure modification

This feature explores the potential to modulate the MLC mode by modifying the ligand's structure. By replacing the carbonyl group or methylating the nitrogen centers, the MLC mode can be deactivated or altered (Figure 1.6). This structural modification provides an opportunity to investigate the significance and role of MLC in the catalyst's reactivity. It allows researchers to gain insights into the contributions of metal-ligand cooperativity to the overall catalytic process.

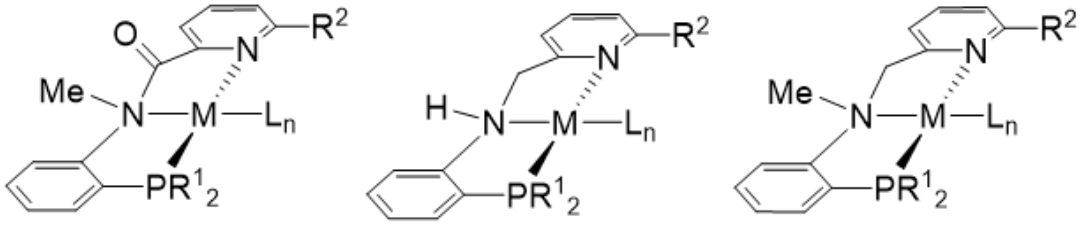

Figure 1.6: Tuning MLC modes by ligand structure modification.

Feature 5. Active sites of the ligand, including the central -NH units and the -C=O group, which can be converted to =C-OH and form hydrogen bonds with the reaction substrate.

This feature highlights the active sites within the ligand design. The central -NH units and the -C=O group can undergo chemical transformations, such as conversion to =C-OH, enabling hydrogen bonding with the reaction substrate. These interactions play a role in facilitating substrate binding and reactivity, leading to efficient catalytic processes.

Feature 6. Dynamic arm-on and arm-off capability within the ligand design to facilitate substrate binding and activation independently of MLC

The ligand design incorporates a dynamic arm-on and arm-off feature, enabling facile substrate binding and activation without relying solely on metal-ligand cooperativity. By altering the R groups attached to the phosphophenyl ring of the ligand, the electronic and steric properties of the metal center can be adjusted (Scheme 1.9). The introduction of a cyclohexyl group onto the phosphophenyl ring is hypothesized to create steric hindrance, causing the metal center to exhibit more nucleophilic behavior.

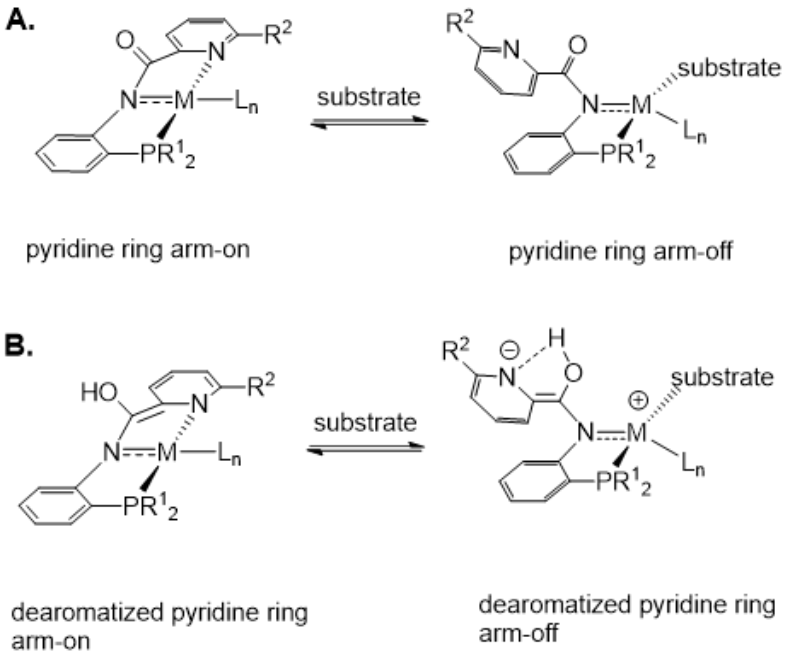

Scheme 1.9: Dynamic arm-on and arm-off events on the ligand design to facilitate substrate binding and activation. For clarity, this scheme does not consider MLC.

Feature 7. **Design incorporating the hemi-liability of the pyridine ring for an arm-on and arm-off dynamic to intensify the reactivity of the catalyst**

This feature focuses on leveraging the hemiliability of the pyridine ring in the ligand design. The term "hemi-liability" refers to the ability of a ligand to partially detach or reorient a coordinating group while maintaining a connection with the metal center. In this case, the pyridine ring serves as the hemilabile arm of the ligand (Scheme 1.9).

The arm-off event in this design allows for the exposure of an additional coordination site on the ligand for substrate binding. By temporarily releasing the coordination of the pyridine arm from the metal center, an open coordination site becomes available,

facilitating the binding of a substrate. This arm-off dynamic enhances the reactivity of the catalyst by providing an additional avenue for substrate coordination.

On the other hand, the arm-on event involves the coordination of the pyridine arm to the metal center, stabilizing organometallic intermediates formed during the catalytic cycle. The coordination of the pyridine arm helps maintain the integrity and stability of the metal-ligand complex, allowing for subsequent catalytic transformations.

The size and electronic properties of the R groups attached to the pyridine ring can influence the hemi-liability of the side arm. Variations in the size or electronic nature of these groups can impact the ease with which the pyridine arm dissociates from and rebinds to the metal center. By carefully selecting the R groups, the ligand's arm-on and arm-off dynamics can be modulated, fine-tuning the reactivity and selectivity of the catalyst.

Overall, this hemiliability feature provides an additional level of control and reactivity modulation in the ligand design, enabling enhanced catalytic performance and expanding the range of transformations achievable by the catalyst.

1.7. Objectives of This Study

In this work, we report the synthesis of a new PNN pincer-type ligand proposed above. The iron and cobalt complexes of the ligand were synthesized and characterized. This work serves as a preliminary step for catalytic amide formation for our future study.

CHAPTER II

EXPERIMENTAL METHODOLOGY

2.1 General Methods

The reactions were conducted either in an MBraun glovebox under a nitrogen atmosphere or using standard Schlenk techniques. To ensure anhydrous conditions, pentane, toluene, diethyl ether, and tetrahydrofuran were deoxygenated by sparging with nitrogen, dried using activated alumina columns from a Pure Solv solvent purification system, and stored in a glovebox filled with nitrogen. Deuterated solvent C_6D_6 was purchased from Cambridge Isotope Lab and dried over sodium/benzophenone before undergoing three cycles of distillation and degassing. $CDCl_3$ obtained from Cambridge Isotope Lab was dried using molecular sieves (4 Å) prior to use. KO^{t}Bu was purchased from Sigma Aldrich and sublimed before being used. Other reagents were purchased from Fisher Scientific, Sigma Aldrich, A2B Chem, Strem Chemicals, Alfa Aesar, and used as received. Silica for column chromatography was purchased from Sorbtech and silica TLC plates used were purchased from Sigma Aldrich.

NMR spectra were recorded using either a JEOL Unity 300 or 500 MHz spectrometer. The ^{31}P NMR spectra were referenced to 85% H_3PO_4 at 0 ppm. Infrared spectra were obtained in the solid state using an Agilent Technologies Cary 630 FT-IR spectrometer equipped with a diamond attenuated total reflectance (ATR) accessory. UV-vis spectra were recorded using a Hewlett-Packard Model 8452A with a diode array. Elemental

analysis was performed by Atlantic Microlab. Mass spectrometry (MS) data were acquired on a Bruker micrOTOF II ESI-MS under positive mode.

2.2 Experimental Methods

2.2.1 Synthesis of $^{Ph}PN^{H}N$ Pincer Ligand L1

2.2.1.1 Unsuccessful Attempt to Synthesize 2-(diphenylphosphino)aniline using DMF solvent (Approach 1)

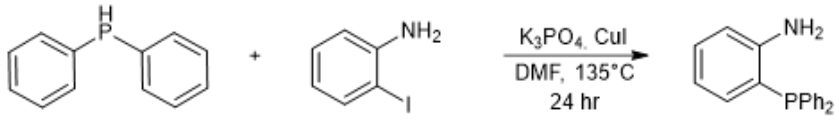

Scheme 2.1: Synthesis of 2-(diphenylphosphino)aniline from diphenylphosphine and 2-iodoaniline.

In the glovebox a 15 mL reaction tube was charged with a stir bar, potassium phosphate (2 mmol, 0.424 g), DMF (1.00 mL), copper iodide (0.05 mmol, 9.50 mg), 2-iodoaniline (1.5 mmol, 0.329 g). and diphenyl phosphine (1 mmol, 174 µL, 1.07 g/mL). The tube was sealed, brought out the box and heated to 135ºC for 24 hours while stirring. Upon ^{31}P NMR analysis it was found that the reaction did not work, and the phosphorus peak correlated to that of the starting material diphenyl phosphine.

2.2.1.2 Synthesis of $^{Ph}PN^{H}N$ Pincer Ligand L1 (Approach 2)

Step 1. Synthesis of 2-(diphenylphosphino)aniline using DMEDA additive

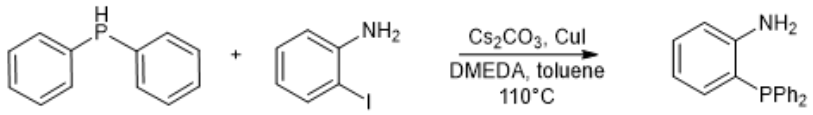

Scheme 2.2: Synthesis of 2-(diphenylphosphino)aniline from diphenylphosphine and 2-iodoaniline**.**

In the glovebox a 500 mL round bottom flask was loaded with a stir bar, copper iodide (1.5 mmol, 286 mg), toluene (100 mL), DMEDA (1.40 mL), diphenylphosphine (6.20 mL, 36.0 mmol) and stir at room temperature for 10 minutes. To the flask was added iodoaniline (30 mmol, 6.57 g) and cesium carbonate (60 mmol, 19.4 g), and the flask was brought out of the box and subjected to heating at 110ºC until reaction completed. The reaction progress was monitored with TLC (1:20 ethyl acetate: hexane, samples dissolved in toluene). The reaction mixture was cooled to room temperature and quenched with 50.0 mL of DI water. Following the liquid extraction with ethyl acetate (50.0 mL x 3), the pure product was obtained by silica column chromatography. The column was started using 1:10 EA:HX. After the compounds begin to elute, the solvent system was switched to 1:20 EA:HX for precise fraction collection. The product was characterized by ^{1}H NMR and ^{31}PNMR. Both analyses confirmed successful synthesis and purification of desired compound. (5.92 g, 71.1 %).

Step 2. Synthesis of ^{Ph}PN^{H}N Pincer Ligand L1

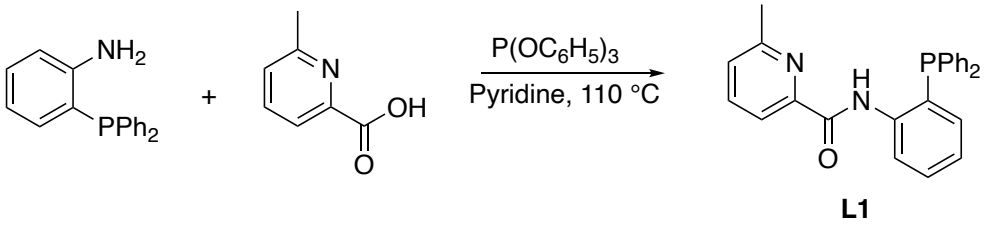

Scheme 2.3: Synthesis of L1 from 2-(diphenylphosphino)aniline and 6-methylpicolinic acid.

This reaction was performed outside of the glovebox. A 25 mL round bottom flask was loaded with a stir bar, 2-(diphenylphosphino)aniline (1.00 g, 3.61 mmol), 6-

methylpicolinic acid (544 mg, 3.97 mmol) and pyridine (3.00 mL). The flask was heated to 110ºC, and triphenylphosphite (1.12 mL, 4.31 mmol) was added by syringe. The reaction continued at 110ºC and was monitored by TLC analysis (1:5 EA:HX). Upon completion, the solvent was removed under vacuum and the crude was analyzed by ^{31}P NMR. Store for further purification.

Step 3 Purification of ^{Ph}PN^{H}N Pincer Ligand L1

Flash column chromatography (1:5 EA:HX) was used for the initial purification to obtain a crude product, which was further purified by crystallization by dissolving the product in ethyl acetate and layering ethanol on top at 0 °C for 2-3 days. The colorless crystals were collected by removing supernatant and dried under vacuum (0.956 g, 66.9 %). The product can be stored on a bench as it is air stable.

^{1}H NMR (500 MHz, Chloroform-*d*) δ 10.88 (s), 8.48 (dd, *J* = 4.6, 1.2 Hz), 8.47 (dd, *J* = 4.5, 1.2 Hz), 8.00 (t, *J* = 0.8 Hz), 7.98 (t, *J* = 0.8 Hz), 7.70 (t, *J* = 7.7 Hz), 7.45 – 7.40 (m), 7.39 – 7.29 (m), 7.24 – 7.23 (m), 7.06 (td, *J* = 7.5, 1.3 Hz), 6.91 (ddd, *J* = 7.6, 4.8, 1.6 Hz), 2.52 (s). ^{31}P{^{1}H} (121 MHz, 298 K, $CDCl_3$): δ (ppm) −19.77. ^{13}C{^{1}H} NMR (126 MHz, $CDCl_3$): δ (ppm) 162.4, 157.2, 149.3, 141.0 (d, J = 19.2 Hz), 137.7, 135.1 (d, J = 8.4 Hz), 134.1 (d, J = 19.2 Hz), 133.8, 130.2, 129.3, 128.9, 127.4 (d, J = 12.0 Hz), 126.1, 124.6, 121.5, 119.4, 24.4. MS spectrum (ESI+): m/z calcd for $[C_{25}H_{22}N_2OP]^+$ 397.1464, found 397.1456.

2.2.2 Synthesis of $^{iPr}PN^{H}N$ Pincer Ligand L2

2.2.2.1 Unsuccessful Attempt to Synthesize L2 from 1-bromo-2-diisopropylphosphinobenzene and 6-methylpicolinamide

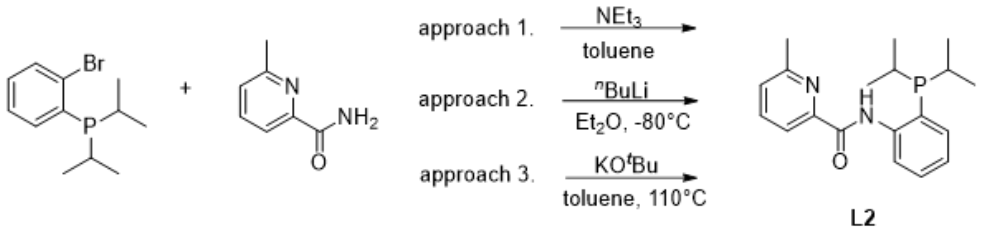

Scheme 2.4: Synthesis of L2 from 1-bromo-2-diisopropylphosphinobenzene and 6-methylpicolinamide.

Approach 1. In a N_2-filled glovebox, a 15 mL reaction tube was prepared by adding a stir bar and the following reagents: 1-bromo-2-diisopropylphosphinobenzene (0.183 mmol, 56.7 mg), 6-methylpicolinamide (0.183 mmol, 28.2 mg), triethylamine (0.201 mmol, 32.0 µL), and toluene (2.00 mL). The flask was then taken out of the glovebox and heated at 110 ºC for 24 hours with continuous stirring. However, no precipitate formation was observed throughout the duration of the reaction. To encourage the formation of precipitate, an attempt was made to push the solid out of the reaction solution by immersing the reaction tube in ice-cold deionized water for 2 hours. Unfortunately, no visible signs of crystallization were observed during this period. Subsequent analysis of the reaction solution using ^{31}P NMR spectroscopy indicated the absence of any signals corresponding to a new product formation. The spectral shift obtained was consistent with that of 1-bromo-2-diisopropylphosphinobenzene, suggesting that no reaction had occurred between the reagents.

Approach 2. This reaction was conducted inside the MBraun glovebox. To prepare the cooling well for the glovebox, an ethanol and liquid N_2 bath was applied to the outside of

the well, lowering the temperature to -80 ºC. The reaction substrates were individually cooled in separate vials within the cooling well for 30 minutes before being removed.

n-Butyl lithium (0.193 mmol, 120 µL, 1.6 M in hexanes) was then carefully added to the vial containing 1-bromo-2-diisopropylphosphinobenzene (0.193 mmol, 52.6 mg), and the mixture was allowed to react at room temperature for approximately 1.5 hours before transferring the vial back into the cooling well. Subsequently, 6-methylpicolinamide (0.193 mmol, 26.2 mg) was added dropwise to the vial over a period of 10 minutes, followed by stirring for 1 hour in the cooling well. The addition of the amide resulted in an immediate change in color to red/purple, suggesting the formation of a radical. However, it is possible that the reaction temperature was not sufficiently low, as maintaining the temperature of the ethanol/liquid N_2 bath for extended periods proved challenging.

Solubility issues arose with the amide reagent, as it was not completely soluble in ether. To overcome this, a small amount of THF was added to fully dissolve the reagent. Subsequent analysis by ^{31}P NMR revealed that the compound detected corresponded solely to the 1-bromo-2-diisopropylphosphinobenzene starting material, indicating an unsuccessful reaction.

Approach 3. The reaction was prepared in the glovebox under a N_2 atmosphere. In a 4 mL vial, 1-bromo-2-diisopropylphosphinobenzene (0.191 mmol, 52.3 mg) was dissolved in toluene (1 mL). In another 4 mL vial, 6-methylpicolinamide (0.191 mmol, 26.3 mg) was dissolved in toluene (1 mL). Both solutions were then combined in a reaction tube with a stir bar, followed by the addition of potassium *tert*-butoxide, KO^{t}Bu (0.211 mmol,

24.4 mg). The reaction tube was sealed and taken out of the glovebox to be placed in an oil bath at 110 ºC for 24 hours.

After the reaction time elapsed, there was visible precipitate suspended in the reaction solution. However, it was uncertain whether it was the desired product or unreacted base. Subsequent analysis using ^{31}P NMR revealed that the detected compound was exclusively associated with the 1-bromo-2-diisopropylphosphinobenzene starting material, indicating an unsuccessful reaction.

2.2.2.2 Synthesis of L2 from diisopropylchlorophosphine and *t*-BOC-aniline

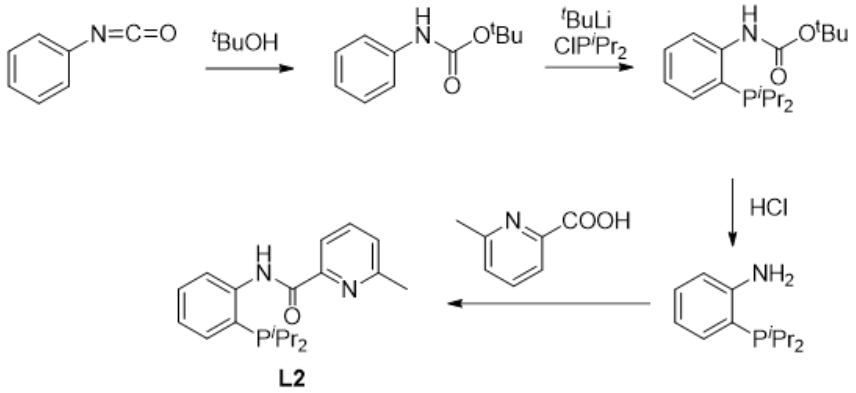

Scheme 2.5: Overview of the synthetic route to ligand L2.

Step 1. Synthesis of *t*-BOC-aniline from phenyl isocyanate

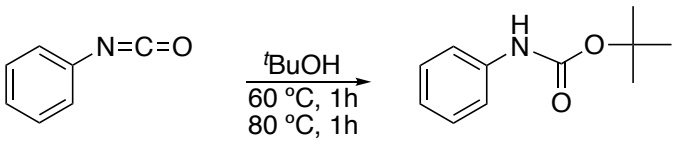

Scheme 2.6: Synthesis of *t*-BOC-aniline from phenyl isocyanate.

A 100 mL Schlenk flask was prepared by adding *tert*-butanol (0.222 mol, 16.4 g) and a stir bar. The flask was capped with a rubber septum, and N_2 gas was introduced into the flask through a Schlenk line while allowing the gas to exit through a bleed needle,

ensuring the removal of all oxygen. After 30 min, phenyl isocyanate (0.201 mol, 24.0 g) was injected into the flask using a needle and syringe. The reaction was carried out under a continuous N_2 atmosphere, initially at 60 ºC for 1 hour, followed by an additional hour at 80 ºC. To isolate the final product, the reaction mixture was vigorously stirred with diethyl ether until complete dissolution (if there were large chunks, an ultrasonicator was employed). The resulting mixture was then filtered using a Buchner funnel and side-arm Erlenmeyer flask, and the filtrate was concentrated and allowed to crystallize. The purity of the product was confirmed through ^{1}H NMR analysis, and the chemical shifts were confirmed according to those reported in the literature.

Step 2. Synthesis of *tert*-butyl (2-(diisopropylphosphino)phenyl)carbamate

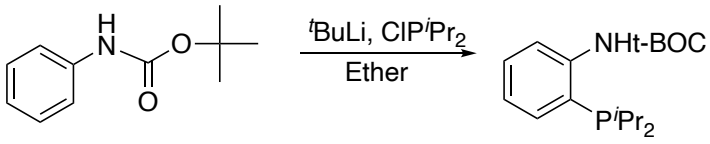

Scheme 2.7: Synthesis of *o*-C_6H_4(NH*t*-BOC)(P^iPr_2) from *t*-BOC-aniline.

The reaction was conducted in the glovebox. A 250 mL Schlenk flask was equipped with a stir bar, *t*-BOC-aniline (18.7 mmol, 3.62 g), and diethyl ether (56.0 mL). ^{t}BuLi (39.9 mmol, 23.5 mL, 1.7 M) was added to the flask. The flask was sealed with a rubber septum fastened by a copper wire before being taken out of the glovebox. It was then connected to the N_2 gas on the Schlenk line and stirred in a bath at -10 ºC for 3 hours. The bath temperature was achieved using dry ice and a NaCl solution. Afterward, chlorodiisopropylphosphine (18.7 mmol, 2.86 g) dissolved in diethyl ether was slowly added to the reaction flask using a syringe and needle. The reaction mixture was stirred at -80 ºC. Subsequently, the reaction was allowed to warm up to room temperature and ran

for 14 hours while maintaining a continuous flow of N_2 gas. Upon completion of the reaction, ice was added to quench the reaction, and brine was introduced. The organic phase was separated and extracted with ether (3 x 50.0 mL). The combined organic extracts were dried over $MgSO_4$, concentrated, and subjected to analysis. ^{31}P NMR spectroscopy confirmed the successful synthesis of the desired product; however, it also indicated the presence of an unknown byproduct. The literature confirmed that this impurity is commonly observed and would not adversely affect further steps in the synthesis process.

Step 3. Synthesis of 2-(diisopropylphosphino)aniline

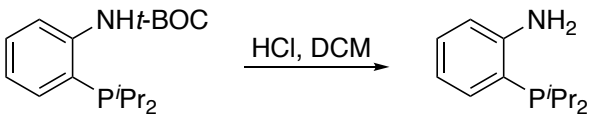

Scheme 2.8: Synthesis of *o*-$C_6H_4(NH_2)(P^iPr_2)$ from *o*-$C_6H_4(NHt\text{-}BOC)(P^iPr_2)$.

The reaction setup was performed inside a glovebox. A 250 mL Schlenk flask was utilized and equipped with *o*-$C_6H_4(NHt\text{-}BOC)(P^iPr_2)$ (57.1 mmol, 16.0 g), dichloromethane (85.0 mL) and a stir bar. To initiate the reaction, hydrochloric acid (15.5 mL, 10M) was slowly added dropwise to the stirring reaction solution. The mixture was then stirred at room temperature for a duration of twenty hours. For the extraction step, the pH of the reaction solution was adjusted to 10 using 10 M sodium hydroxide (NaOH). Separation of the reaction phases was accomplished by utilizing a separatory funnel. The organic phase was dried using magnesium sulfate ($MgSO_4$) and subsequently concentrated. To dissolve the concentrated organic phase, it was transferred to an Erlenmeyer flask containing ether (Et_2O). The resulting solution was subjected to gravity filtration to eliminate any suspended material. The filtrate was then further concentrated.

Further purification was carried out by dissolving the concentrated filtrate in pentane within an Erlenmeyer flask, followed by gravity filtration to remove any remaining suspended material. Once again, the filtrate was concentrated. The final product was characterized using ^{31}P NMR, which confirmed the successful synthesis of the desired compound. However, analysis of the spectral data revealed the presence of an impurity peak at 52.6 ppm.

Step 4. Synthesis of $^{iPr}PN^{H}N$ Pincer Ligand L2

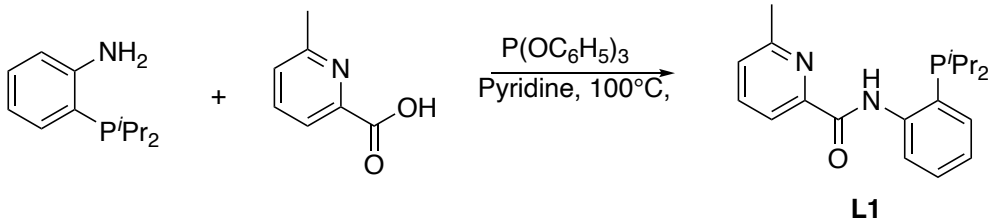

L1

Scheme 2.9: Synthesis of L2 from *o*-$C_6H_4(NH_2)(P^iPr_2)$ and 6-methylpicolinic acid**.**

The reaction setup was performed in the glovebox. A 250 mL Schlenk flask was equipped with *o*-$C_6H_4(NH_2)(P^iPr_2)$ (2.38 mmol, 0.500 g), pyridine (2.50 mL), and 6-methyl picolinic acid (2.39 mmol, 0.327 g). A reflux condenser and rubber septa were attached to the apparatus for proper sealing. The Schlenk flask was brought out of the box and connected to a Schlenk line and filled with N_2 gas to establish an inert atmosphere. The reaction mixture was then heated to 110 ºC before introducing triphenylphosphite (2.85 mmol, 0.749 mL) to the reaction flask. The mixture was stirred at 110 ºC for a duration of 12 hours. The reaction yielded a partially successful outcome, as the purification process presented challenges, limiting the ability to obtain a pure form of the product. To confirm the synthesis of the desired product, GC/MS analysis was

performed. The calculated and hypothesized fragments observed in the analysis were consistent with the predicted structure, confirming the synthesis of the product.

2.2.3 Synthesis of Fe and Co Complexes of $^{Ph}PN^{H}N$ ligand

2.2.3.1 Synthesis of $(^{Ph}PNN)_2Fe$ Complex

Inside the glovebox, a 150 mL vacuum flask was loaded with a stir bar, $^{Ph}PN^{H}N$ ligand (100 mg, 0.252 mmol), iron (II) chloride (16.0 mg, 0.126 mmol), potassium *tert*-butoxide (28.3 mg, 0.252 mmol), and toluene 15.0 mL. The reaction flask was taken out of the box and heated at 110 °C for 24 hours. After the reaction was completed, the reaction flask was brought back to the box, and the reaction mixture was filtered through a celite plug and concentrated under vacuum. The purple crystal was grown by layering pentane over concentrated toluene solutions at -20 °C (89.2 mg, yield 75%). ^{1}H NMR (500 MHz, 298 K, C_6D_6): δ (ppm) 11.37, 10.50 (d, J = 8.3 Hz), 9.13, 7.99 (d, J = 8.3 Hz), 7.87 (d, J = 8.1 Hz), 7.63 (d, J = 7.4 Hz), 7.14-6.83 (m), 6.76 (t, J = 8.3 Hz), 6.60 (m), 6.49 (m,), 6.27 (d, J = 7.3 Hz), 5.94 (d, J = 7.2 Hz), 3.68, 3.30, 2.15, 2.05, 1.85, 1.75, 1.32 (m), 1.18 (m), 0.91, 0.80 (m). UV-vis [toluene; λ, nm (ε, M-1cm^{-1})]: 422 (4.95×10^3). ESI-HRMS-TOF m/z: $[M + H]^+$ calc. for $C_{50}H_{40}FeN_4O_2P_2$, 846.1971; found, 846.1963. Anal. Calcd. for C, 70.93; H, 4.76; N, 6.62. Found: C, 70.84; H, 4.76; N, 6.63.

2.2.3.2 Synthesis of $(^{Ph}PNN)_2Co$ Complex

Inside the glovebox, a 150 mL vacuum flask was loaded with a stir bar, $^{Ph}PN^{H}N$ ligand (100 mg, 0.252 mmol), cobalt (II) chloride (16.4 mg, 0.126 mmol), potassium *tert*-butoxide (28.3 mg, 0.252 mmol), and toluene (15.0 mL). The reaction flask was taken out of the box and heated at 110 °C for 24 hours. After the reaction was completed, the reaction flask was brought back to the box, and the reaction mixture was filtered through

a celite plug and concentrated under vacuum. Red brown crystals were grown by layering pentane over concentrated toluene solutions at -20 °C. (93.9 mg, yield 79.0%). ^{1}H NMR (500 MHz, 298 K, C_6D_6): δ (ppm) 36.12, 27.11, 14.85, 13.71, 9.78, 9.39, 7.09, 5.50, 5.30, 2.18, 1.05, 0.29, -2.02, -8.14, -13.96. UV-vis [toluene; λ, nm (ε, $M^{-1}cm^{-1}$)]: 418 (4.88×10^3). ESI-HRMS-TOF m/z: $[M + H]^+$ calc. for $C_{30}H_{43}ClCoN_2P_3$, 618.1654; found, 618.1661. Anal. Calcd. for C, 70.67; H, 4.74; N, 6.59. Found: C, 70.59; H, 4.76; N, 6.61.

2.2.3.3 Unsuccessful Attempt to Synthesize (^{Ph}PNN)FeCl$_2$ Complex

Inside the glovebox, a 15 mL reaction vessel was loaded with a stir bar, $^{Ph}PN^{H}N$ ligand (20.0 mg, 0.050 mmol), iron (II) chloride (12.2 mg, 0.050 mmol), and toluene (2.00 mL). The vessel was heated at 110 °C for 24 hours. The reaction mixture was then filtered through a celite plug and concentrated under vacuum. Crystallization was set up by layering pentane over a concentrated toluene reaction mixture. Colorless needle crystals were grown along with black non-crystal residue. The colorless crystal was identified to be L1 ligand by single crystal X-Ray diffraction.

2.2.3.4 Unsuccessful Attempt to Synthesize (^{Ph}PN^{H}N)CoCl$_2$ Complex

Inside the glovebox, a 15 mL reaction vessel was loaded with a stir bar, $^{Ph}PN^{H}N$ ligand (20.0 mg, 0.050 mmol), cobalt (II) chloride (12.3 mg, 0.050 mmol), and toluene (2.00 mL). The vessel was heated at 110 °C for 24 hours. Then the reaction mixture was filtered through a celite plug and concentrated under vacuum. Crystallization was set up by layering pentane over a concentrated toluene reaction mixture at -20 °C. No crystal was successfully grown from the sample.

2.2.3.5 Unsuccessful Attempt to Synthesize (^{Ph}PN^{H}N)Co(PPh$_3$)Cl Complex

A 15 mL reaction vessel was loaded with a stir bar, ^{Ph}PNN ligand (20.0 mg, 0.050 mmol), cobalt (II) chloride (6.60 mg, 0.050 mmol), potassium *tert*-butoxide (5.70 mg, 0.050 mmol), triphenylphosphine (13.2 mg, 0.050 mmol) and toluene (2.00 mL). The reaction mixture was stirred at 110 °C for 24 hours and filtered by a celite plug. A diffusion method (Et_2O/toluene) was used for crystallization; however, no crystal was grown from the sample. NMR analysis of the sample revealed a pure ligand ^{Ph}PN^{H}N starting material. No desired product was observed.

2.2.3.6 Unsuccessful Attempt to Synthesize Co(^{Ph}PN^{H}N)(PPh$_3$)$_3$ complex

A 150 mL vacuum flask was loaded with a stir bar, ^{Ph}PN^{H}N ligand (20.0 mg, 0.050 mmol), chlorotris(triphenylphosphine)cobalt(I) (44.1 mg, 0.050 mmol), potassium *tert*-butoxide (5.60 mg, 0.050 mmol), and toluene (2.00 mL). The reaction mixture was heated in an oil bath at 110 °C for 24 hours. NMR analysis of the sample revealed a pure ligand ^{Ph}PN^{H}N starting material. No desired product was observed.

2.2.4. X-ray Crystallographic Data Collection and Refinement of the Structure.

2.2.4.1 Data Collection for ^{Ph}PN^{H}N ligand L1

Single colorless plate-shaped crystals of ^{Ph}PN^{H}N ligand were isolated from toluene. A suitable crystal 0.18×0.11×0.06 mm^3 was selected and mounted on a suitable support on a SuperNova, Dual, Cu at home/near, Pilatus 200K diffractometer. The crystal was kept at a steady T = 99.97(10) K during data collection. The structure was solved with the ShelXT structure solution program using the Intrinsic Phasing solution method and by using Olex2 as the graphical interface. The model was refined with version 2018/1 of ShelXL 2018/1 using least squares minimization. [16], [17]

2.2.4.2 Data Collection for (^{Ph}PNN)$_2$Fe complex

Single brown needle-shaped crystals of (^{Ph}PN^{H}N)$_2$Fe complex were isolated from Toluene. A suitable crystal 0.78×0.07×0.07 mm^3 was selected and mounted on a suitable support on a SuperNova, Dual, Cu at home/near, Pilatus 200K diffractometer. The crystal was kept at a steady T = 99.98(15) K during data collection. The structure was solved with the ShelXT structure solution program using the Intrinsic Phasing solution method and by using Olex2 as the graphical interface. The model was refined with version 2018/1 of ShelXL 2018/1 using least squares minimization. [16], [17]

2.2.4.3 Data Collection for (^{Ph}PNN)$_2$Co complex

Single brown plate-shaped crystals of (^{Ph}PN^{H}N)$_2$Co complex were isolated from Toluene. A suitable crystal 0.46×0.34×0.28 mm^3 was selected and mounted on a suitable support on a SuperNova, Dual, Cu at home/near, Pilatus 200K diffractometer. The crystal was kept at a steady T = 100.00(11) K during data collection. The structure was solved with the ShelXT structure solution program using the Intrinsic Phasing solution method and by using Olex2 as the graphical interface. The model was refined with version 2018/1 of ShelXL 2018/1 using least squares minimization. [16], [17]

CHAPTER III

RESULTS & DISCUSSION

3.1 Synthesis of $^{Ph}PN^{H}N$ Pincer Ligand L1

3.1.1 Synthesis of 2-(diphenylphosphino)aniline

3.1.1.1 Literature Survey of the Synthesis of 2-(diphenylphosphino)aniline.

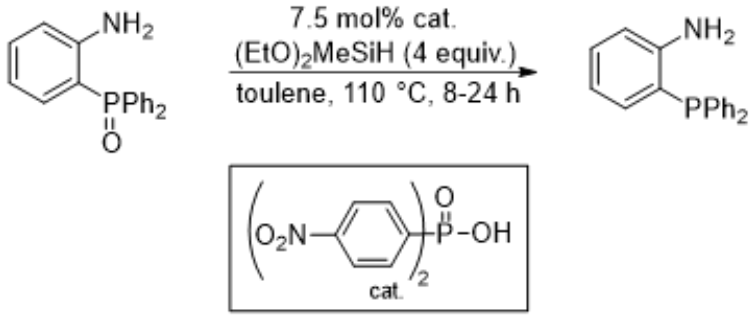

Scheme 3.1: Synthesis of 2-(diphenylphosphino)aniline from 2-aminophenyl(diphenyl) phosphine oxide conducted by Beller. [18]

The Beller group has worked to develop synthetic strategies for the chemoselective reduction of phosphine oxides with catalytic amounts of appropriately selected Brønsted acids. This reductive pathway is achievable under optimized conditions with the support of inexpensive silanes and reducible functional groups. Through this synthetic design, the group was able to demonstrate the organo-catalytic reduction of organophosphines to phosphines under metal-free conditions. They have demonstrated the ability to achieve a catalytic reduction with broad functional group tolerance and air-insensitivity with acceptable yields. [18]

Scheme 3.2: Synthesis of 2-(diphenylphosphino)aniline from phosphorylate *o*-fluoroaniline and potassium diphenylphosphate reported by Holland. [19]

The Holland group has demonstrated the ability to phosphorylate *o*-fluoroaniline via a microwave irradiation technique. This synthetic strategy is unlike the conventional thermal process. In using microwaves, the group has reported an increase in yields using this technique. Their synthetic strategy offers the benefits of convenience and efficiency to prepare aryl-substituted aminoarylphosphine ligands from inexpensive materials and decreasing the total reaction time required by its ability to maintain an elevated reaction temperature. [19]

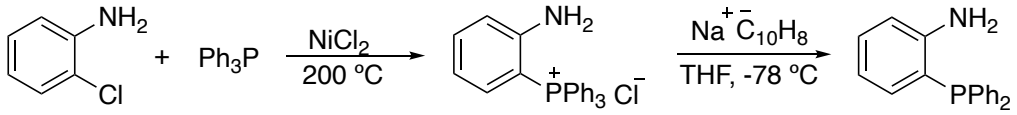

Scheme 3.3: Synthesis of 2-(diphenylphosphino)aniline from 2-chloroaniline and triphenylphosphine reported by Wang. [20]

The Wang group was able to demonstrate the synthesis of the aryl aniline compound through a catalytic reaction of nickel chloride treating 2-chloroaniline with triphenylphosphine. The intermediate product must be treated with reductant sodium naphthalene to achieve the desired structure. [20]

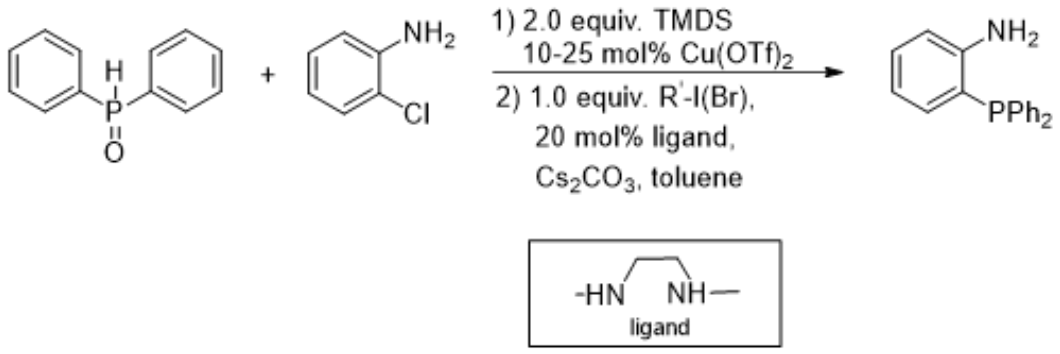

Scheme 3.4: Synthesis of 2-(diphenylphosphino)aniline from 2-chloroaniline and phosphine oxide reported by Beller. [21]

The Beller group has developed synthetic strategies for the catalytic reductions of tertiary and secondary phosphine oxides to phosphines. With the support of mild reducing agent, TMDS, and copper complexes, the selective reduction of PO occurs in the presence of other reducible functional groups. This synthetic strategy is considered to be a one pot reduction-phosphination domino sequence that is applicable to a variety of functionalized aromatic and aliphatic phosphines. [21]

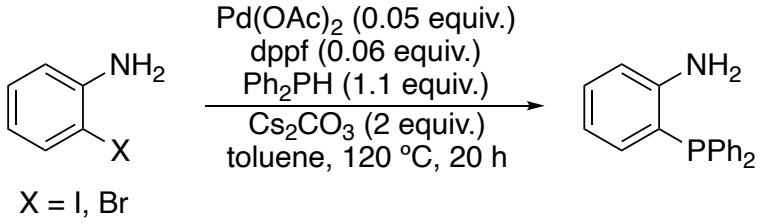

Scheme 3.5: Synthesis of 2-(diphenylphosphino)aniline from aryl aniline halides via a transition metal catalyzed pathway reported by Franchino and Xia. [22], [23]

The Franchino and Xia Groups independently synthesized the target aryl phosphine compounds via copper-catalyzed or palladium-catalyzed C-P cross-coupling reactions, employing aryl halides and phosphine reagents as the initial reactants. Both groups successfully achieved the synthesis of 2-(diphenylphosphino)aniline under air and

moisture-free conditions using similar reagents. However, variations were observed in the workup and purification techniques, including the choice of drying agents and solvents for flash column chromatography. [22], [23]

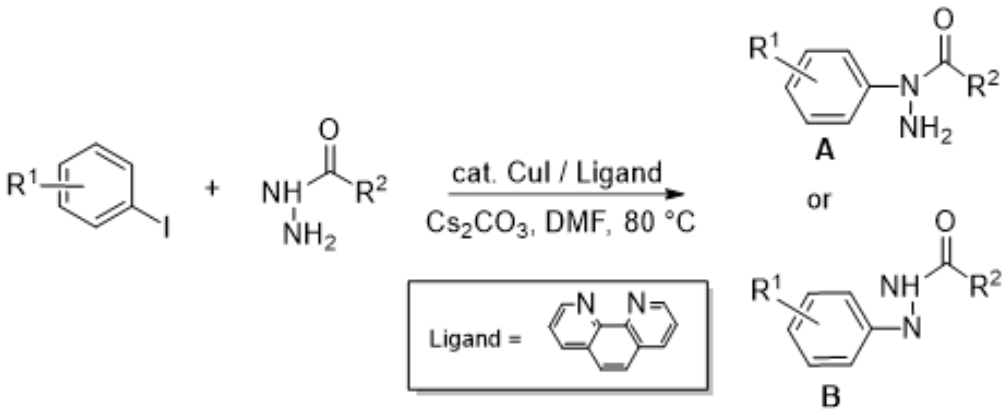

Scheme 3.6: N-arylation of hydrazides with substituted aryl halide in presence of copper catalysts reported by the Buchwald group. [24]

The Buchwald group reported the successful coupling of aryl halides with amines with the synthesis of catalyst copper iodide with ligand 1,10-phenanthroline, and solvent dimethylformamide (DMF). The C—N coupling reaction afforded N-arylated products from para- and meta-substituted aryl halides. Regioselectivity of this synthetic pathway to afford coupling with the amine versus the amide was proved with ortho-substituted aryl halides. [24]

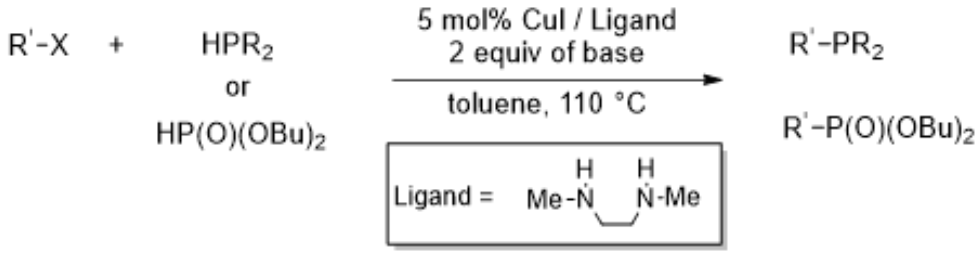

Scheme 3.7: Coupling of aryl and vinyl halides with diaryl and dialkyl phosphines with copper catalysts and DMEDA as reported by Buchwald group. [25]

The Buchwald group reported coupling of aryl and vinyl halides with diaryl and dialkyl phosphines via a copper-catalyzed synthetic pathway with N, N-dimethylethylenediamine (DMEDA) as the ligand and toluene as the reaction solvent. It was discovered the chelating diamine ligand enhances the efficiency of copper-catalyzed reactions. This synthetic design afforded the direct coupling and facilitation of C—P bond construction between substrates. Sterically hindered or functionalized substrate were found to react in good yields under these reaction conditions. [25]

3.1.1.2 Synthesis of 2-(diphenylphosphino)aniline (Approach 1)

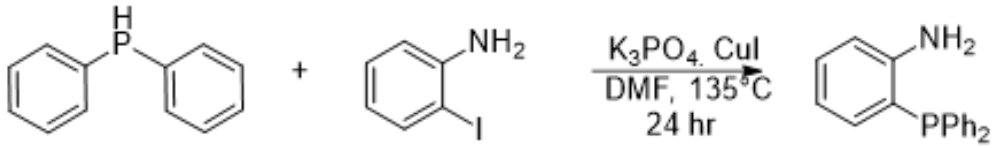

Scheme 3.8: Synthesis of 2-(diphenylphosphino)aniline from diphenylphosphine and iodoaniline.

Initially, our experiment aimed to synthesize 2-(diphenylphosphino)aniline by utilizing copper (I) iodide (CuI) as the catalyst, potassium phosphate (K_3PO_4) as the base, and dimethylformamide (DMF) as the solvent. The reaction was conducted under air and

moisture-free conditions at 135 ºC for an extended period. After completion, the reaction mixture was subjected to analysis using ^{31}P NMR, which revealed a singular peak. However, this peak corresponded to the starting material, diphenylphosphine, indicating the failure of the reaction.

3.1.1.3 Synthesis of 2-(diphenylphosphino)aniline (Approach 2)

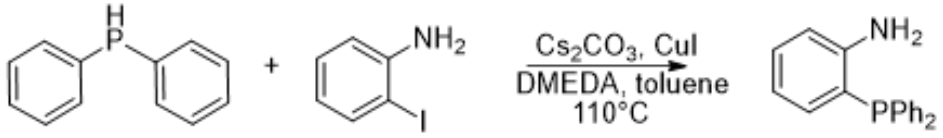

Scheme 3.9: Synthesis of 2-(diphenylphosphino)aniline from diphenylphosphine and iodoaniline.

In accordance with the methodology described by the Buchwald group we introduced Cs_2CO_3 as an additive and replaced DMF with DMEDA in approach 1. It has been reported that DMEDA can enhance the catalytic efficiency of copper-catalyzed C-P cross-coupling reactions. [25]

Upon analyzing the ^{31}P NMR spectrum of the crude sample, we observed the presence of the desired product. However, the mixture also contained several impurities. To eliminate these impurities, we performed flash column chromatography (FCC) on the crude sample, utilizing silica gel and a 1:20 ethyl acetate: hexane eluent system. Despite following the procedure described in the literature, the isolated yield of the pure product was less than 30%, and the column procedure yielded inconsistent results.

3.1.1.3.1 Optimization of Approach 2

In order to enhance the yield of 2-(diphenylphosphino)aniline from approach 2, modifications were made to the reaction time and purification procedures. Instead of

following the literature-reported 20-hour reaction duration, the progress of the reaction is now monitored using TLC analysis with a 1:20 ethyl acetate: hexane eluent system. A sample of iodoaniline is dissolved in toluene and spotted alongside the reaction mixture. The reaction is considered complete when the starting material spot disappears, as illustrated in Figure 3.1. This revised approach allows for a reaction time ranging from 4 to 6 days, ensuring the complete utilization of the limiting reagent, and facilitating higher yields.

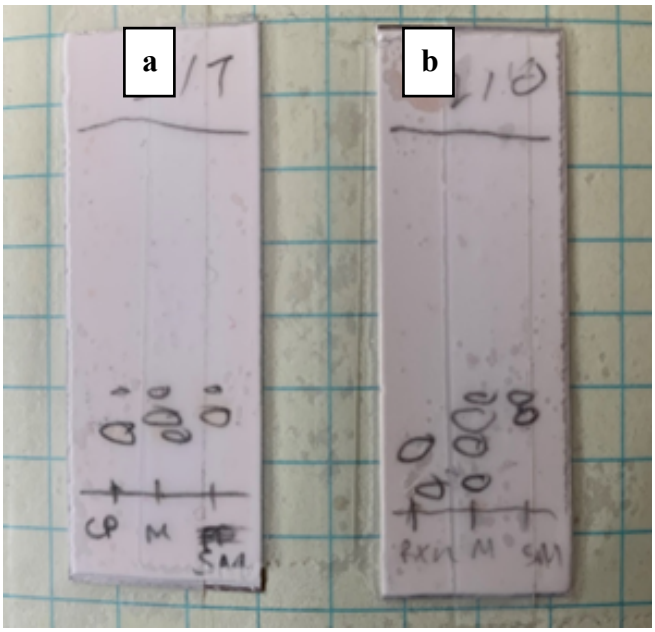

Figure 3.1: TLC Analysis of 2-(diphenylphosphino)aniline reaction progress a) after 72 hours of heating and b) upon completion of reaction after 96 hours of heating.

Furthermore, the flash column chromatography procedure was modified to reduce solvent usage, minimize purification time, and improve the reaction yield. Instead of employing a solution of 1:20 ethyl acetate: hexane throughout the entire column, we initiated the column using a more polar 1:10 ethyl acetate: hexane eluent. This adjustment enables the desired product to traverse the column more rapidly, while the majority of impurities

remain localized near the top. Once TLC analysis confirms the initiation of product elution, the solvent system is switched from 1:10 to 1:20 to facilitate efficient separation between the desired product and impurities. We monitor the elution of the product by examining the UV activity of the eluent every 80-100 mL. The crude product appears as a dark brown sticky oil, while the post-column material forms a white, powdery precipitate, as depicted in Figure 3.2.

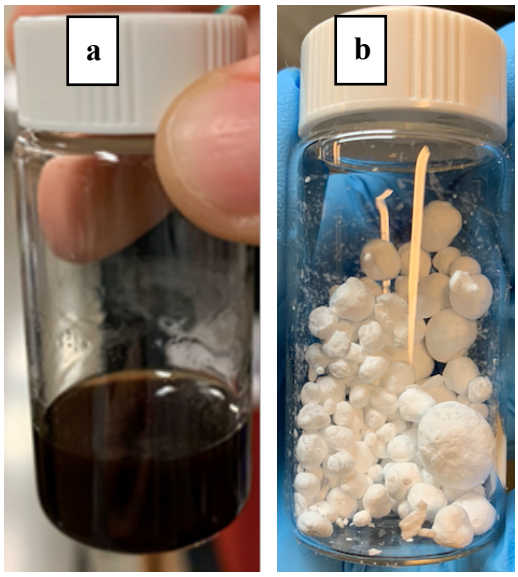

Figure 3.2: 2-(Diphenylphosphino)aniline reaction scheme 3.9 products. a) Crude product pre-column and b) pure product post-column.

The above modification has not only decreased the amount of materials used to synthesize 2-(diphenylphosphino)aniline but also increased yields consistently to >70%. The final product is characterized by ^{31}P NMR to confirm its purity before being used in the synthesis of ligands. A single peak at ~ −20 ppm ($CDCl_3$) correlates with that of the pure product, as seen in Figure A.1. This reaction was repeated multiple times yielding approximately 25.0 g of pure compound (71.1 %).

3.1.2 Synthesis of $^{Ph}PN^{H}N$ Pincer Ligand L1

3.1.2.1 Literature Survey of L1 Synthesis

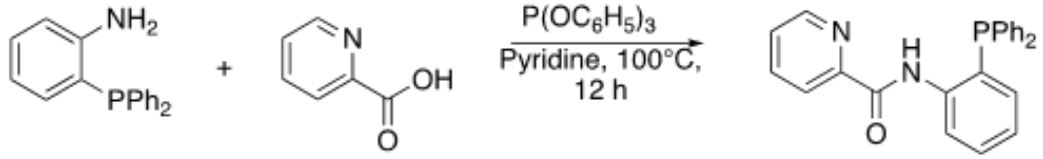

Scheme 3.10: Synthesis of N-(2-(diphenylphosphino)phenyl)pyridine-1-1carboxamide from 2-aminodiphenylphosphine and 2-picolinic acid reported by Gupta. [26]

In a recent study, the Gupta group employed a condensation mechanism, combining 2-aminodiphenylphosphine and 6-methylpicolinic acid as substrates, to synthesize the ligand N-(2-(diphenylphosphino)phenyl)pyridine-1-1carboxamide. This molecule belongs to the class of phosphine-carboxamide-based tridentate ligands and bears a striking resemblance to our proposed ligand. The Gupta group successfully synthesized a mononuclear ruthenium complex utilizing this tridentate ligand as a catalyst for the transfer hydrogenation of various carbonyl compounds, employing isopropanol as the hydrogen source. However, to date, there have been no reported first-row transition metal complexes of this ligand. [26]

3.1.2.2 Synthesis of L1: Method Development and Design

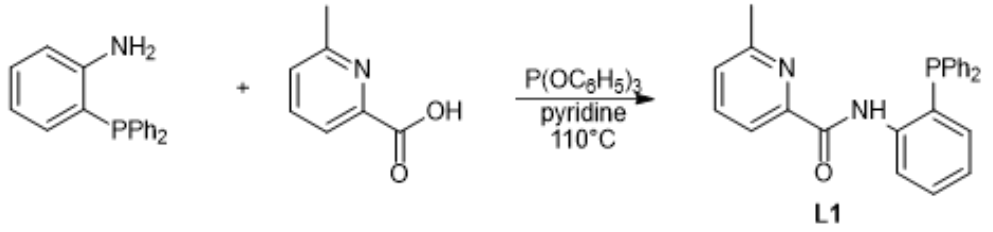

Scheme 3.11: Synthesis of L1 from 2-(diphenylphosphino)aniline and 6-methylpicolinic acid.

In accordance with the procedure employed by the Gupta group, we adopted a similar synthetic method for the synthesis of L1. However, we adjusted the reaction time, temperature, and post-workup procedure. The Gupta group reported a reaction temperature of 100 °C for 12 hours, resulting in yields of 92.0 %. After conducting further investigations into our ligand design's synthetic process, we found it optimal to run the reaction at 110 °C while monitoring the progress using TLC analysis (SiO_2; 1:5 ethyl acetate: hexane) as illustrated in Figure 3.3. The selection of the solvent system was determined by our group, evaluating various ratios of ethyl acetate and hexane (1:20, 1:10, and 1:5). We determined that a ratio of 1:5 provided the most distinct separation between products. This method was adopted to ensure the complete reaction of substrate 2-(diphenylphosphino)aniline, thereby leading to increased yields. Notably, we observed that higher yields could be achieved by raising the reaction temperature.

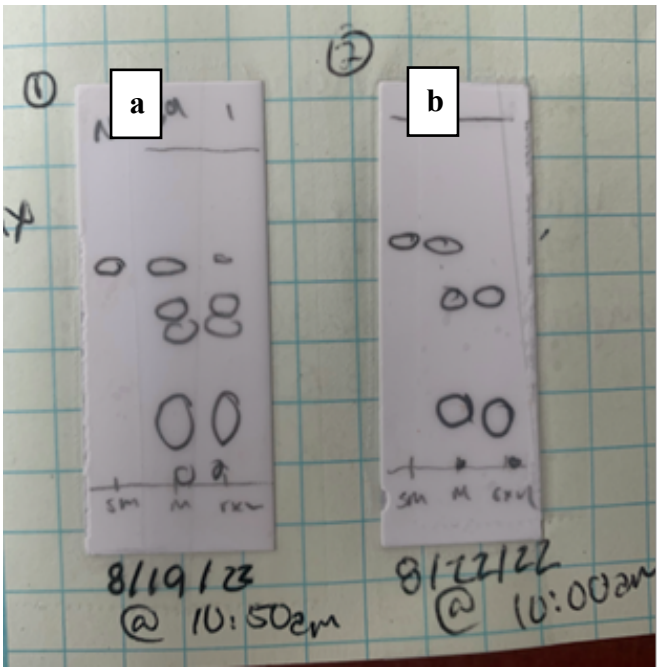

Figure 3.3: TLC monitoring of reaction progress at a) 24 hours and b) 96 hours for reaction scheme 3.11.

The second modification involved the post-workup and purification method. The Gupta procedure includes solvent removal under vacuum, cold water washing of the crude product, and precipitation of the final product using ether. However, when we followed this work-up procedure, instead of obtaining a white precipitate as reported by the Gupta group, we obtained a viscous, amber-colored, sticky oil. We suspected issues with the solubility of our product in ether and attempted to use dichloromethane (DCM) as an alternative solvent. Unfortunately, this change did not yield conclusive results.

A suitable purification method needed to be devised for this synthetic pathway. Neither crystallization nor distillation provided pure products or viable samples. Consequently, we turned to flash column chromatography (FCC) using the same solvent system employed in TLC analysis. Due to the close proximity of the various products generated in this reaction, as revealed by TLC analysis, approximately 100 g of silica gel was

required for every 1.00 g of crude product. FCC allowed for successful separation of the desired product from the majority of impurities. To attain absolute purity of the compound, the product collected and concentrated from FCC underwent a two-solvent crystallization method. This involved dissolving the column product in ethyl acetate, layering ethyl alcohol on top, and storing the mixture in the freezer. This optimized purification method resulted in the formation of white crystals, as shown in Figure 3.4C. The purity of the product was confirmed by ^{31}P, ^{1}H and ^{13}C NMR (Figures A.4 - A.7). Additionally, the predicted structure of the compound was further supported by HRMS (Appendix R.1) and single X-ray crystal analysis, as depicted in Figure 3.5.

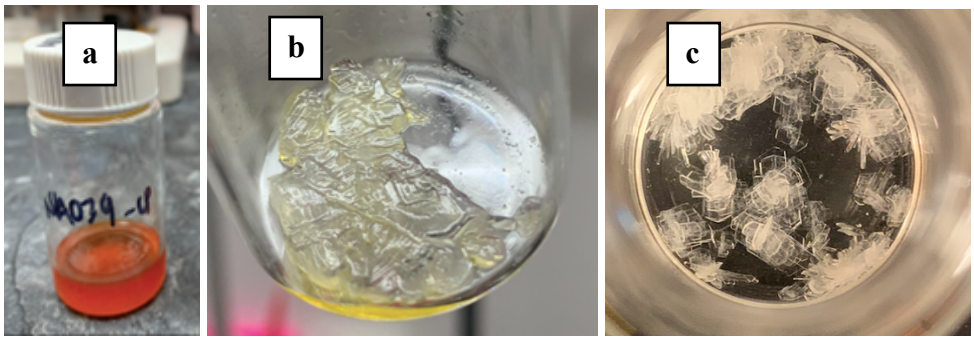

Figure 3.4: Reaction scheme 3.11 products through the purification process. a) Crude product post removal of solvent, b) product post column, and c) pure product post crystallization.

Initially, we handled the reaction process with caution regarding air and moisture sensitivity. To ensure a controlled environment, we employed an inert atmosphere using the Mbraun glovebox for the preparation of the reaction. However, upon further investigation, we discovered that this synthetic scheme is air and moisture stable. As a result, it can be prepared outside of the glovebox in an ambient atmosphere, simplifying the synthetic method for L1.

Although L1 has exhibited signs of air and moisture stability, it is still subjected to drying using a high vacuum and stored inside the Mbraun glovebox under an inert atmosphere. This is necessary due to its utilization in subsequent reactions of organometallic synthesis for complex coordination, where maintaining an inert environment is crucial.

3.1.2.3 Characterization of ligand L1

Single colorless plate-shaped crystals of the ligand were isolated from toluene. A suitable crystal 0.18×0.11×0.06 mm^3 was selected and mounted on a suitable support on a SuperNova, Dual, Cu at home/near, Pilatus 200K diffractometer. The crystal was kept at a steady T = 99.97(10) K during data collection. The structure was solved with the ShelXT structure solution program using the Intrinsic Phasing solution method and by using Olex2 as the graphical interface. The model was refined with version 2018/1 of ShelXL 2018/1 using least squares minimization. The final wR2 was 0.1695 (all data) and R1 was 0.0592 (I > 2(I)). [16], [17]

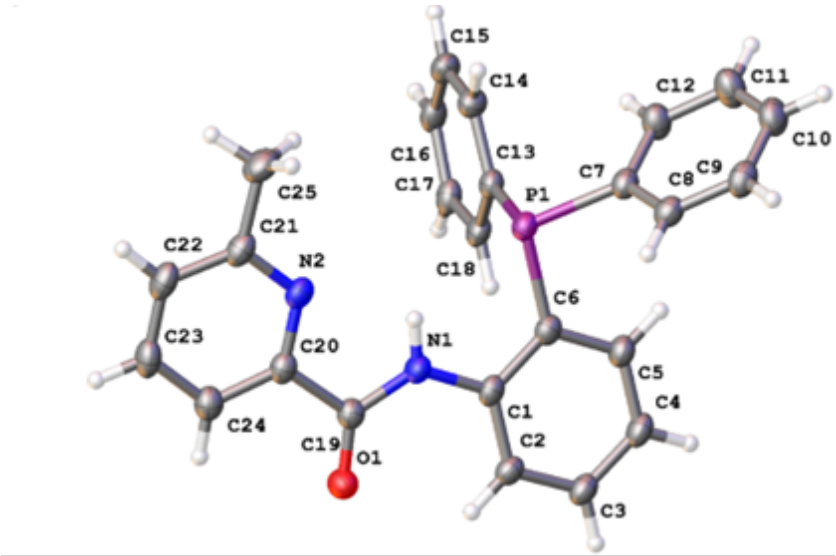

Figure 3.5: Solid-State Structure of $^{Ph}PN^{H}N$ Ligand L1 by Single Crystal X-ray Crystallography. Drawn at 50% thermal ellipsoid probability.

The crystal structure shows an expected tridentate pincer ligand structure with a phosphine donor, a pyridine donor and an amide bond that can potentially serve as an electron donor as well. L1 can act as a neutral ligand or an anionic ligand when the amide is deprotonated.

Table 3.1: Selected Bond Lengths (Å) and Angles (deg) for $^{Ph}PN^{H}N$ pincer ligand L1.

Bond	**Length**
P1—C6	1.835(2)
N1—C1	1.410(3)
N1—C19	1.355(2)
C19—C20	1.508(3)
C19—O1	1.225(3)
C20—N2 C20—C24	1.339(3) 1.387(3)
	Angles
C13—P1—C7	103.92(10)
C1—N1—C19	129.17(19)
O1—C19—N1	125.94(19)
O1—C19—C20	121.05(17)
C21—N2—C20	118.52(16)
C7—P1—C6	101.51(10)
C13—P1—C6	102.88(10)
P1—C6—C1	119.72(16)
N1—C1—C6	119.72(16)

The IR spectrum of each compound exhibited a very strong absorption at 3272 cm^{-1}, consistent with the presence of the amide N-H bond (Figure A.20). This was supported by the appearance in the ^{1}H NMR spectrum of the ligand of a singlet at 10.88 ppm (Figure A.5). The ^{31}P NMR spectrum of the ligand (Figure A.4) shows a singlet at −18.2 ppm, consistent with one environment for the two PPh_2 groups in the ligand. The electrospray (ESI) mass spectrum of MeCN or MeOH solutions of L1 exhibited a peak envelope at *m/z* 397.1456 assigned to $[C_{25}H_{22}N_2OP]^+$ and an isotope pattern consistent with this formulation.

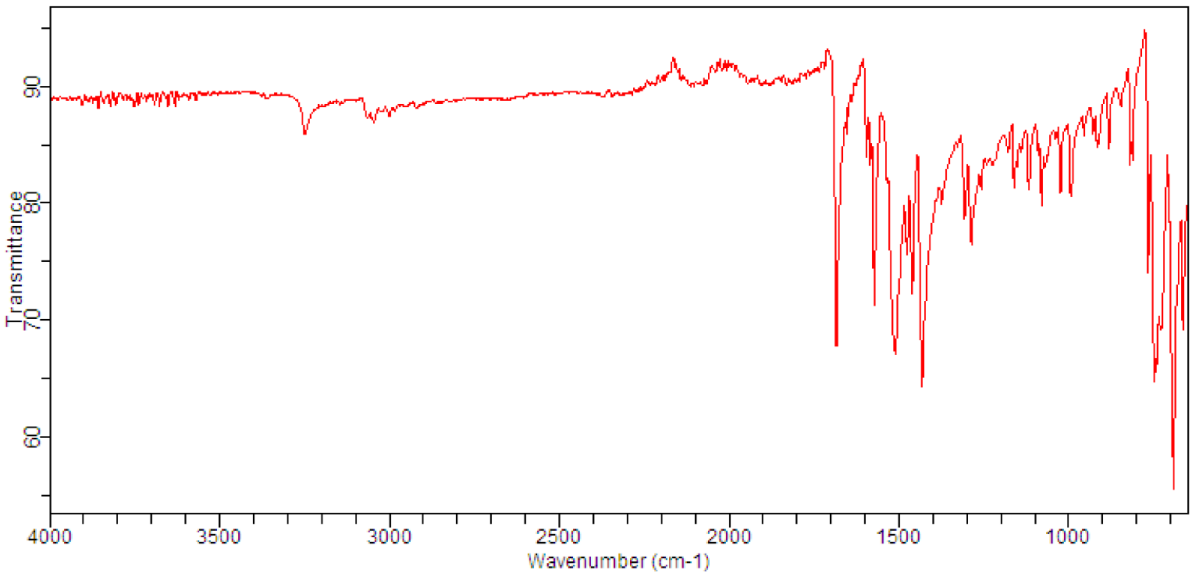

Figure A.20: IR Spectrum of L1

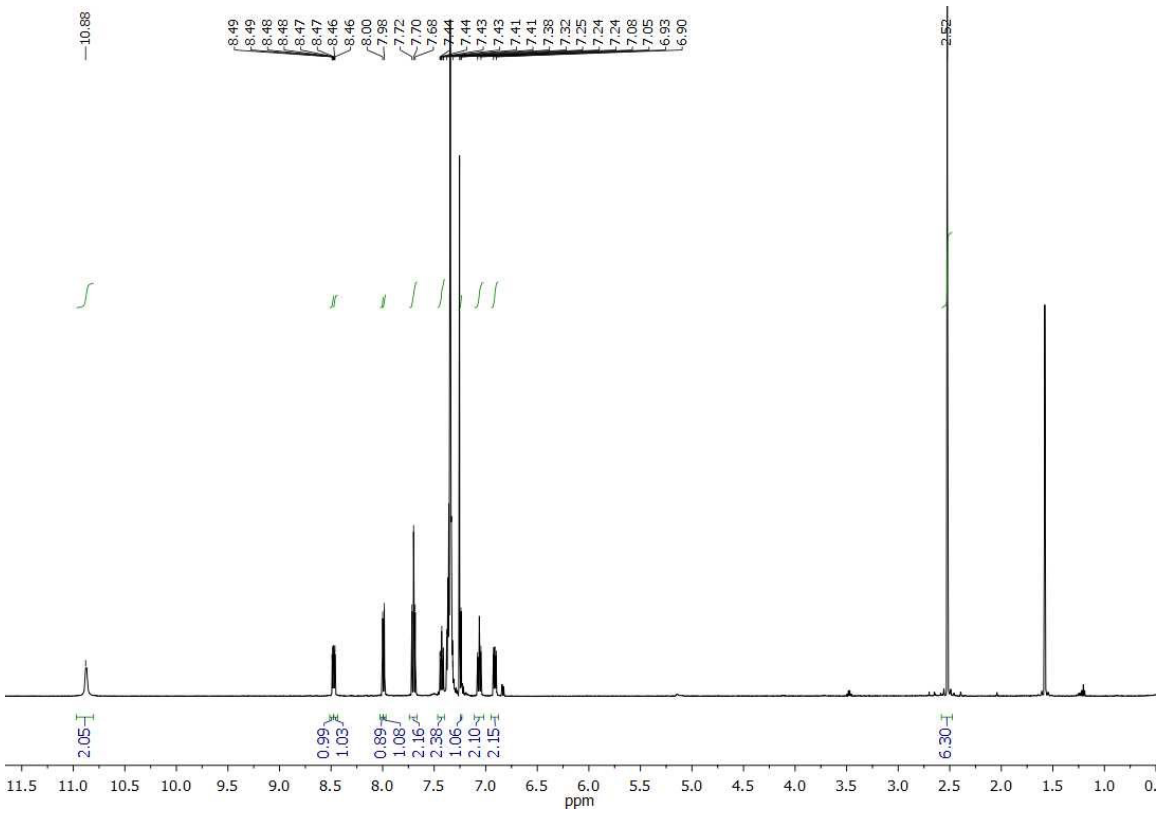

Figure A.5: ^{1}H NMR ($CDCl_3$, 500 MHz) of product L1

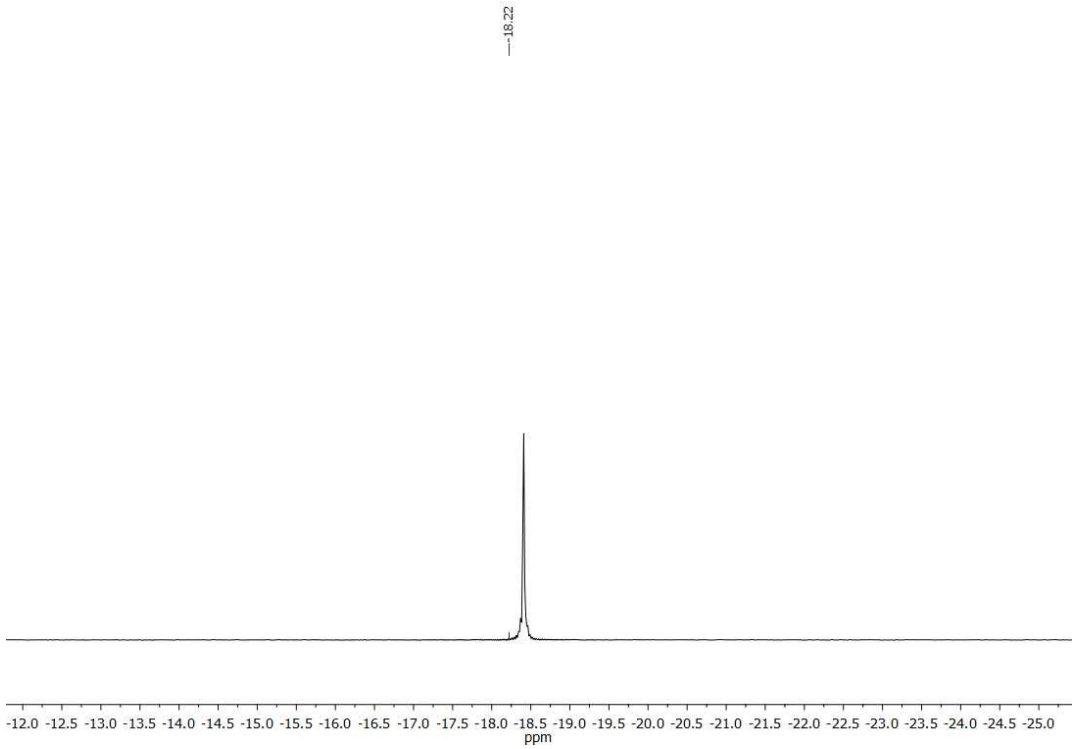

Figure A.4. ^{31}P NMR ($CDCl_3$, 500 MHz) of product L1.

3.2 Synthesis of $^{iPr}PN^{H}N$ Pincer Ligand L2

3.2.1 Unsuccessful Attempt to Synthesize L2 from 1-bromo-2-diisopropylphosphinobenzene and 6-methylpicolinamide

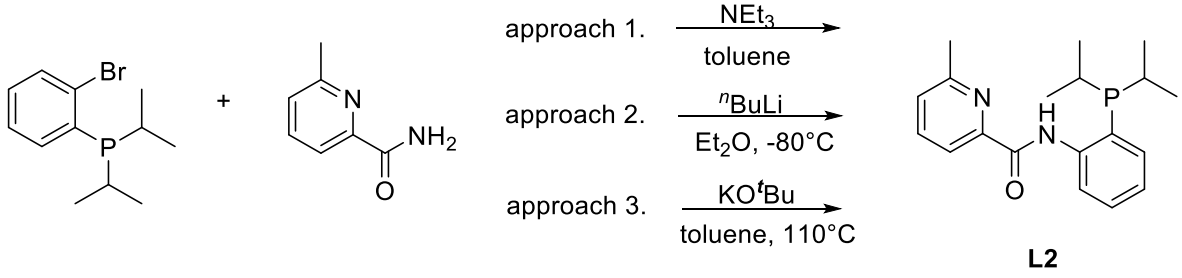

Scheme 3.12: Unsuccessful Synthesis of L2 from 1-bromo-2-diisopropylphinobenzene and 6-methyl-2-pyridinecarboxamide (Approach 1-3).

Approaches 1-3 were prepared in the Mbraun glovebox, while reagent 1-bromo-2-diisopropylphosphinobenzene was synthesized in the laboratory by colleagues.

Approach 1: A flask was set up with reagents 1-bromo-2-diisopropylphosphinobenzene and 6-methyl-2-pyridinecarboxamide, along with triethylamine as the base, in an attempt to carry out a direct coupling reaction. The reaction mixture was prepared inside the Mbraun glovebox and left to react overnight at room temperature. It was expected that a precipitate would form as a result of the reaction. However, upon visual inspection after completion, no precipitate was observed. Analysis of the ^{31}P NMR spectrum indicated that the two substrates did not couple, as the spectrum matched that of the 1-bromo-2-diisopropylphosphinobenzene substrate shown in Figure A.14. This indicates that triethylamine was not a strong enough base to promote coupling between the two substrates.

Approach 2: Considering that triethylamine may not have been sufficient as a base, *n*-butyl lithium was employed to attempt the coupling of the two substrates. To facilitate the removal of the bromine group from 1-bromo-2-diisopropylphosphinobenzene, *n*-butyl lithium was added prior to introducing 6-methyl-2-pyridinecarboxamide. Upon addition of the amide, an immediate color change to red/purple was observed, indicating the possible generation of a radical from the pyridine substrate. Analysis of the ^{31}P NMR spectrum revealed that it matched that of the starting material, 1-bromo-2-diisopropylphosphinobenzene, as depicted in Figure A.14, similar to Approach 1.

Approach 3: The use of potassium *tert*-butoxide as the base in the previous method yielded similar results to Approach 1 and 2. There was visible solid suspended in the reaction mixture, but it remains uncertain whether it was unreacted potassium *tert*-

butoxide or the potential formation of potassium bromide. The ^{31}P NMR analysis confirmed no reaction had taken place and correlated with the substrate 1-bromo-2-diisopropylphosphinobenzene, as observed in Figure A.14.

All three methods were evaluated to address the possibility of reagent contamination by testing the dryness of the various solvents and starting materials. Both substrates were found to be pure, as shown in Figures A.15, A.16, and A.17. Additionally, all solvents passed the dryness tests. Thus, we can rule out contamination as a potential complication for the lack of success in this synthetic pathway. Overall, approach 1-3 present challenges in terms of reactivity and selectivity in the direct coupling reaction.

3.2.2 Synthesis of L2 from diisopropylchlorophosphine and *t*-BOC-aniline

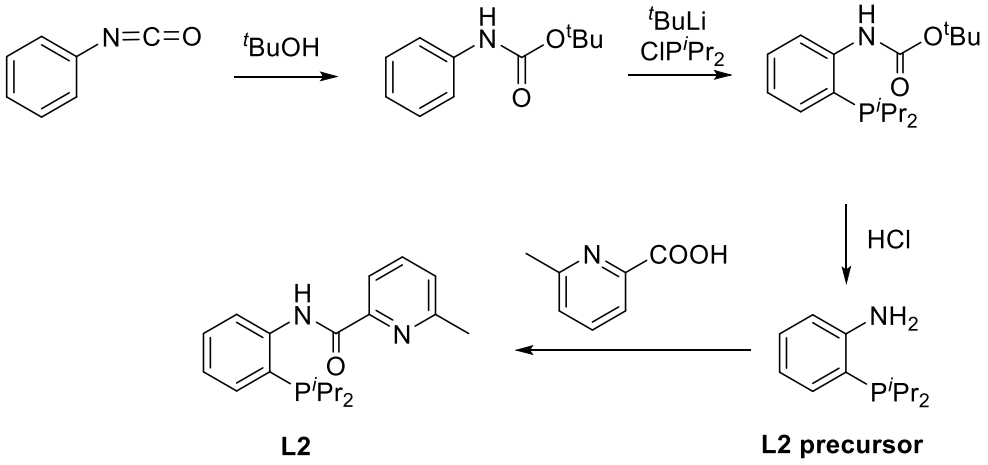

Scheme 3.13: Overview of the Synthetic Route to Ligand L2.

An alternative synthetic pathway for ligand L2 is proposed in Scheme 3.13. This approach consists of four individual steps, each of which will be discussed separately below.

3.2.2.1 Literature Survey of *o*-diisopropylphosphinoaniline

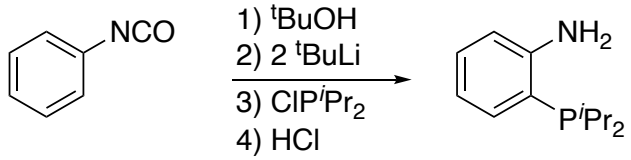

Scheme 3.14: Synthesis of *o*-diisopropylphosphinoaniline from phenyl isocyanate.

The Fryzuk group successfully synthesized *o*-diisopropylphosphinoaniline (L2 precursor) via a double lithiation of *t*-BOC-aniline using *tert*-butyl lithium, chloro-diisopropylphosphine, and hydrochloric acid for the deprotection of the amine group. The synthesized compound is utilized in the synthesis of pincer ligands as a generated bis(phosphine) imidazolinium salt to be coordinated to a metal center. [27]

3.2.2.2 Synthesis of *o*-diisopropylphosphinoaniline

The synthetic schemes described below were conducted with reference to the work of the Fryzuk group. While most of the synthetic procedures followed the reported protocols of the Fryzuk group, certain reaction preparations and work-up procedures were modified as deemed appropriate. [27]

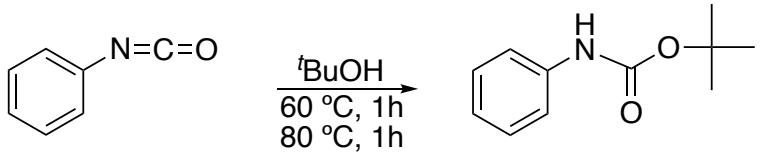

Scheme 3.15: Synthesis of *t*-BOC-aniline from phenyl isocyanate.

In the initial step of this synthetic pathway, a protecting group was introduced using *tert*-butanol to safeguard the nitrogen group from the strong base *tert*-butyl lithium used in the second step. Due to the pyrophoric nature of phenyl isocyanate, this reaction preparation was carried out on the Schlenk line. Regarding reagent loading, we employed a different

method than the Fryzuk group. The Schlenk flask was loaded with *tert*-butanol, and the flask was subsequently flushed with N_2 gas before adding phenyl isocyanate by a syringe. This precautionary step ensured that no oxygen reacted with the phenyl isocyanate substrate. Upon dropwise addition of phenyl isocyanate to *tert*-butanol, an immediate visible formation of precipitate occurred in the reaction mixture. Once the reaction was complete, it resulted in a solid white precipitate that had to be crushed to be removed from the reaction flask. To ensure the complete removal of *tert*-butanol from the reaction, the reaction solvent was removed by rotavap and subsequently high vacuum line. We were able to further purify the product by dissolving the crude with ether and filtering the solution through a Büchner funnel. Upon removal of the solvent under vacuum, the final product would crystallize. The ^{1}H NMR, as depicted in Figure A.10, confirmed the purity of the product. This compound was not air-sensitive and could be handled and stored outside of the Mbraun glovebox.

Figure 3.6. *t*-BOC-aniline product.

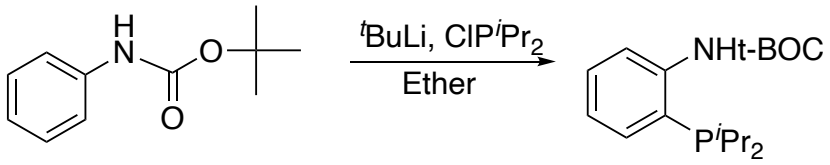

Scheme 3.16: Synthesis of *o*-C_6H_4(NH*t*-BOC)(P^iPr_2) from *t*-BOC-aniline.

In the second step of the synthesis, a strong base, *tert*-butyl lithium, was utilized to deprotonate the ortho position of *t*-BOC aniline in preparation for the addition of the diisopropylphosphine group. As a result, butanol and lithium chloride were generated as byproducts, both of which could be easily removed in the work-up procedure. To prepare the reaction, the required amount of *t*-BOC-aniline was first added to a Schlenk flask before transferring it into the Mbraun glovebox. Inside the glovebox, diethyl ether was added, and the flask was sealed with a rubber septum before bringing it out of the glovebox. This step was necessary to maintain the integrity of the reaction mixture and ensure safe handling of the reagents. The flask was then purged with N_2 gas before the dropwise addition of *tert*-butyl lithium at -20 °C. To achieve this reaction temperature, a cooling bath was created using dry ice, sodium chloride, and deionized water. The reaction solution was stirred at -20 °C for 3 hours before transitioning the bath to -80 °C using acetone and dry ice. Subsequently, chloro-diisopropylphosphine was added dropwise to the reaction solution. The reaction flask was slowly raised to room temperature and stirred for 14 hours. Upon completion of the reaction time, the reaction mixture exhibited an orange/red color, as depicted in Figure 3.7.

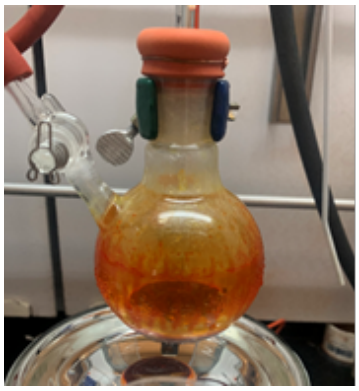

Figure 3.7. Reaction mixture from scheme 3.16 after heating.

Initially, the bright orange/red color raised concerns about possible decomposition of the product. However, through analysis of ^{1}H NMR and with reference to the reported literature, we were able to confirm the successful synthesis of the desired product. Additionally, there were a few impurities present, as shown in Figure A.11, but these same peaks were reported in the literature too. The work-up procedure was carried out precisely as reported by the Fryzuk group. The final product obtained was an orange/yellow oil, as seen in Figure 3.8. [27]

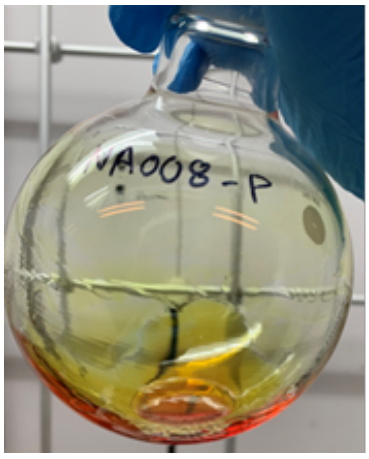

Figure 3.8. Reaction product from scheme 3.16.

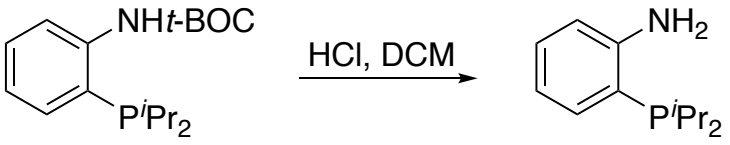

Scheme 3.17: Synthesis of *o*-diisopropylphosphinoaniline from *o*-C_6H_4(NH*t*-BOC)(P^{i}Pr$_2$).

The final step of the synthetic pathway involved an acid-base reaction mechanism to deprotect and convert the amide group to an aniline group, resulting in the formation of *o*-diisopropylphosphinoaniline (L2 precursor). In this step, there was no need to handle the reaction or reagents inside the Mbraun glovebox due to the air and moisture stability of the compounds involved. A round-bottom flask was charged with *o*-C_6H_4(NH*t*-BOC)(P^{i}Pr$_2$), 10 M hydrochloric acid, and dichloromethane, and the mixture was stirred at room temperature for a duration of twenty hours. This procedure was followed precisely as reported by the Fryzuk group. Upon the addition of hydrochloric acid, the color of the reaction mixture changed from yellow to orange/brown. After approximately five minutes of stirring, the reaction solution transformed into a green, non-transparent color, as depicted in Figure 3.9. [27]

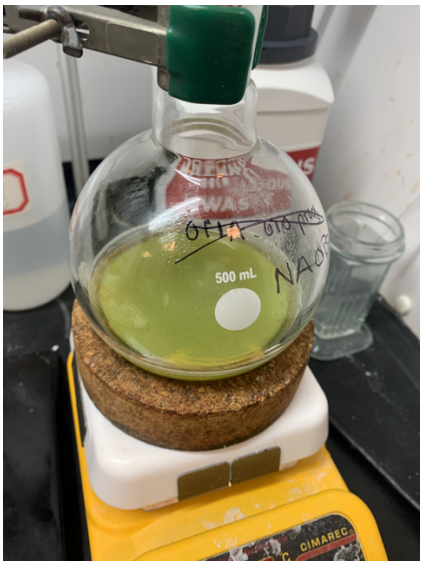

Figure 3.9. Reaction mixture of scheme 3.17 post heating.

The work-up procedure was followed as the Fryzuk group reported. The final product affords a yellow oil and was characterized via ^{31}P NMR; as seen in Figure A.12. In addition to the final product at -14.8 ppm there is an impurity peak at 52.9 ppm, however, this peak is reported in literature and is thought to correlate to P^iPr_2OH. The impurity at 60.3 ppm is believed to have carried over from the previous step as both spectrums (A.10 ad A.11) have the same peak. We believe conducting the reaction under inert atmosphere in the future may help to eliminate or decrease the presence of this impurity. At this point in the work, we moved forward without further purification. [27]

3.2.2.3 Synthesis of ligand L2

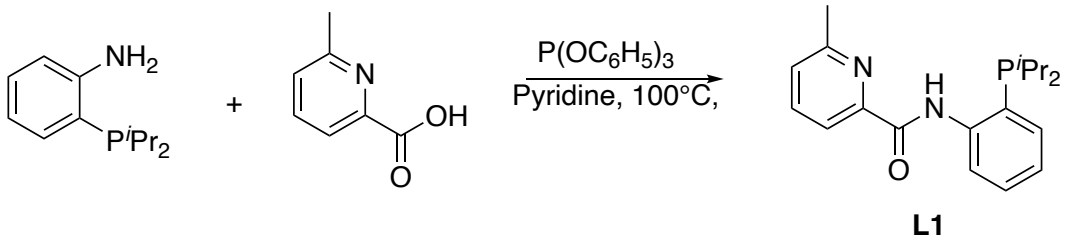

Scheme 3.18: Synthesis of L2 from *o*-C_6H_4(NH*t*-BOC)(P^iPr_2) and 6-methylpicolinic acid.

In the synthesis of L2, a condensation mechanism was performed following the procedure of the Gupta group with a change in the apparatus setup and workup procedure. Unlike the Gupta group, we prepared the reaction in a Schlenk flask with a reflux condenser and connected the flask to the Schlenk line to achieve an inert atmosphere (Figure 3.10). The purpose of introducing the reflux condenser to the apparatus was to ensure no solvent was lost during the heating process. [26]

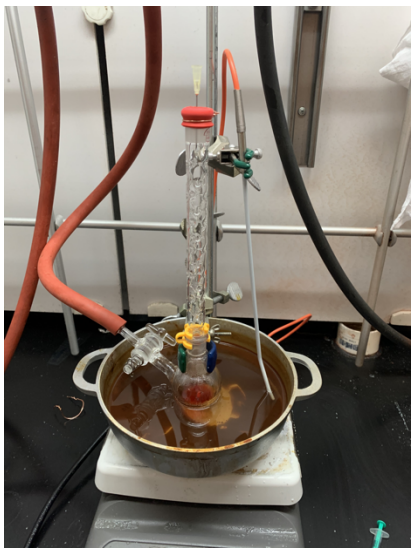

Figure 3.10. Apparatus for reaction scheme 3.18.

Upon addition of triphenyl phosphite, the reaction color changes from yellow to red. It is unclear as to why this occurs but does indicate a reaction is occurring. The Gupta workup procedure was initially followed, however, as there was no visible formation of precipitate upon addition of ether, we decided to perform a liquid-liquid extraction, collect the organic layer, dry it over magnesium sulfate, and concentrate the sample. The final product afforded a bright orange oil as seen in Figure 3.11. Upon analysis of ^{31}P NMR as seen in Figure A.13, the spectrum indicated that the final product was not pure due to the presence of several peaks versus a single peak which would indicate purity. It is possible this is due to not purifying step two or three in the synthesis of *o*-diisopropylphosphinoaniline.

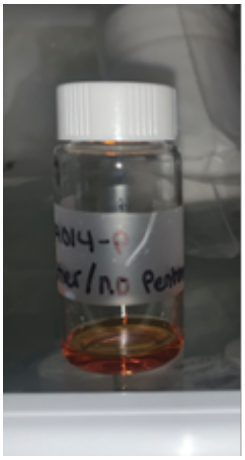

Figure 3.11: Crude product from reaction scheme 3.18.

3.2.3 Purification of L2

In attempt to purify L2 from the impure mixture, the sample was setup for diffusion crystallization by dissolving the sample in ethyl acetate and layering it with ethyl alcohol. After 24 hours stored in the freezer there was no visible signs of crystal growth. This may be due to issues of product solubility in ethyl alcohol. Considering the success of flask

column chromatography used for L1, this purification method was adopted in a second attempt to isolate L2 from the impure mixture. The sample was tested with TLC analysis against solvent systems 1:10 ethyl acetate: hexane, 1:5 ethyl acetate: hexane, and 1:3 hexane: DCM. It was decided 1:5 ethyl acetate: hexane provided the best separation as seen Figure 3.12. Using TLC analysis, we see some separation between compounds, especially in fractions 7, 8, and 9. As we were working with a 30 mg crude sample, there was not enough material to obtain a clear ^{1}H NMR spectrum for analysis. This purification method may provide promising results of obtaining a pure ligand sample but must be optimized in the future.

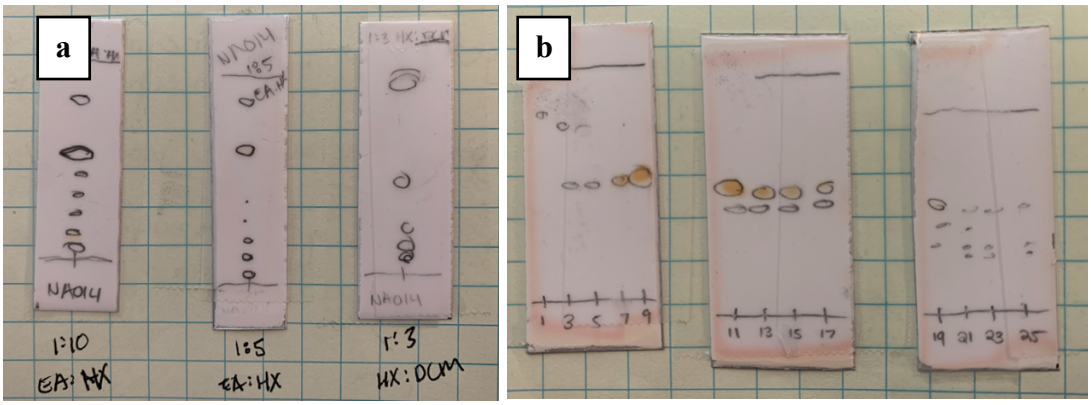

Figure 3.12: TLC analysis of column chromatography for reaction scheme 3.18. a) Analysis of solvent system for L1 column chromatography and b) analysis of fractions collected from column chromatography.

3.4 Synthesis of Iron and Cobalt Complexes of L1

All organometallic reactions were prepared in the Mbraun glovebox due to air and moisture sensitivity of metal reagents and base. L1 is thoroughly dried under high vacuum before being stored in the Mbraun glovebox to maintain the integrity of its

dryness for coordination reactions. All reaction workups were performed inside the Mbraun glovebox.

3.4.1 Synthesis of Fe Complex with $^{Ph}PN^{H}N$ ligand

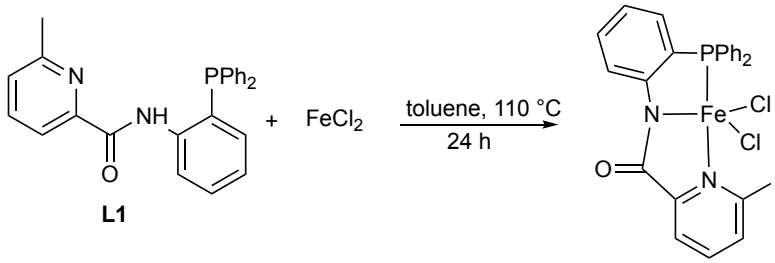

Scheme 3.19: Proposed reaction scheme of iron complex from neutral L1 and iron (II) chloride.

The ^{Ph}PNN ligand can act as either neutral ligand or anionic ligand upon deprotonation. Our first goal was to obtain an iron complex [($^{Ph}PN^{H}N$)$FeCl_2$] coordinated with the neutral $^{Ph}PN^{H}N$ ligand. The $^{Ph}PN^{H}N$ ligand was allowed to react with $FeCl_2$ precursor in 1:1 ratio without any external base being used. This reaction was performed in toluene, THF or DCM at room temperature. However, no desired product was successfully obtained. The reaction was also performed at 110 °C in toluene without success. Later, a colorless crystal sample was obtained after crystallizing the reaction mixture in toluene/pentane. It was revealed to be the $^{Ph}PN^{H}N$ ligand, instead of the iron complex.

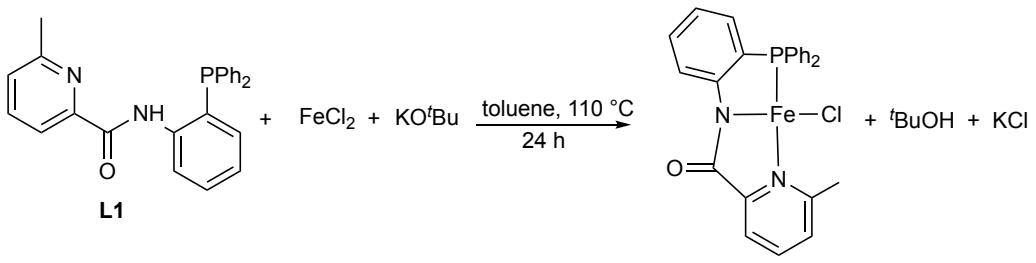

Scheme 3.20. Proposed reaction scheme of iron complex from anionic L1 and iron (II) chloride

Our second goal was to obtain an iron complex with the anionic form of the ligand. Our approach is to add one equivalence of the base potassium *tert*-butoxide (KO^{t}Bu) to the mixture of $^{Ph}PN^{H}N$ ligand and $FeCl_2$. KO^{t}Bu serves to deprotonate the amide and achieve its anionic form. By principle, this should create a mono-chelated iron complex [(^{Ph}PNN)FeCl] and *tert*-butanol and potassium chloride byproducts as shown in Scheme 3.20. When $^{Ph}PN^{H}N$ ligand, $FeCl_2$ and KO^{t}Bu were allowed to react in a 1:1:1 ratio, a purple mixture with white precipitates were generated. Purple crystals were isolated by crystallization out of toluene layered with pentane. Surprisingly, the X-ray single crystal diffraction analysis showed a bis-chelated iron complex [(^{Ph}PNN)$_2$Fe]. Despite manipulating the equivalences of metal to ligand to a 1:1 ratio, the ligand has shown to continuously bond in a two to one ratio with the metal, and this causes unreacted metal left at the end of the reaction. Therefore, the reaction conditions have been optimized to be conducted in a 2:1:2 ratio of ligand to metal to base to achieve good yields. The coordination geometry of the complex is shown in Figure 3.14.

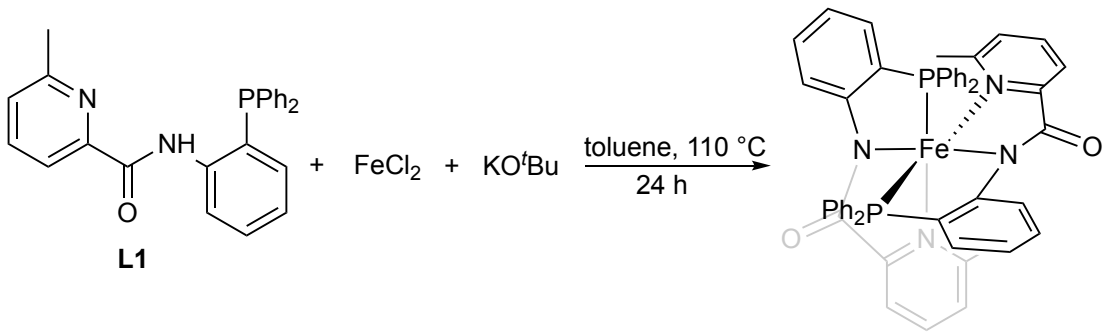

Scheme 3.21: True synthetic scheme of iron complex from anionic L1 and iron (II) chloride.

Crystallization was found to be the best method of purifying the complex. In small reaction scales <10 mg, diffusion method is most efficient. However, in larger scale

reaction >50 mg, layering method proves to be more efficient. Three solvent systems for crystallization were tested against the complex: toluene/pentane, tetrahydrofuran/pentane, and dichloromethane/pentane. In the toluene/pentane system, there is visible crystal growth. In the tetrahydrofuran/pentane system, there is some crystal growth. Lastly, in the dichloromethane/pentane system, there was no visible sign of crystal growth.

3.4.1.1 Characterization of Fe Complex of $^{Ph}PN^{H}N$ ligand

Elemental analytical data for the iron complex was consistent with the stoichiometry of [(^{Ph}PNN)$_2$Fe] complex. The strong absorption at 3272 cm^{-1} in the IR spectrum of $^{Ph}PN^{H}N$ ligand was gone in the IR spectrum of [(^{Ph}PNN)$_2$Fe] complex, indicating a successful deprotonation of amide N-H bond of the ligand (Figure A.18). The [(^{Ph}PNN)$_2$Fe] complex was poorly soluble in C_6D_6, and this hampered the collection of ^{13}C NMR data. The electrospray (ESI) mass spectrum of MeCN solutions of [(^{Ph}PNN)$_2$Fe] (Appendix R.2) exhibited a peak envelope at *m/z* 846.1963 assigned to $[C_{50}H_{40}FeN_4O_2P_2]^+$ and an isotope pattern consistent with this formulation.

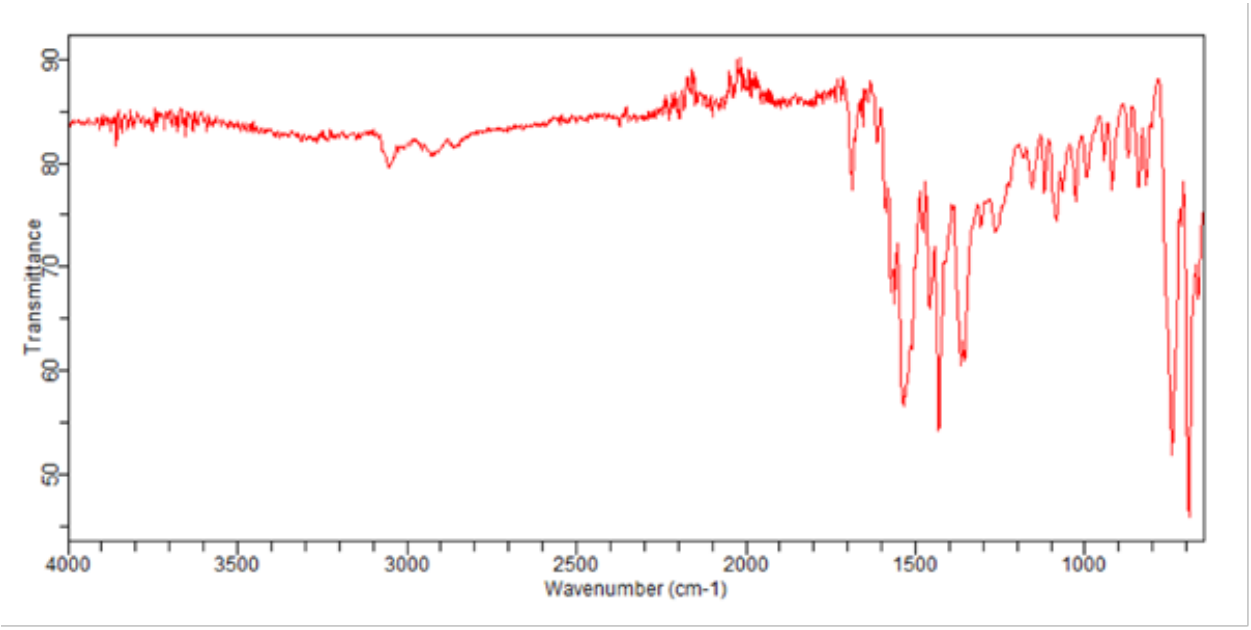

Figure A.18: IR Spectrum of bis chelate iron complex [(^{Ph}PNN)$_2$Fe].

Figure A.16 (below) shows the electronic absorption spectra of toluene solutions of the [(^{Ph}PNN)$_2$Fe] complex. The spectra shows that the absorptions in the UV region 425 nm is due to ligand to metal charge transfer and d-d * transition band of the metal in the complex.

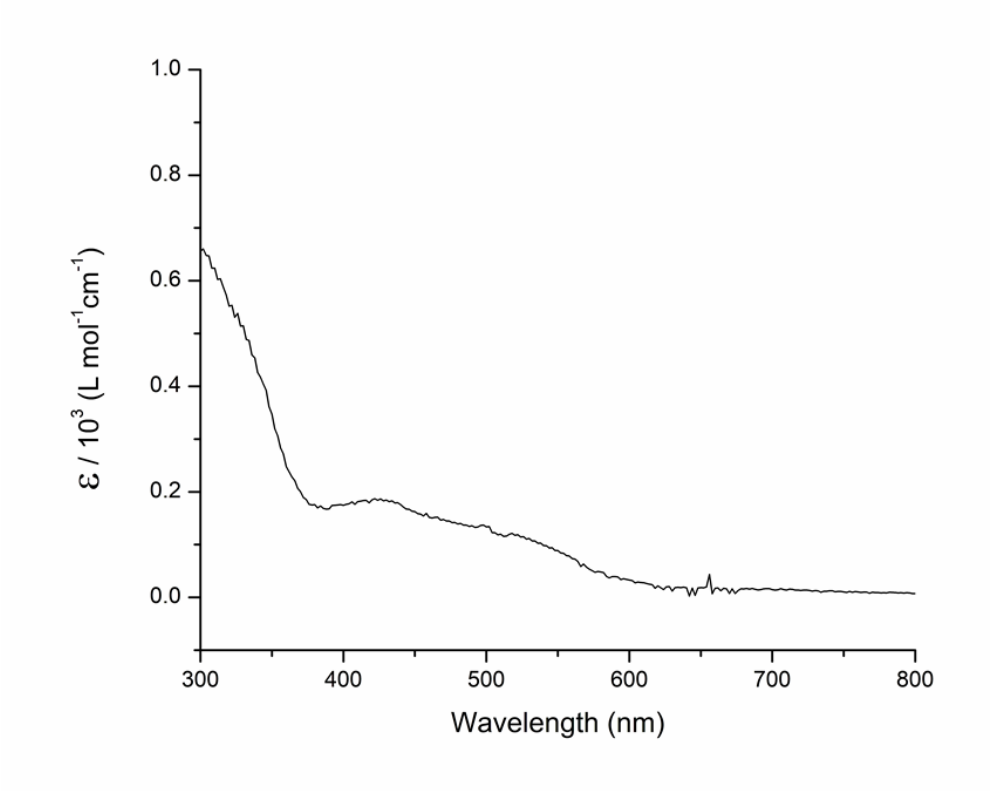

Figure A.16: UV-Vis Analysis of bis-chelated iron complex[(^{Ph}PNN)$_2$Fe].

The complex stability was tested in several solvents: toluene, dichloromethane, tetrahydrofuran, and methanol. After twenty-four hours there were no visible signs of decomposition in any of these solvents.

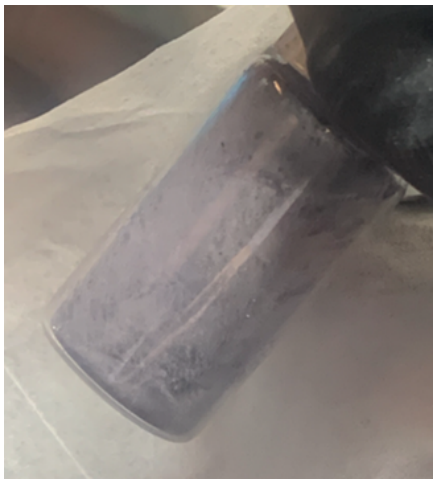

Figure 3.13: Image of crystal product for bis chelated iron complex.

3.4.1.2 Crystal Analysis of Fe Complex

Purple needle crystals of [(^{Ph}PNN)$_2$Fe] grew from toluene solutions of the bulk material layered with pentane. The structure of the complex is shown in Figure 3.14 and bond parameters are given in Table 2. The iron is in a distorted octahedral environment, coordinated by atoms of P1, N1, N2 of one ligand and P2, N3, N4 of the second. Like other examples in the literature, both ^{Ph}PNN ligands are coordinated to the Fe center in a meridional fashion. The *trans* N-Fe-P angles of the pincer ligands are 164.44(4)° for both N2-Fe-P1 and N3-Fe-P2, showing significant distortion from the ideal octahedral geometry. The values observed for average bond distances between Fe-P and Fe-N agree well with the results reported earlier for other iron pincer PNN compounds. The Fe-P distances are 2.23 Å for both Fe-P1 and Fe-P2. The Fe amido distance in *cis* position to the P atom is 1.98 Å for each ligand, and the Fe-N distance in the *para* position to the P atom is 2.05 Å for each ligand.

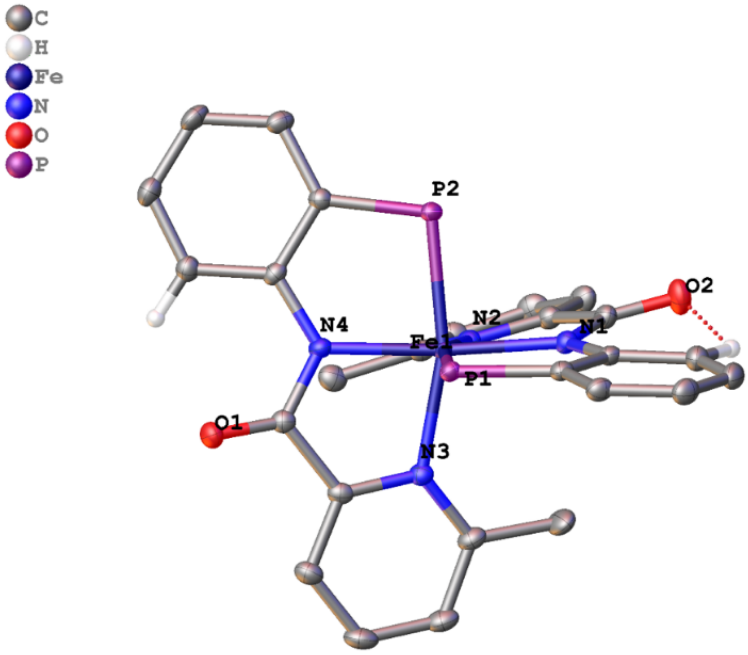

Figure 3.14: Solid-state structure of bis-chelated iron complex. Drawn at 50% thermal ellipsoid probability. Hydrogen atoms not participating in hydrogen bonding are omitted for clarity.

Table 3.2: Selected Bond Lengths (Å) and Angles (deg) for bis-chelated iron complex.

Bond	**Length**
Fe1—N1	1.9874
Fe1—N2	2.0457
Fe1—N3	2.0491
Fe1—N4	1.9830
Fe1—P1	2.2255
Fe1—P2	2.2289
	Angle
N2—Fe1—P1	164.44(4)
N1—Fe1—N4	174.36(7)
N3—Fe1—P2	164.44(4)
N1—Fe1—P1	84.36(5)
N1—Fe1—P2	91.29(5)
N1—Fe1—N3	103.95(6)
N1—Fe1—N2	81.33(7)
N2—Fe1—N3	89.07(7)
N2—Fe1—N4	101.82(7)
N2—Fe1—P2	90.17(5)
N3—Fe1—P1	89.03(5)
N3—Fe1—N4	80.90(6)
N4—Fe1—P1	92.91(5)
N4—Fe1—P2	84.05(5)
P1—Fe1—P2	95.67(2)

3.4.2 Synthesis of Co Complex with $^{Ph}PN^{H}N$ ligand

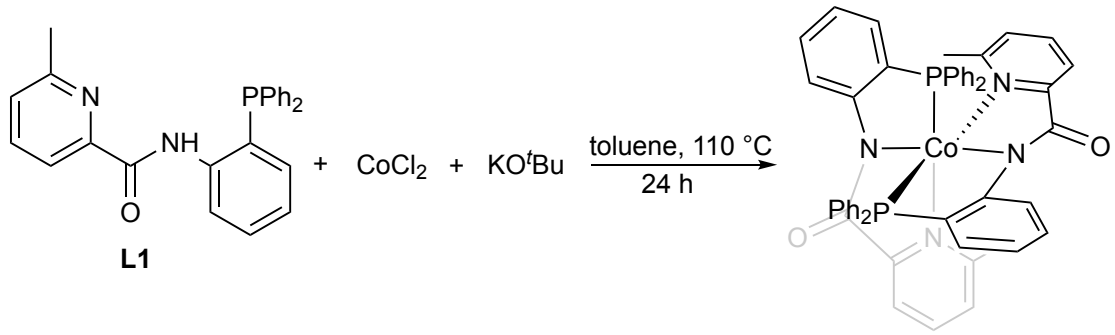

Scheme 3.22: Synthesis of cobalt complex from L1 and cobalt (II) chloride.

L1 ligand coordinates with cobalt (II) in a similar manner as with iron (II). It binds in a 2:1 ratio to Co (II) center and generates a bis-chelate complex [(^{Ph}PNN)$_2$Co]. Optimized crystallization method determined for iron (II) complex was utilized for the cobalt (II) complex and afforded red-brown need crystals with good yields.

3.4.2.1 Characterization of Co Complex of $^{Ph}PN^{H}N$ ligand

Elemental analytical data for the iron complex was consistent with the stoichiometry of [(^{Ph}PNN)$_2$Co] complex. The strong absorption at 3272 cm^{-1} in the IR spectrum of $^{Ph}PN^{H}N$ ligand was gone in the IR spectrum of [(^{Ph}PNN)$_2$Co] complex, indicating a successful deprotonation of amide N-H bond of the ligand (Figure A.22). The [(^{Ph}PNN)$_2$Co] complex is paramagnetic, as evidenced by its ^{1}H NMR spectrum in C_6D_6 solution. The electrospray (ESI) mass spectrum of MeCN solutions of [(^{Ph}PNN)$_2$Co] (Appendix R.3) exhibited a peak envelope at *m/z* 849.1953 assigned to $[C_{50}H_{40}CoN_4O_2P_2]^+$ and an isotope pattern consistent with this formulation.

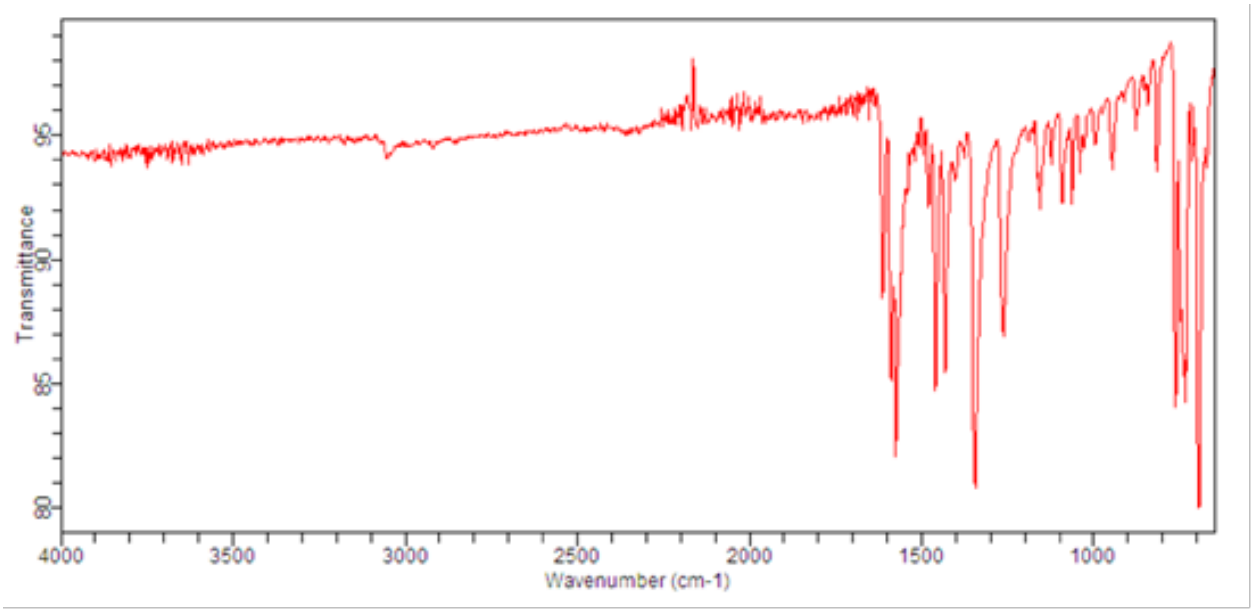

A.22: IR Spectrum of Cobalt (II) Complex

Figure A.19 shows the electronic absorption spectra of toluene solutions of the [(^{Ph}PNN)$_2$Co] complex. The spectra shows that the absorptions in the UV region 418 nm is due to ligand to metal charge transfer and d-d * transition band of the metal in the complex.

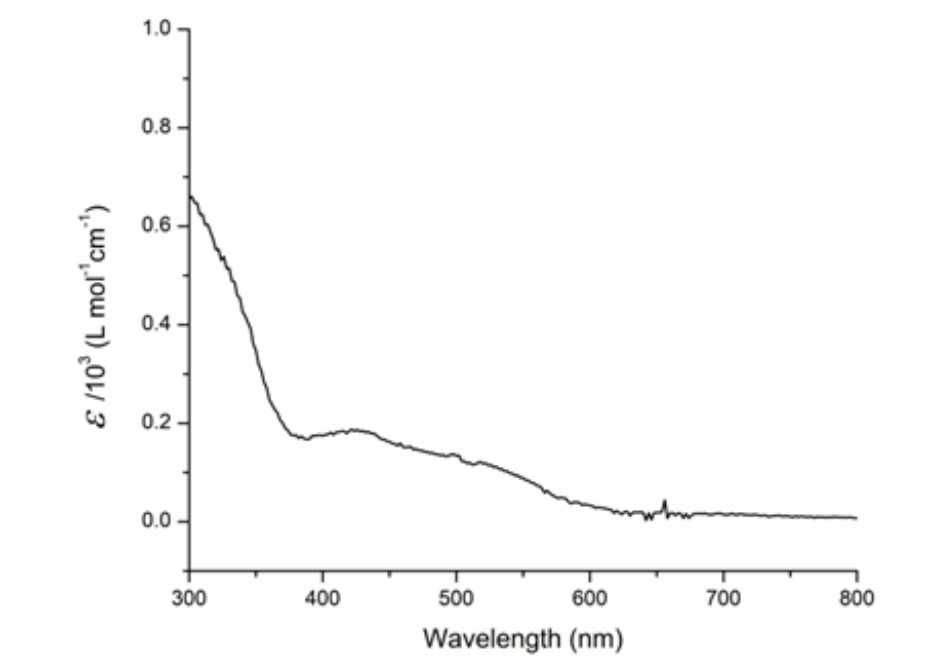

Figure A.19: UV-Vis Spectrum of bis-chelated cobalt complex [(^{Ph}PNN)$_2$Co]

Figure 3.15 Image of crystal product for bis chelated cobalt complex.

3.4.2.2 Crystal structure analysis of [(^{Ph}PNN)$_2$Co] complex with no auxiliary ligand

Red brown needle crystals of [(^{Ph}PNN)$_2$Co] grew from toluene solutions of the bulk material layered with pentane. The structure of the complex is shown in Figure 3.16, and bond parameters are given in Table 3. The cobalt is in a distorted octahedral environment, coordinated by atoms of P1, N3, N4 of one ligand and P2, N1, N2 of the second. Similar

to [(^{Ph}PNN)$_2$Fe], both ^{Ph}PNN ligands are coordinated to the Co center in a meridional fashion. The *trans* N-Co-P angles of the pincer ligands is 164.1(2)° for N3-Co-P1 and 165.0(2)° for N1-Fe-P2, showing significant distortion from the ideal octahedral geometry. The Co-P distances are 2.29 Å for Co-P1 and 2.27 Å for Co-P2. The Co amido distance in *cis* position to the P atom is 1.93 Å for each ligand, and the Co-N distance in the *para* position to the P atom is 2.16 Å for Co-N1 on one ligand and 2.20 for Co-N3 on the other ligand.

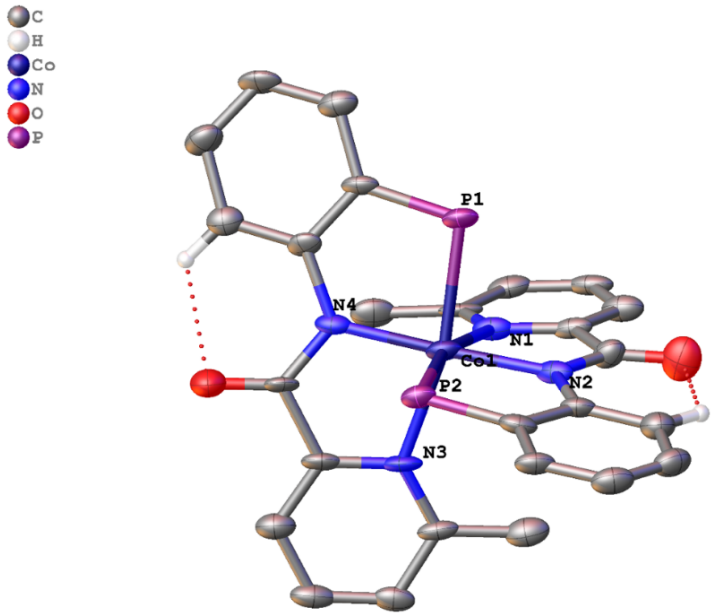

Figure 3.16: Solid-state structure of bis-chelated cobalt complex. Drawn at 50% thermal ellipsoid probability. Hydrogen atoms not participating in hydrogen bonding are omitted for clarity.

Table 3.3: Selected Bond Lengths (Å) and Angles (deg) for bis-chelated cobalt complex.

Bond	Length
Co1—N1	2.159
Co1—N2	1.934
Co1—N3	2.201
Co1—N4	1.935
Co1—P1	2.293
Co1—P2	2.271
	Angles
N1—Co1—P2	165.0(2)
N2—Co1—N4	176.3(3)
N3—Co1—P1	164.1(2)
N2—Co1—P1	91.5(3)
N4—Co1—P1	85.9(2)
P1—Co1—N1	89.6(3)
P1—Co1—P2	98.75(10)
N2—Co1—N1	80.8(3)
N1—Co1—N3	85.6(3)
N1—Co1—N4	101.6(3)
N1—Co1—P1	89.6(3)
N3—Co1—N2	102.7(3)
N2—Co1—P2	86.4(3)
N3—Co1—N4	80.3(3)
N3—Co1—P2	89.4(3)
N4—Co1—P2	91.5(3)

3.4.3 Synthesis of Co complex with $^{Ph}PN^{H}N$ complex and an auxiliary ligand

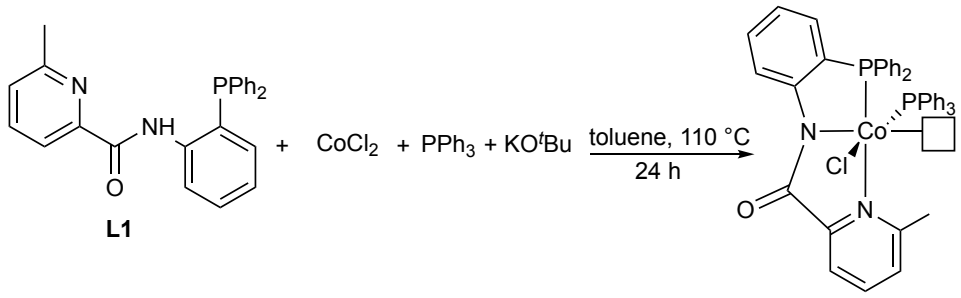

Scheme 3.23: Synthesis of cobalt complex from L1, cobalt (II) chloride, and triphenylphosphine.

In an attempt to prevent the formation of a bis-chelated complex, an auxiliary ligand PPh_3 was added to the reaction of $CoCl_2$ and L1. The goal of this strategy was to prevent the binding of a second equivalence of L1 and ensure an open site on the metal center for substrate binding. However, through single crystal X-ray analysis it is observed that L1 will out-compete the auxiliary ligand for binding and continue to form the bis-chelated cobalt (II) [(^{Ph}PNN)$_2$Co].

3.4.4 Synthesis of Co complex [(^{Ph}PNN)$_2$Co(PPh$_3$)$_3$] with ^{Ph}PN^{H}N and Co (I)

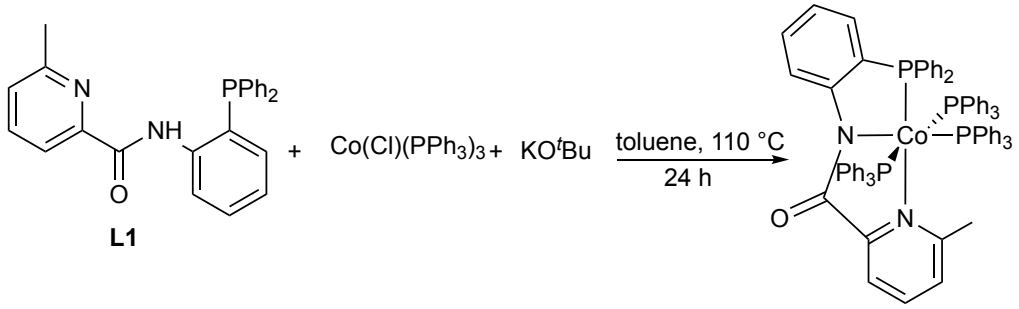

Scheme 3.24: Synthesis of cobalt complex from L1 and cobalt (I) triphenylphosphine chloride.

In a second attempt to prevent the formation of the bis-chelated complex, chlorotris(triphenylphosphine) cobalt (I) compound was allowed to react with L1 in the presence of KO^{t}Bu in toluene at 110 °C for 24 hours. No desired product was isolated.

3.4.5 Steric Influence on Mono- and Bis-Chelated Complex Formation: Role of R Group and X Ligand

It appeared that the formation of mono- and bis-chelated complexes is influenced by both the steric bulk of the R group on the PNN ligand and the choice of X ligand. Milstein et al. observed that a PNN ligand with a Ph substituent consistently formed bis-chelated complexes regardless of the reaction conditions or the X ligand used (X = Cl, Br).

However, when the ligand had an iPr group, it could yield either the mono- or bis-chelated complex, depending on the molar ratio of the iron salt to the PNN ligand. On the other hand, the ligand with a tBu group exclusively provided the mono-chelated complex. While a comprehensive steric analysis of pincer ligands is still being investigated, it is worth noting that the values of Tolman's cone angle (θ°) for the mono-dentate phosphine, PR_3 (R = Ph, iPr, tBu), increase in the order Ph (145) < iPr (160) < tBu (182). Also, in previous reports by Kamitani group and the Rauchfuss group, it was observed that PNN ligands with increased steric bulk tend to form mono-chelated complexes. These findings indicate that a higher steric bulk on the ligand can hinder the formation of sterically crowded bis-chelated structure. Furthermore, formation of a bis-chelated organometallic complex could pose challenges for substrate compatibility in a catalytic cyclic and hinder the organometallic complexes ability to possess characteristics of catalysis. In forming the mono-chelated organometallic complex we may observe the difference in the two complexes ability to perform in the proposed features of catalysis.[28], [29], [30], [31]

3.5 Catalysis

A catalytic study is to be conducted on the existing complexes, [($^{Ph}PN^{H}N)_2Fe$] and [($^{Ph}PN^{H}N)_2Co$], to determine if they show catalytic activities for dehydrogenation of alcohols. The complexes will also be tested against synthesis between primary alcohols with primary and secondary amines, in addition to esters with primary and secondary amines as seen in Figure 3.17 below.

A catalytic study will provide insight on the effects of the mono- vs bis- chelated structure regarding substrate compatibly.

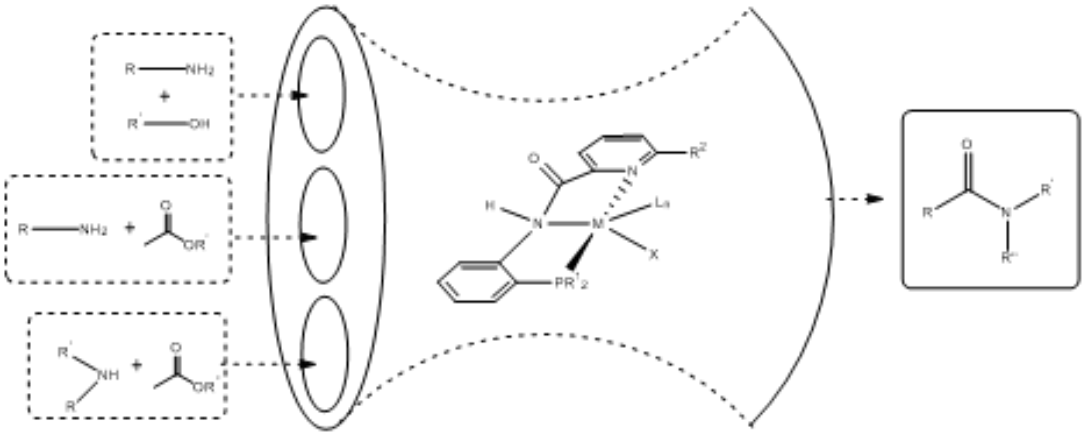

Figure 3.17: Proposed substrate reactions to conduct catalytic study on new organometallic complexes for amide synthesis.

CHAPTER IV

CONCLUSIONS

In summary, a new PNN pincer ligand, $^{Ph}PN^{H}N$, was successfully synthesized and purified through the optimization and design of synthetic and purification techniques of flash column chromatography and crystallization. The $^{Ph}PN^{H}N$ ligand was then successfully coordinated to two types of base transition metals, Fe (II) and Co (II), to form two new organometallic complexes [$(^{Ph}PNN)_2Fe$] and [$(^{Ph}PNN)_2Co$].

The new organometallic complex with serve as a catalyst for the formation of amide bonds through and dehydrogenative coupling reaction between primary alcohols and amines. The utilization of this mechanistic route coupled with the use of environmentally benign substrates with serve to replace the currently used methods of heavy metal catalysis, peptide coupling and the DCC/HOBT method which possess challenges in regard to environmental safety and sustainability.

Future study should optimize the synthesis and purification methods for the $^{iPr}PN^{H}N$ ligand to investigate the change in the organometallic complex's modes of MLC due to the change in ligand structure.

REFERENCES

[1] Bode, J. W.; Pattabiraman, V. R. Rethinking amide bond synthesis. *Nature*. **2011**. 480, 471-479.

[2] Seavill, P. W.; Wilden, J. D.; *Green Chemistry* **2020**, 22.

[3] Guo, F.; Liu, K.; Liu, W.; Xie, J. Enantioselective effects of chiral amide herbicides napropamide, acetochlor and propisochlor: The more efficient R-enantiomer and its environmental friendly. *Science of The Total Environment.* **2018.** *626*, 860-866.

[4] Falque, V.; Montalbetti, C. A. G. N. Amide Bond Formation and Peptide Coupling. *Tetrahedron.* **2005.** *61,* 10827-10852.

[5] Abo-Elenien, O. M.; Zohdy, K. M. Synthesis and Characterization of New Poly (Urethane Amide) Composites From L-Ascorbic Acid as Protective Materials for Petroleum Equipment. *The International Conference on Chemical and Environmental Engineering.* **2012**. 1-18.

[6] Shi, S.; Szostak, M. Pd-PEPPSI: a general Pd-NHC precatalyst for Buchwald-Hartwig cross-coupling of esters and amides (transamidation) under the same reaction conditions. *Chemical Communications.* **2017**. *53*, 10584-10587.

[7] Ullmann, H. F. Goldberg, I. Uber Phenylirungen bei Gegenwart von Kupfer als Katalysator. *Berichte der Deutschen Chemischen Gesellschaft.* **1906**. *39*, 2691-1692.

[8] Gunanathan, C.; Ben-David, Y.; Milstein, D. Direct Synthesis of Amides from Alcohols and Amines with Liberation of H_2. *Science.* **2007**, *317*, 790–792.

[9] Stahl, S. S.; Zhao, J.; Zultanski, S. L. Practical Synthesis of Amides via Copper/ABNO-Catalyzed Aerobic Oxidative Coupling of Alcohols and Amines. *Journal of American Chemical Society.* **2016.** *138,* 6416-6419.

[10] Bernskoetter, W. H.; Hazari, N.; Lane, E. M.; Uttley, K. B. Iron-Catalyzed Amide Formation from the Dehydrogenative Coupling of Alcohols and Secondary Amines. *Organometallics.* **2017**. *36*, 2020-2025.

[11] Bernskoetter, W. H.; Hazari, N.; Lane, E. M. Iron-Catalyzed Urea Synthesis; Dehydrogenative Coupling of Methanol and Amines. *Chemical Science.* **2018**. *9*, 4003-4008.

[12] Beller, M.; Neumann, H.; Pena-Lopez, M. Iron (II) Pincer-Catalyzed Synthesis of Lactones and Lactams Through a Versatile Dehydrogenative Domino Sequence. *ChemCatChem.* **2015**. *7*, 865-871.

[13] Avram, L.; Diskin-Posner, Y.; Espinosa-Jalapa, N.; Kumar, A.; Leitus, G.; Milstein, D. Direct Synthesis of Amide by Dehydrogenative Coupling of Amines with Either Alcohols or Esters; Managanese Pincer Complex as Catalyst. *Angewandte Chemie International Edition.* **2017**. *56*, 14992-14996.

[14] Avram, L.; Chakraborty, S.; Diskin-Posner, Y.; Gellrich, U.; Leitus, G.; Milstein, D. Manganese-Catalyzed N-Formylation of Amines by Methanol Liberating H_2: A Catalytic and Mechanistic Study. *Angewandte Chemie International Edition.* **2017.** *56,* 4229-4233.

[15] Green, K.; Lawrence, M. A. W.; Lorraine, S. C.; Nelson, P. N. Review: Pincer ligands – Tunable, Versatile, and Applicable. *Polyhedron*. **2018.** *143*, 11-27.

[16] Sheldrick, G. M. Crystal structure refinement with SHELXL. *Acta Crystallographica*. **2015**. *C71*, 3–8.

[17] Dolomanov, O. V.; Bourhis, L. J.; Gildea, R. J.; Howard, J.A.K.; Puschmann, H. Olex2: A complete structure solution, refinement, and analysis program. *Journal of Applied Crystallography*. **2009**. *42*, 339-341.

[18] Beller, M.; Das, S.; Junge, K.; Li, Y.; Lu, L.; Pisiewicz, S. Highly Chemoselective Metal-Free Reduction of Phosphine Oxides to Phosphines. *Journal of the American Chemical Society.* **2012**. *134*, 18325 – 18329.

[19] Holland, A. W.; Nguyen, M.; Platt, Z. H.; Seipel, K. R. Microwave-Assisted Synthesis of Phenylene-Bridges Aminophosphine Ligands: Acceleration of N-Arylation and Aryl Fluoride Phosphorylation Reactions. *Journal of Organic Chemistry.* **2008**. *73*, 4291 – 4294.

[20] Feng, Y.; Li, Y.; Li, Y.; Lu. L; Song, L.; Suo, F.; Wang, K. Synthesis and Biological Evaluation of Vanadium Complexes as Novel Anti-Tumor Agents. *European Journal of Medicinal Chemistry.* **2019.** *176*, 1 – 10.

[21] Beller, M.; Das, S.; Junge, K.; Li, Y.; Zhou, S. General and Selective Copper-Catalyzed Reduction of Tertiary and Secondary Phosphine Oxides: Convenient Synthesis of Phosphines. *Journal of the American Chemical Society.* **2012**. *134*, 9727 – 9732.

[22] Echavarren, A. M.; Franchino, A.; Martí, À.; Nejrotti, S. Silver-Free Au(I) Catalysis Enabled by Bifunctional Urea- and Squaramide-Phosphine Ligands via H-Bonding. *Chemistry – A European Journal.* **2021.** *27*, 11989 – 11996.

[23] Cai, C.; Chen, J.; Ding, Y.; Liu, B.; Liu, H.; Xia, Y. Cobalt-Catalyzed *E*-Selective Isomerization of Alkene with A phosphine-Amido-Oxazoline Ligand. *ACS Omega.* **2020.** *5*, 11655 – 11670.

[24] Wolter. M; Klapars, A.; Buchwald, S. L. Synthesis of N-Aryl Hydrazides by Copper-Catalyzed Coupling od Hydrazides with Aryl Iodides. *Organic Letters.* **2001**. *3*, 23, 3803-3805.

[25] Gelman, D.; Jiang, L.; Buchwald, S. L. Copper-Catalyzed C—P Bond Conctruction via Direct Coupling of Secondary Phosphines and Phosphites with Aryl and Vinyl Halides. *Organic Letters*. **2003**. *5*, 2315-2318.

[26] Yadav, S.; Vijayan, P.; Yadav, S.; Gupta, R. Ruthenium Complexes of Phosphine-Amide Based Ligands as Efficient Catalysts for Transfer Hydrogenation Reactions. *Dalton Transactions*. **2021**. *50*, 3269 – 3279.

[27] Steinke, T.; Shaw, B. K.; Jong, H.; Patrick, B. O.; Fryzuk, M. D. Synthesis and Coordination Chemistry of a Tridentate *o*-Phenylene-Bridges Disphosphine – NHC System. *Organometallics.* **2009.** *28*, 2830 – 2836.

[28] T. Zell, R. Langer, M. A. Iron, L. Konstantinovski, L. J. W. Shimon, Y. Diskin-Posner, G. Leitus, E. Balaraman, Y. BenDavid and D. Milstein. Synthesis, structures, and dearomatization by deprotonation of iron complexes featuring bipyridine-based PNN Pincer ligands. *Inorganic Chemistry.* **2013**, *52*, 9636–9649.

[29] C. A. Tolman. Electron donor-acceptor properties of phosphorus ligands. Substituent additivity *Journal of the American Chemical Society* **1970**, *92*, 2956–2965.

[30] M., Kamitani. Chemically robust and readily available quinoline-based PNN iron complexes: application in C-H borylation of arenes**.** *Chemical Communications.*, **2021**, *57*, 13246.

[31] R. Gilbert-Wilson, W.-Y. Chu, T. B. Rauchfuss. Phosphine-iminopyridines as platforms for catalytic hydrofunctionalization of alkenes. *Inorganic Chemistry.* **2015**, *54*, 5596–5603.

APPENDIX

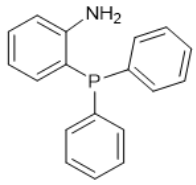

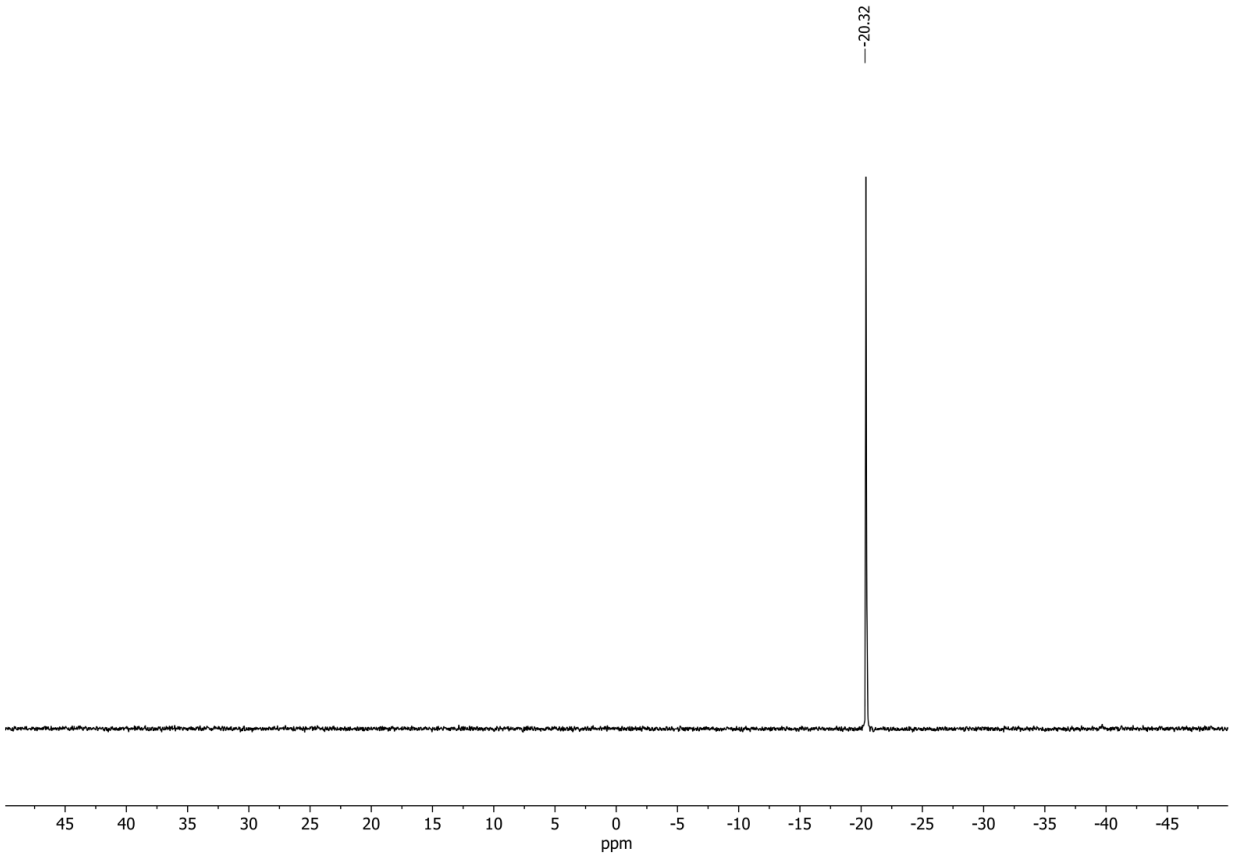

Figure A.1: ^{31}P NMR ($CDCl_3$, 500 MHz) of product 2-(diiphenylphosphino)aniline.

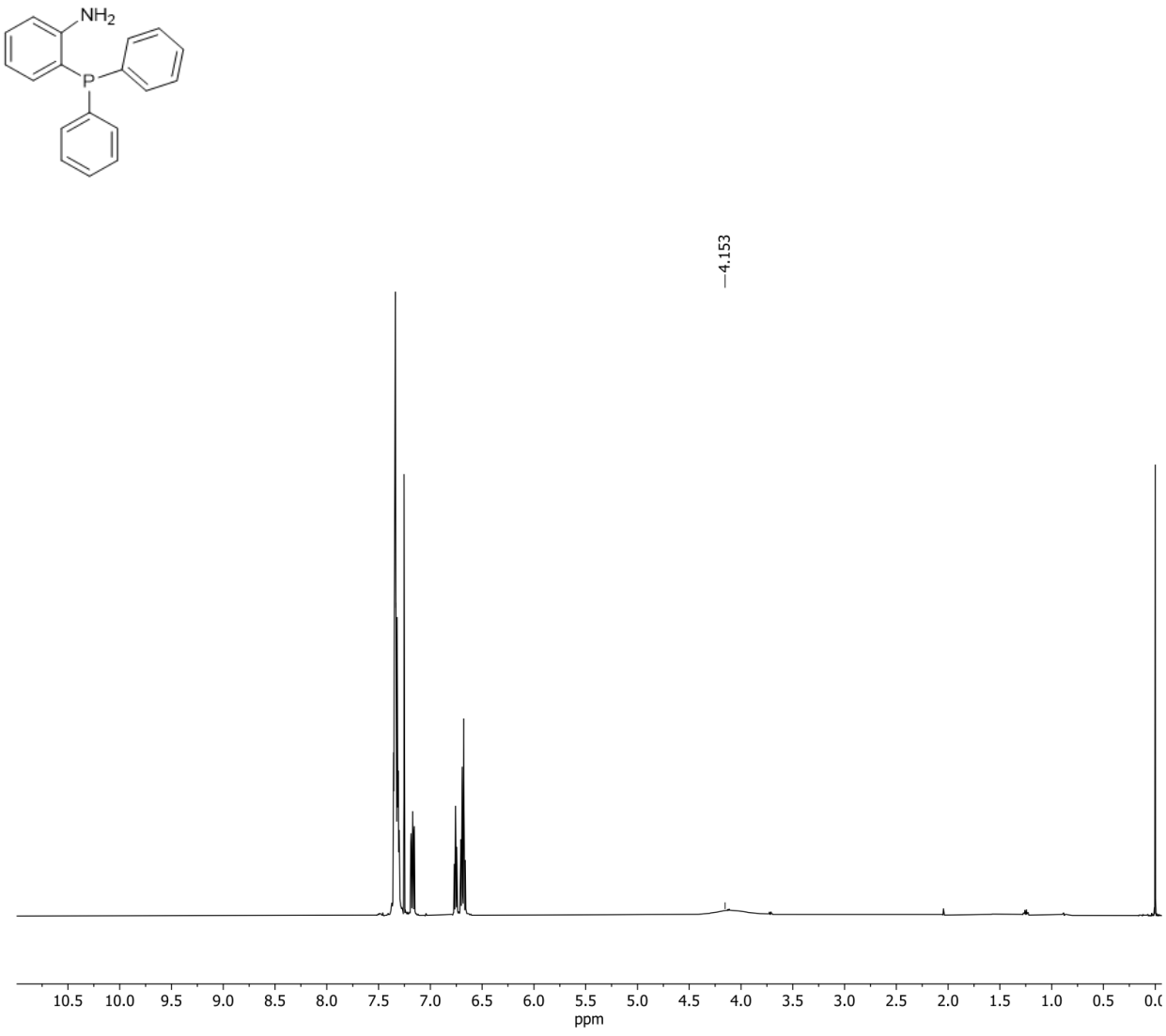

Figure A.2: ^{1}H NMR ($CDCl_3$, 500 MHz) of product 2-(diiphenylphosphino)aniline.

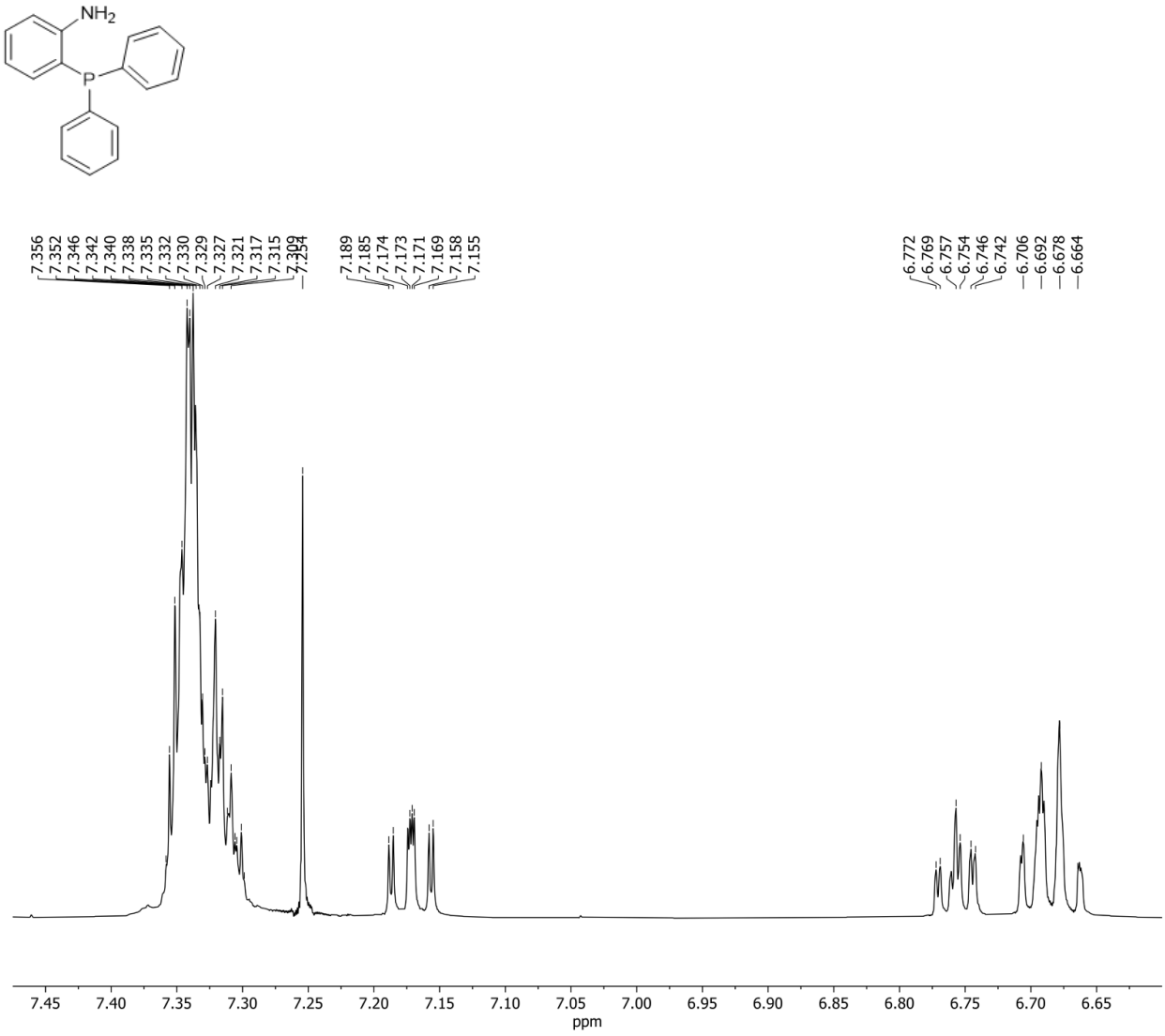

Figure A.3: ^{1}H NMR ($CDCl_3$, 500 MHz) of product 2-(diiphenylphosphino)aniline.

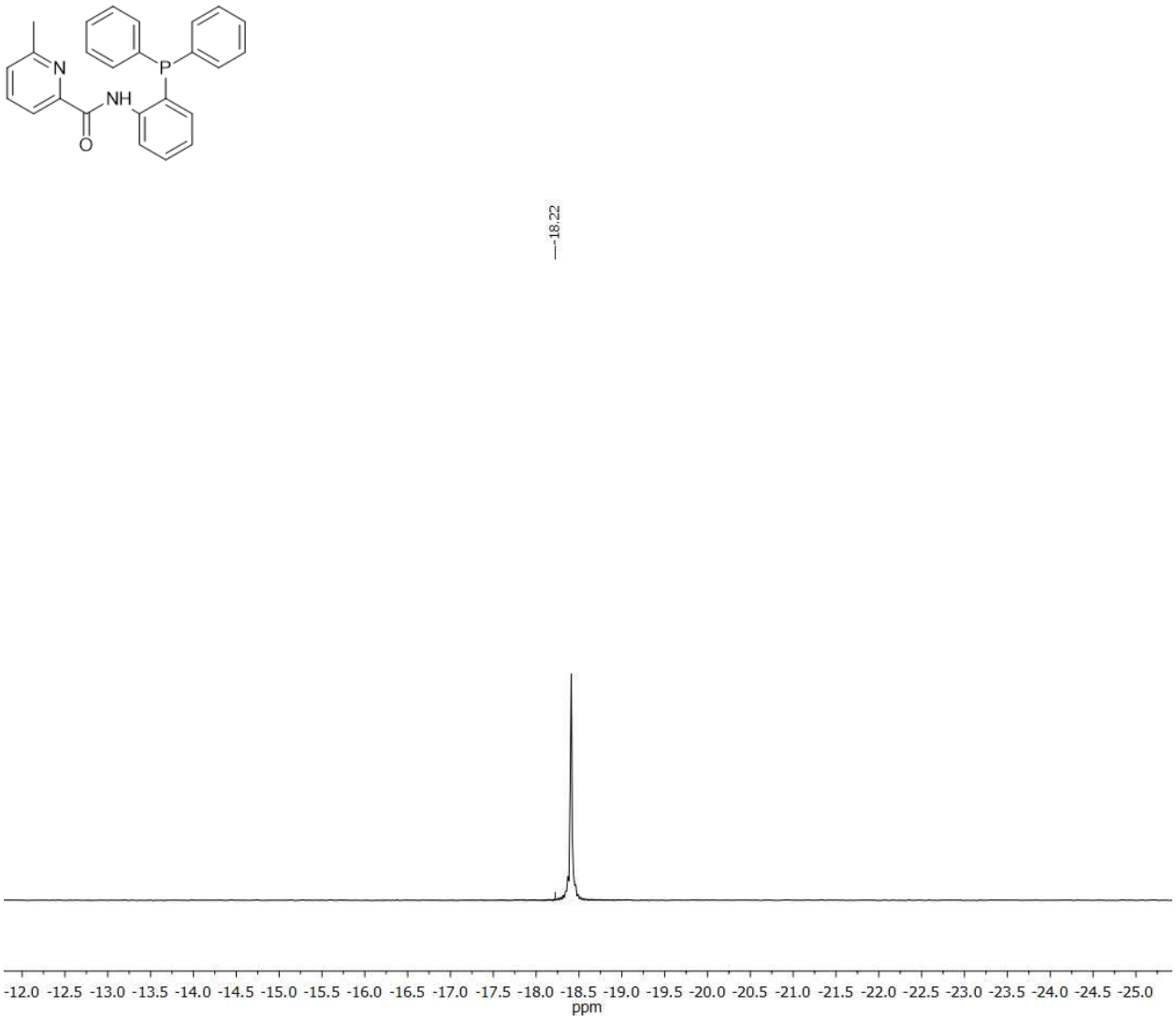

Figure A.4: ^{31}P NMR ($CDCl_3$, 500 MHz) of product L1

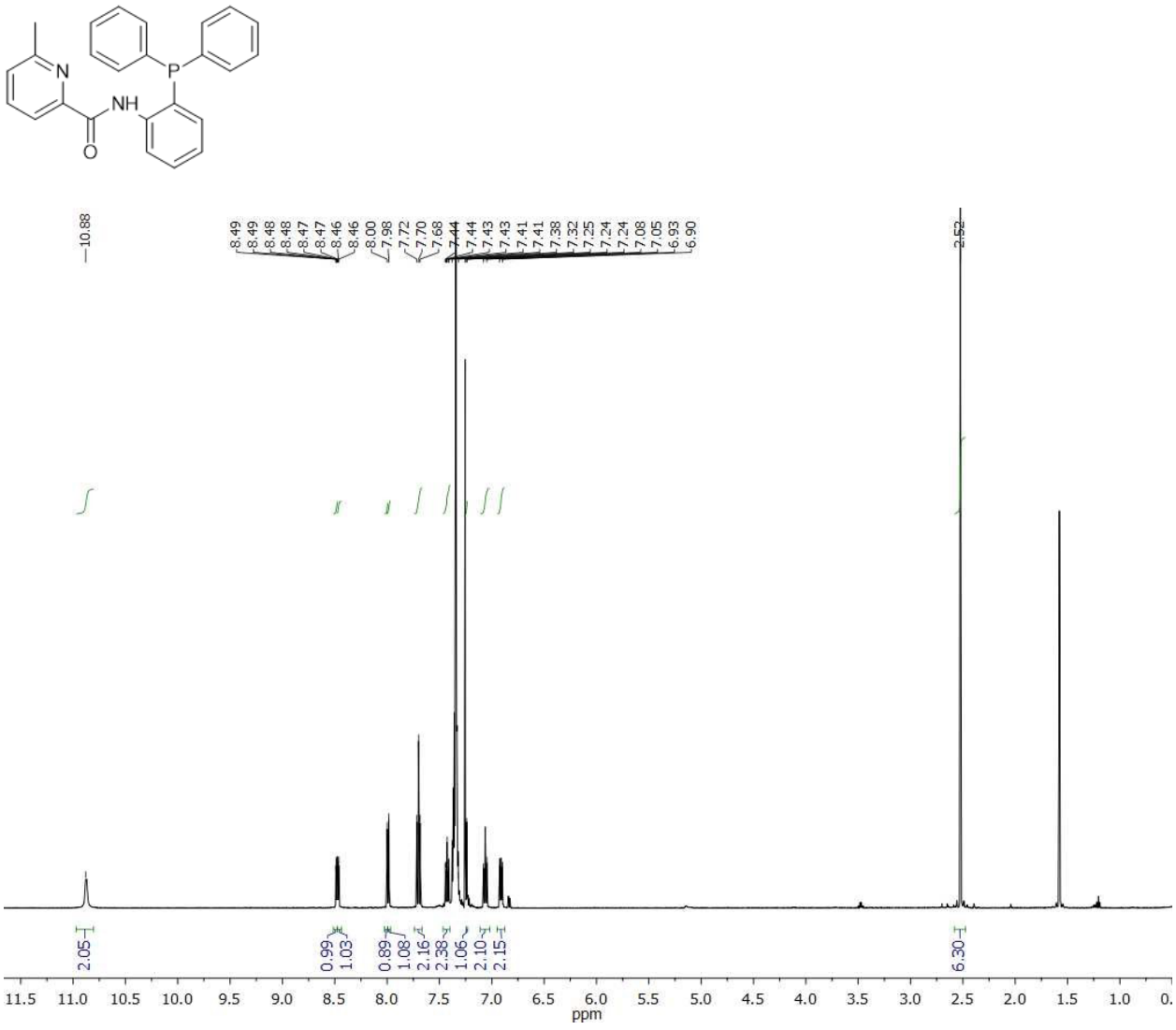

Figure A.5: ^{1}H NMR ($CDCl_3$, 500 MHz) of product L1.

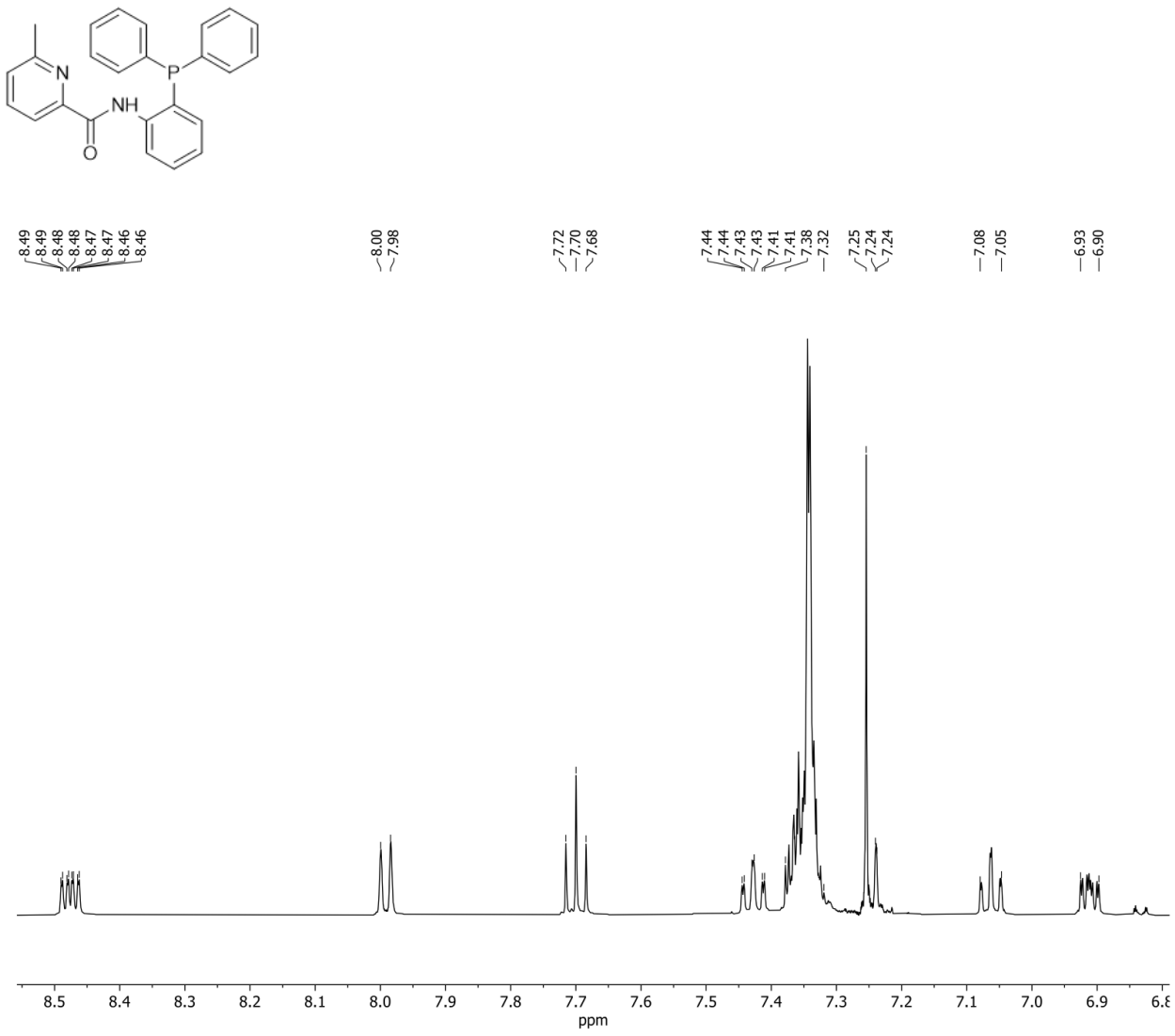

Figure A.6: ^{1}H NMR ($CDCl_3$, 500 MHz) of product L1.

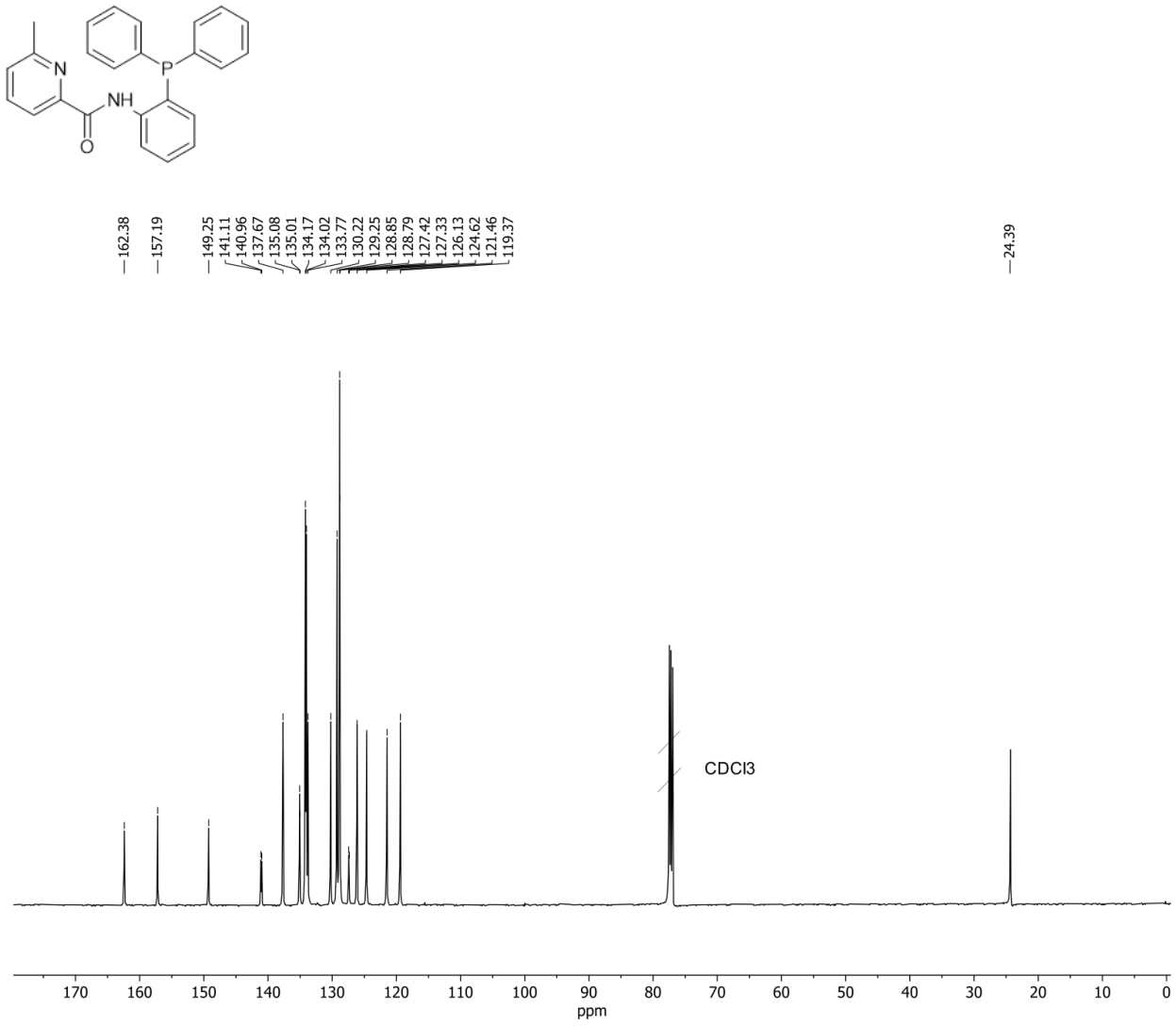

Figure A.7: ^{13}C NMR ($CDCl_3$, 500 MHz) of product L1.

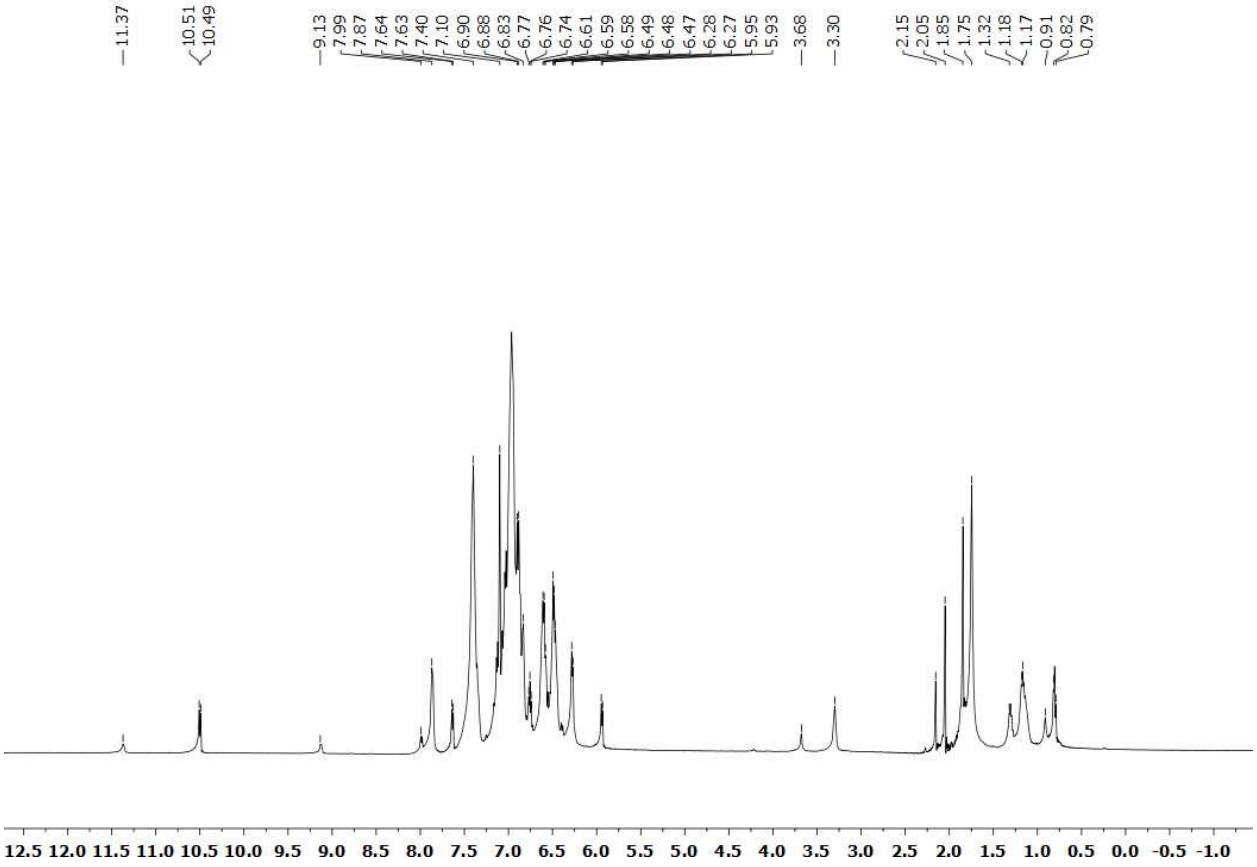

Figure A.8: ^{1}H NMR (C_6D_6, 500 MHz) of bis chelate iron complex [(^{Ph}PNN)$_2$Fe].

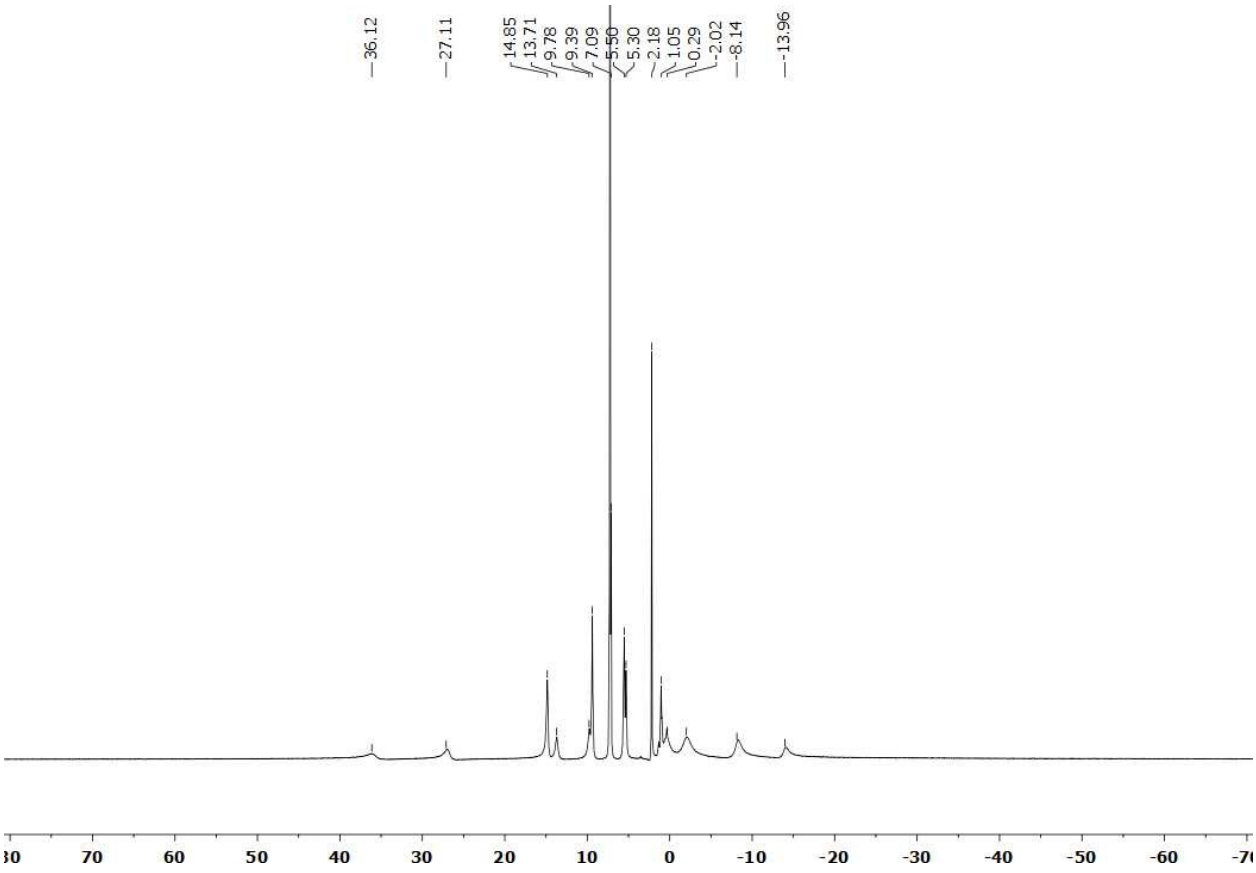

Figure A.9: ^{1}H NMR (_) of cobalt complex.

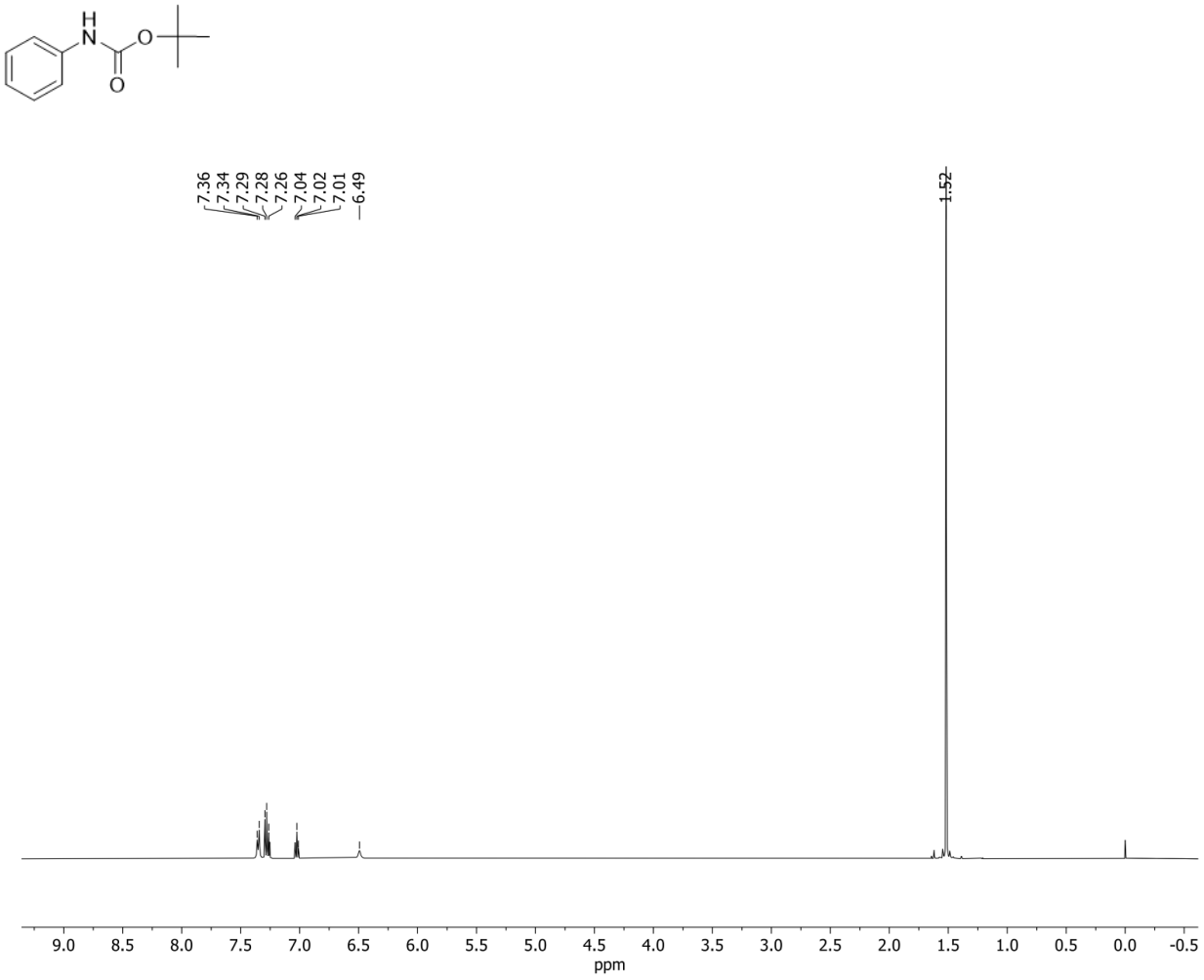

Figure A.10: ^{1}H NMR ($CDCl_3$, 500 MHz) of product *t*-BOC-aniline.

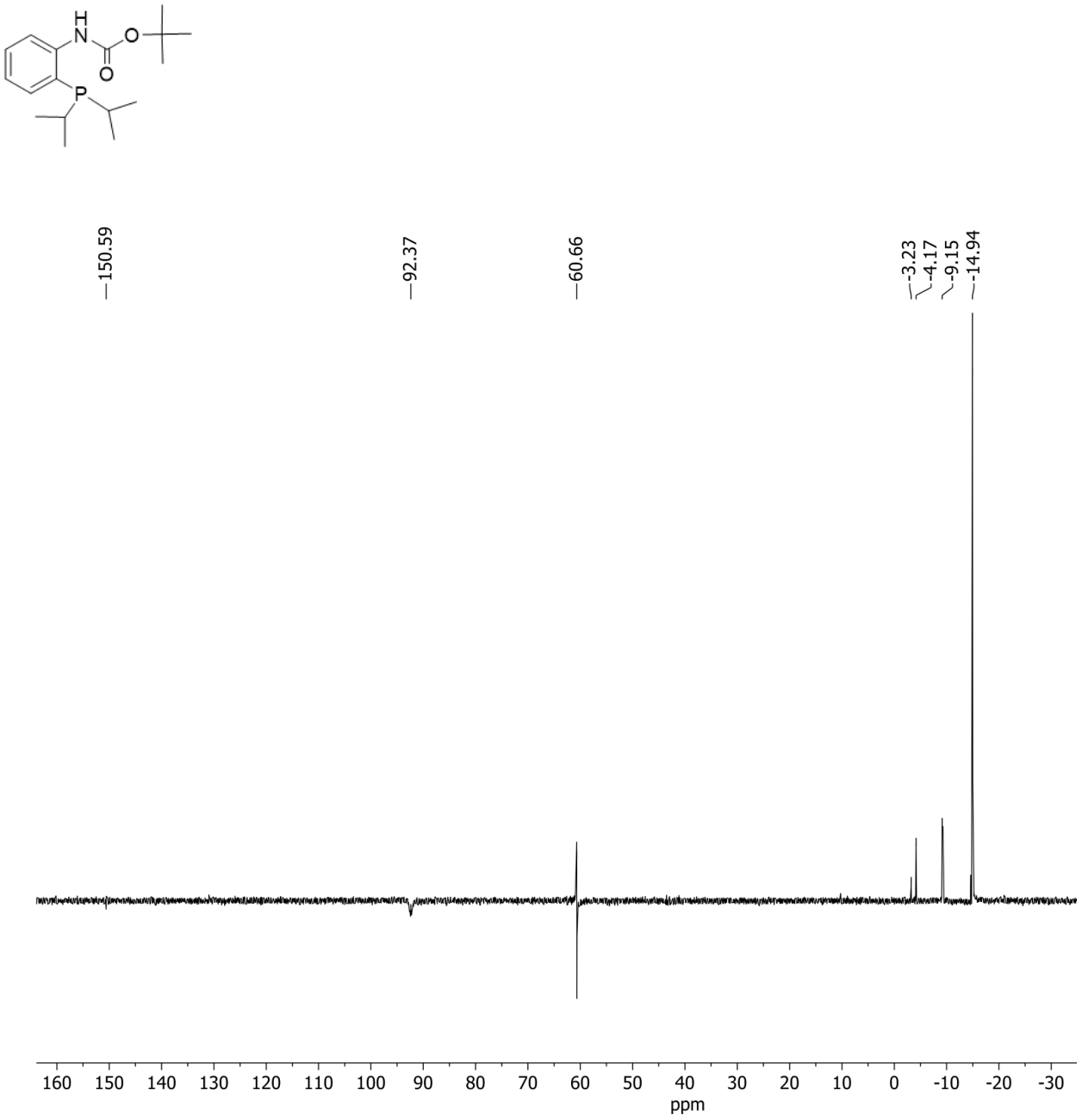

Figure A.11: ^{31}P NMR (CDCl3, 500 MHz) of *o*-C_6H_4(NH*t*-BOC)(P^{i}Pr$_2$). Product found at -14.94 ppm. Reported impurities from literature [8] found at -9.15 ppm, -4.14 ppm, and 92.37 ppm. Other impurities included in spectrum at -3.23 ppm, 60.66 ppm, and 150.59 ppm.

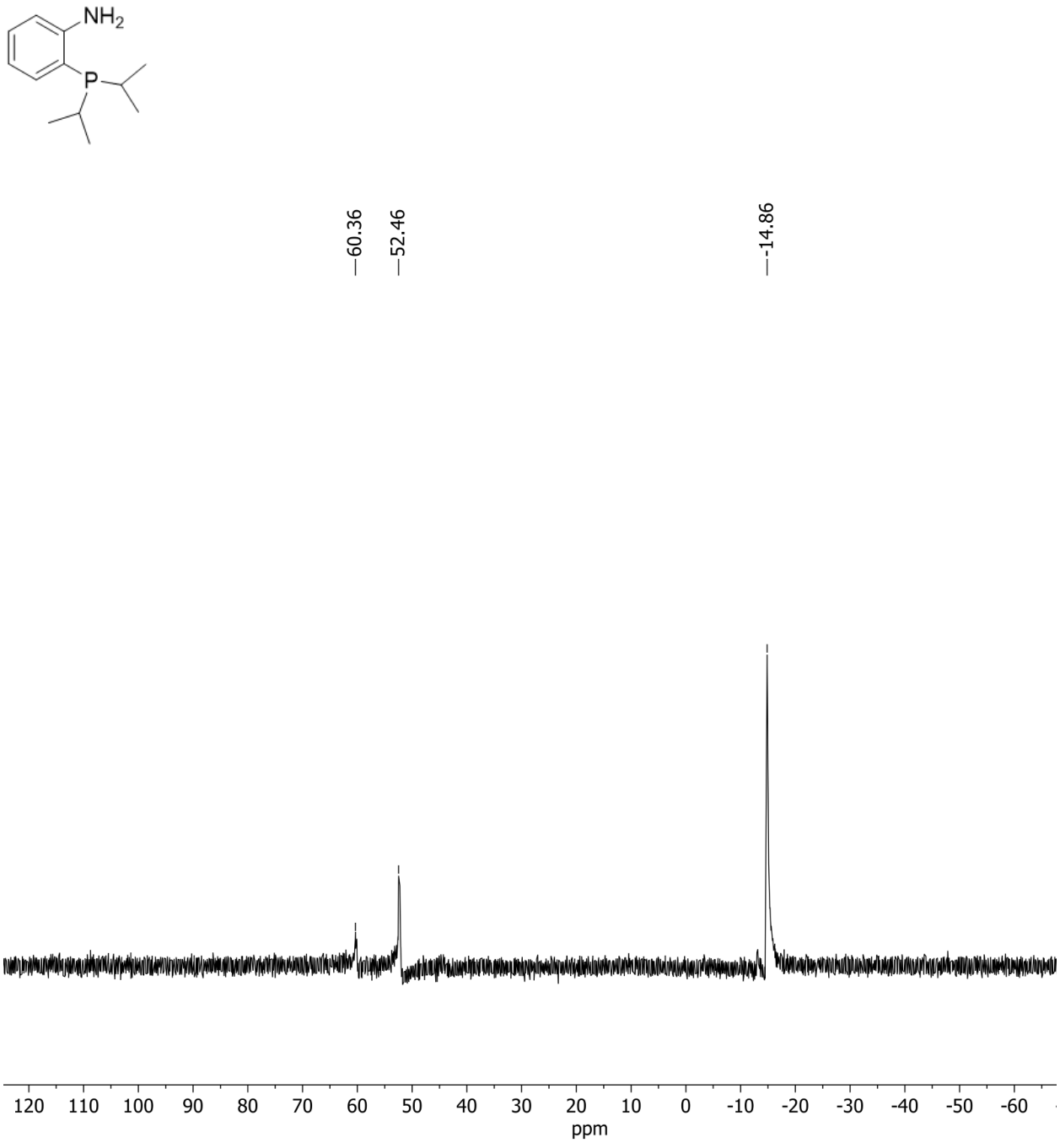

Figure A.12: ^{31}P NMR (CDCl3, 500 MHz) of *o*-$C_6H_4(NH_2)(P^iPr_2)$. Product found at -14.86 ppm. Reported impurity from literature [8] found at 52.46 ppm. Additional impurity not reported in literature found at 60.36 ppm.

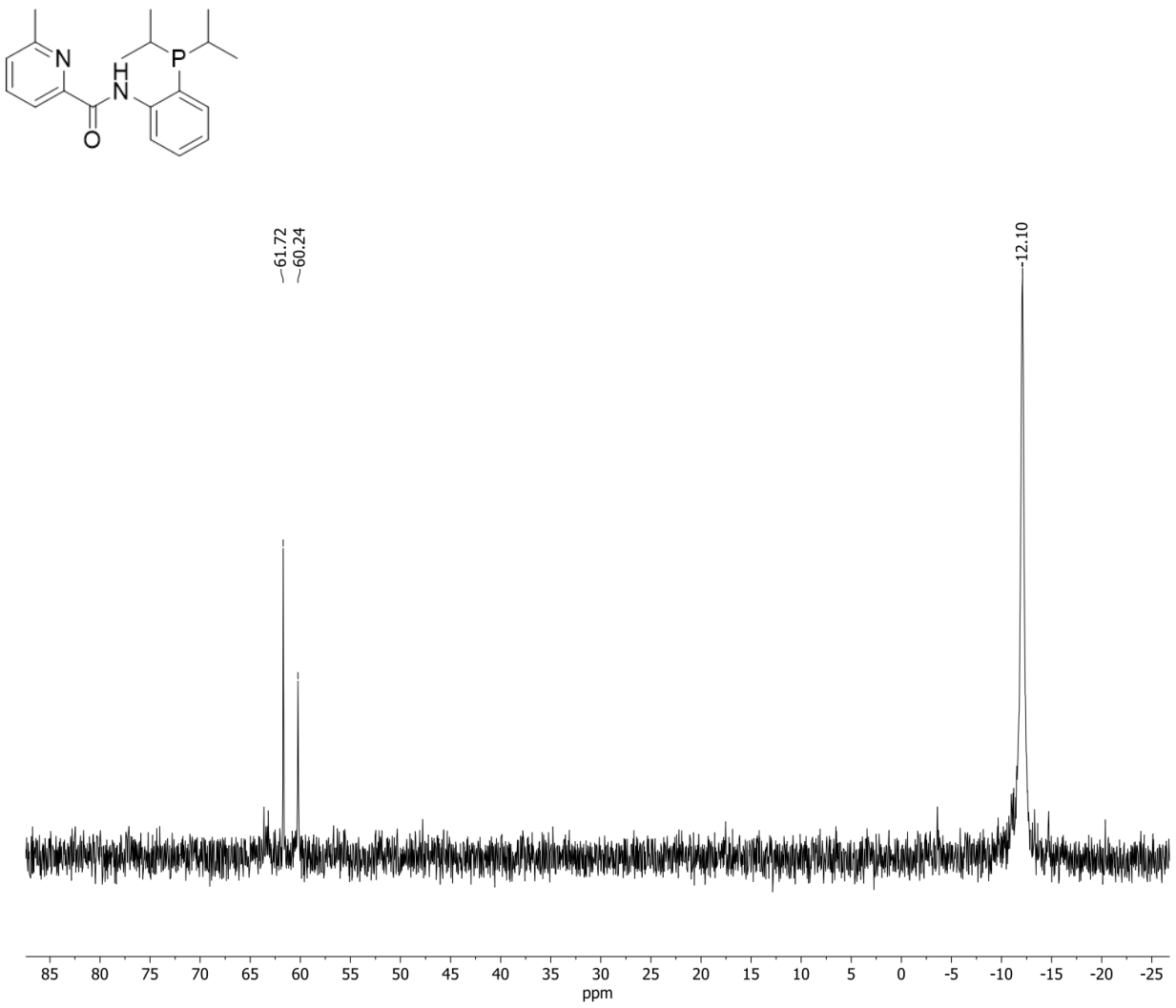

Figure A.13: ^{31}P NMR (CDCl3, 500 MHz) of L2.

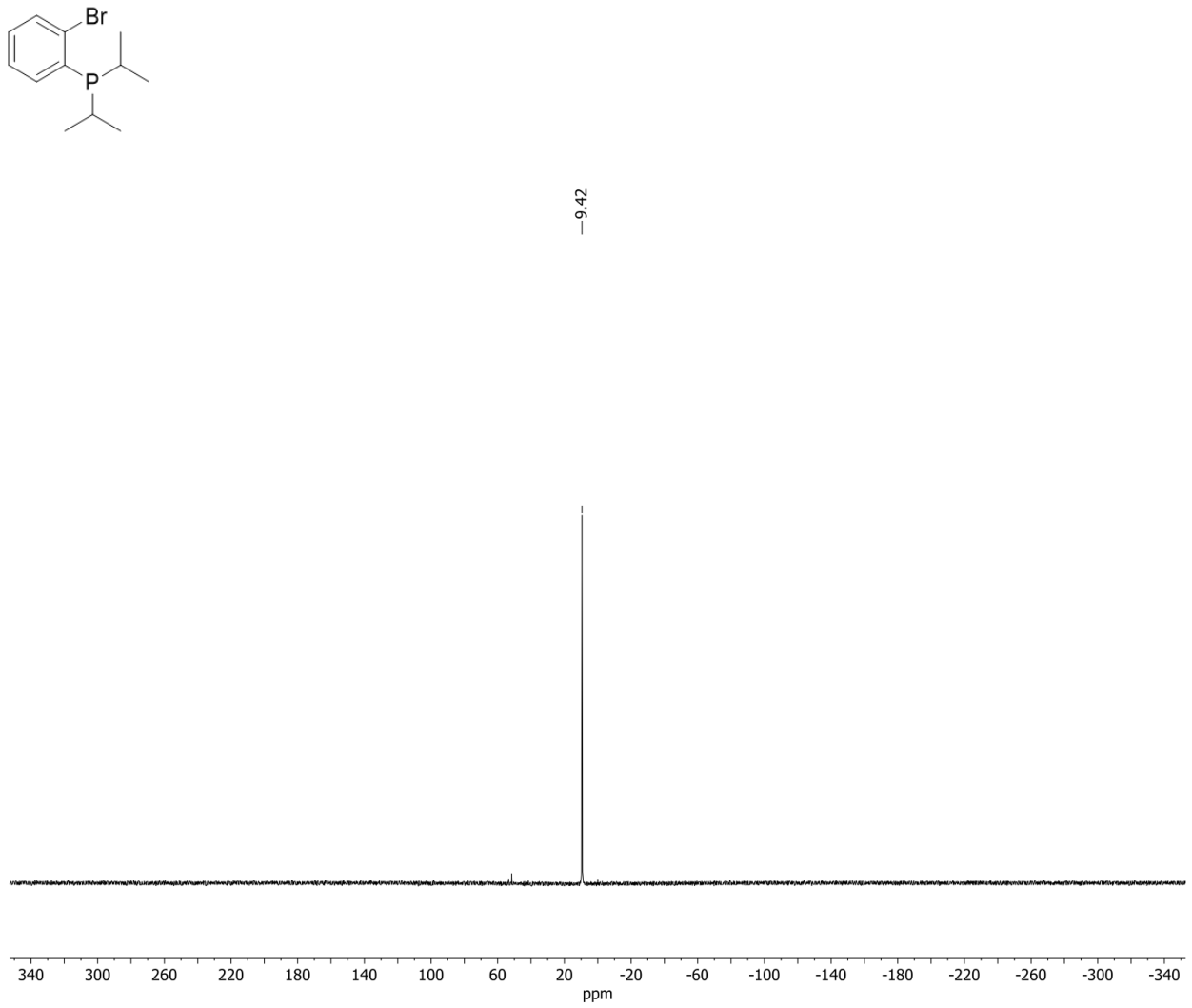

Figure A.14: ^{31}P NMR ($CDCl_3$, 500 MHz) of reaction product from method L2-2A. Peak corresponds with that of reagent 1-bromo-2-diisopropylphosphinobenzene.

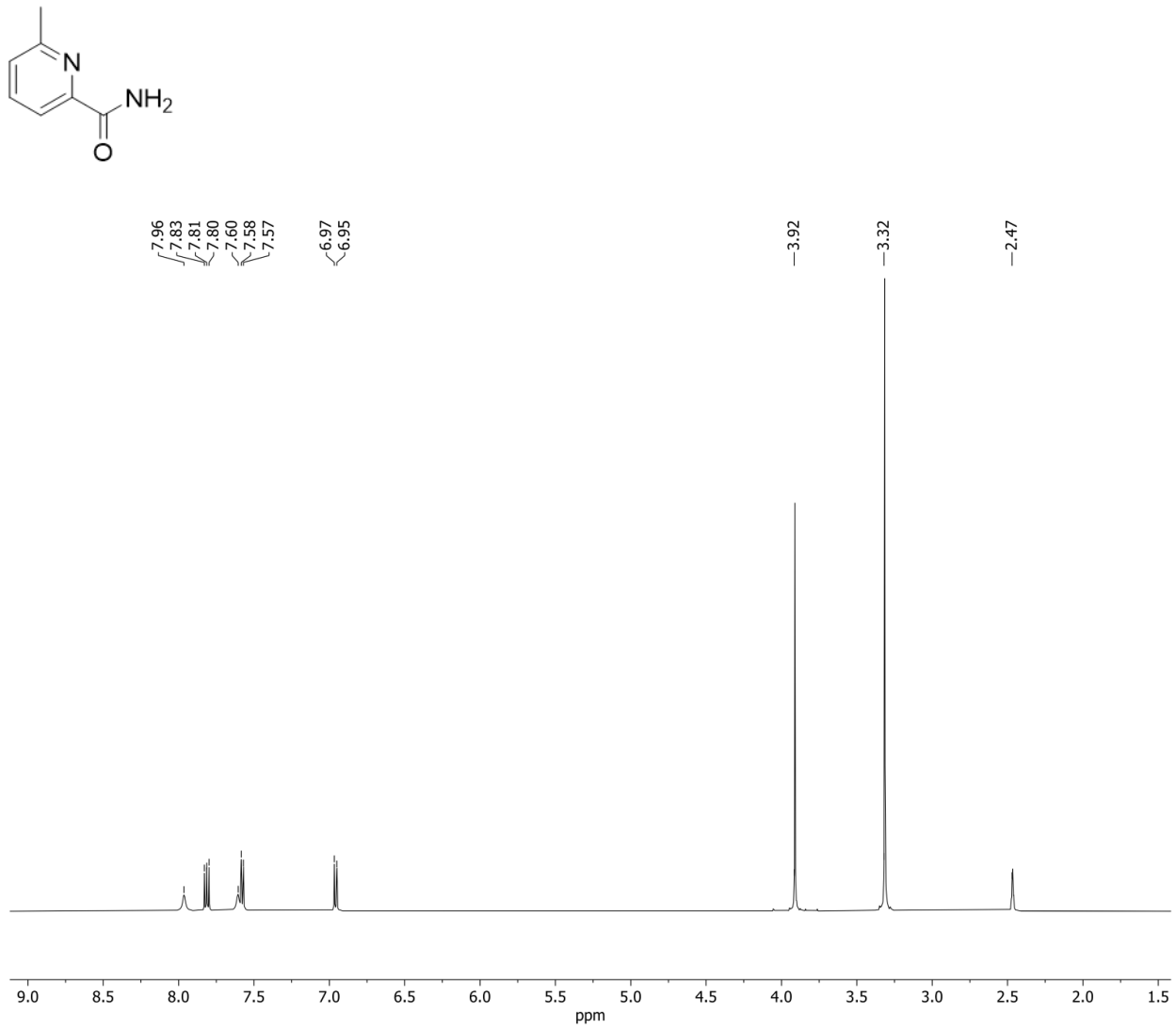

Figure A.15: ^{1}H NMR (DMSO, 500 MHz) of 6-methylpyridinecarboxamide.

Figure A.16: ^{31}P NMR ($CDCl_3$, 500 MHz) of 1-bromo-2-diisopropylphosphinobenzene.

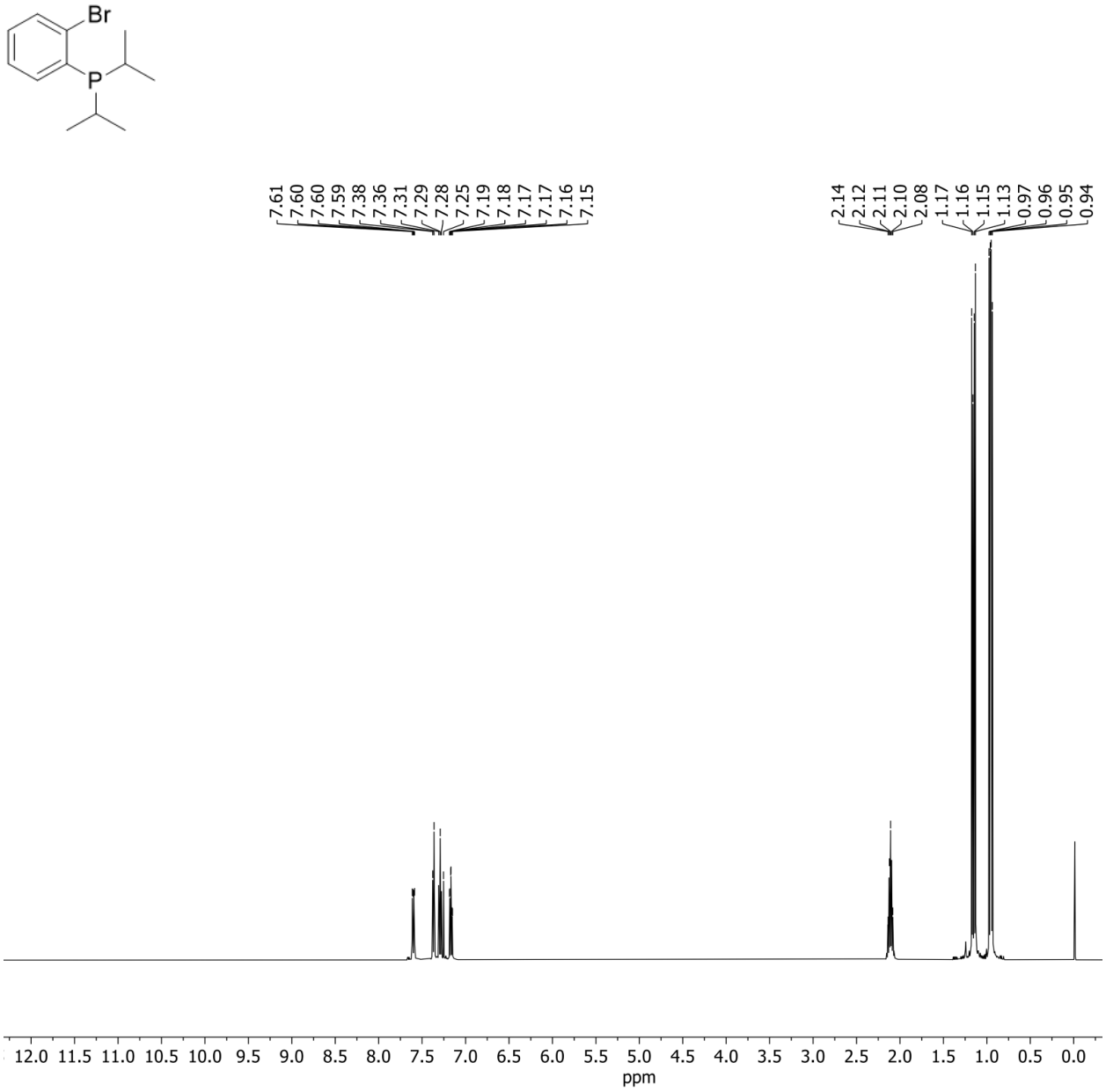

Figure A.17: ^{1}HNMR ($CDCl_3$, 500 MHz) of 1-bromo-2-diisopropylphosphinobenzene.

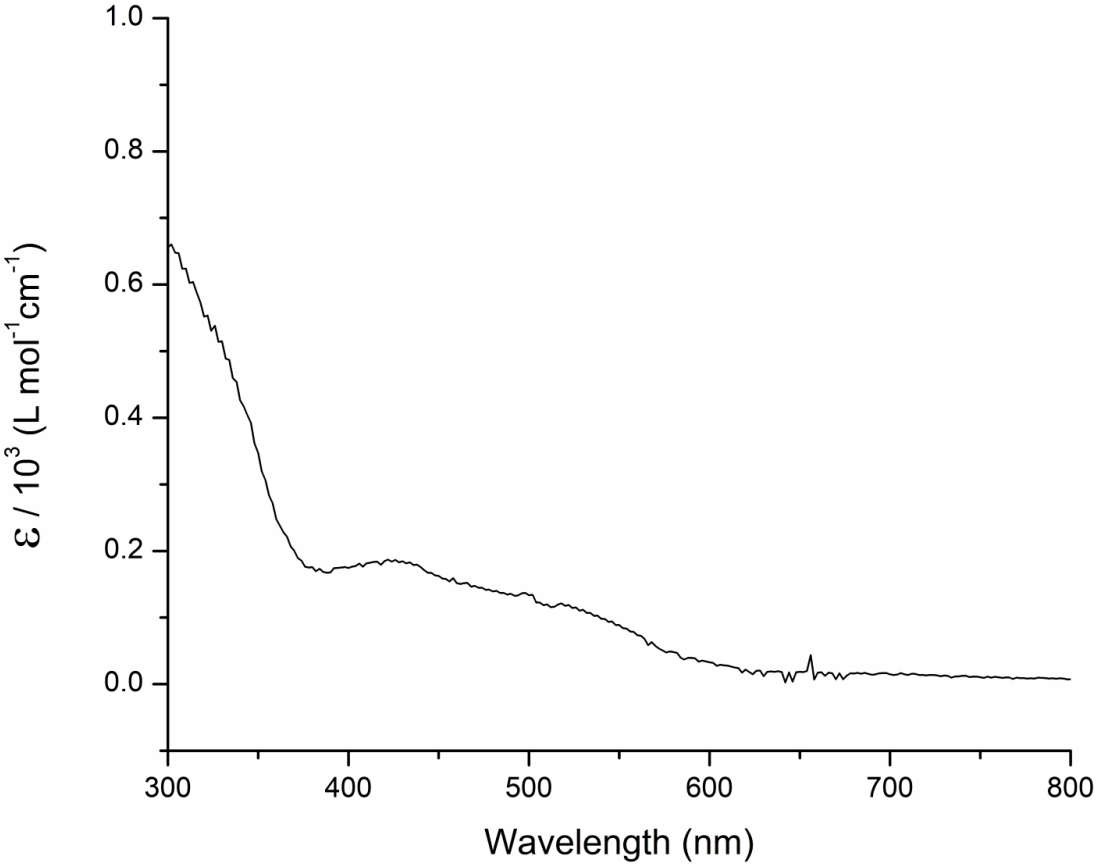

Figure A.18: UV-Vis Spectrum of Iron (II) Complex.

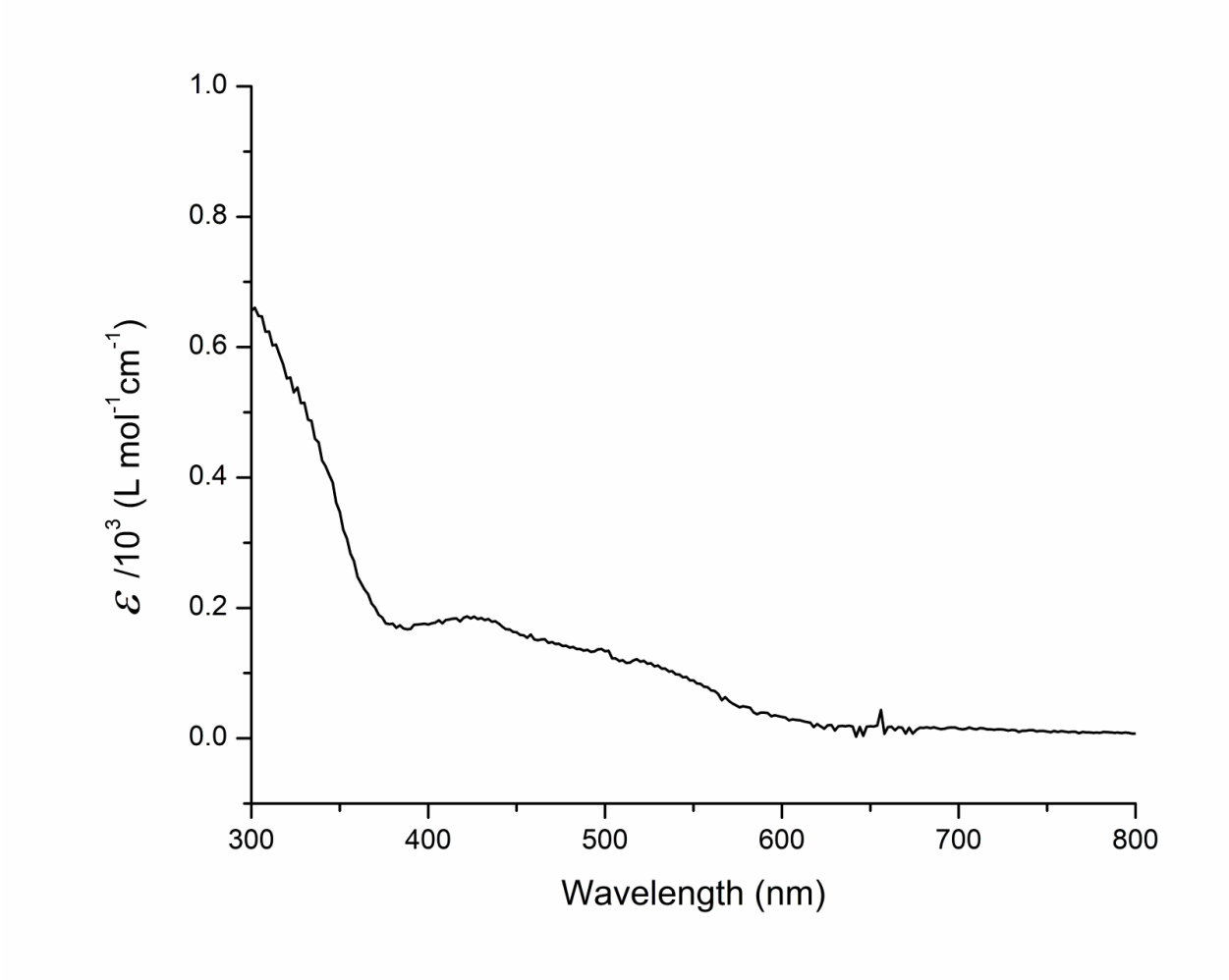

Figure A.19: UV-Vis Spectrum of Cobalt (II) Complex.

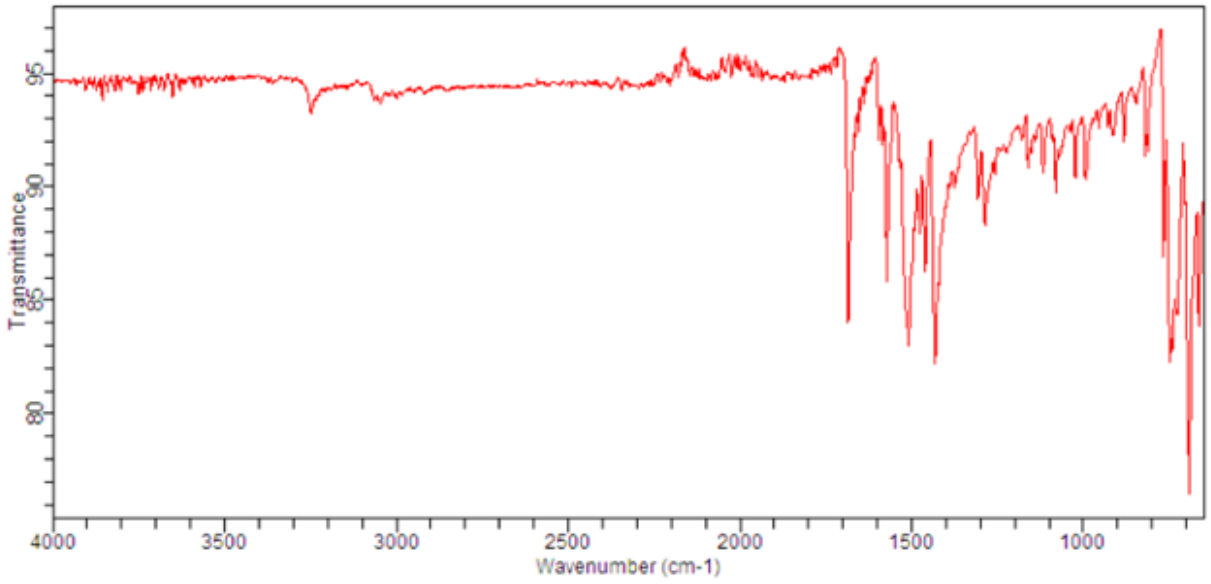

Figure A.20: IR spectrum of L1.

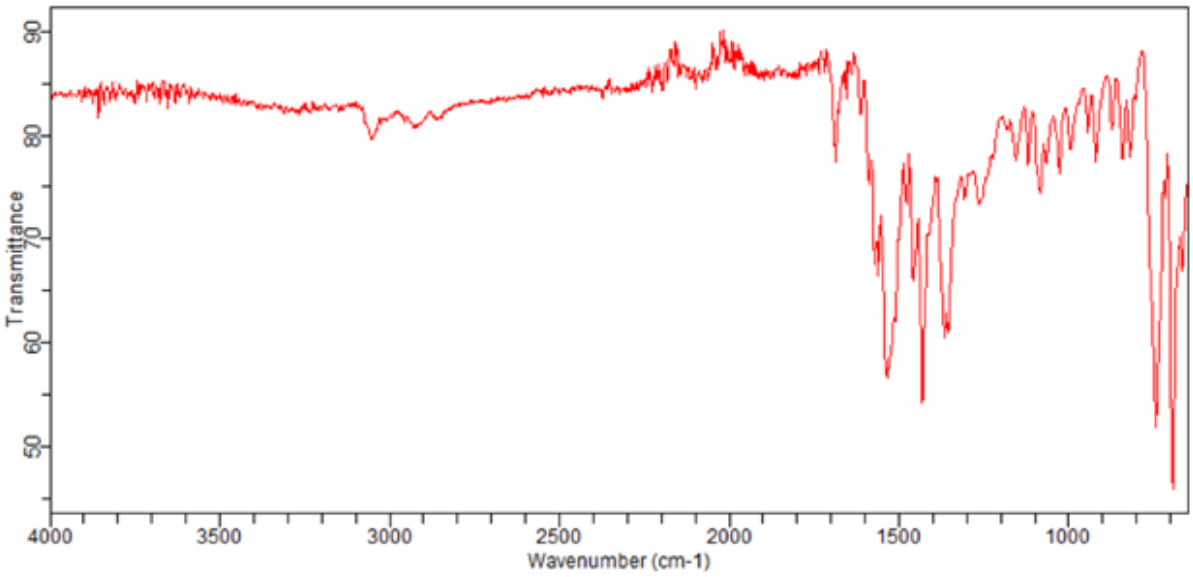

A.21: IR Spectrum of Iron (II) Complex.

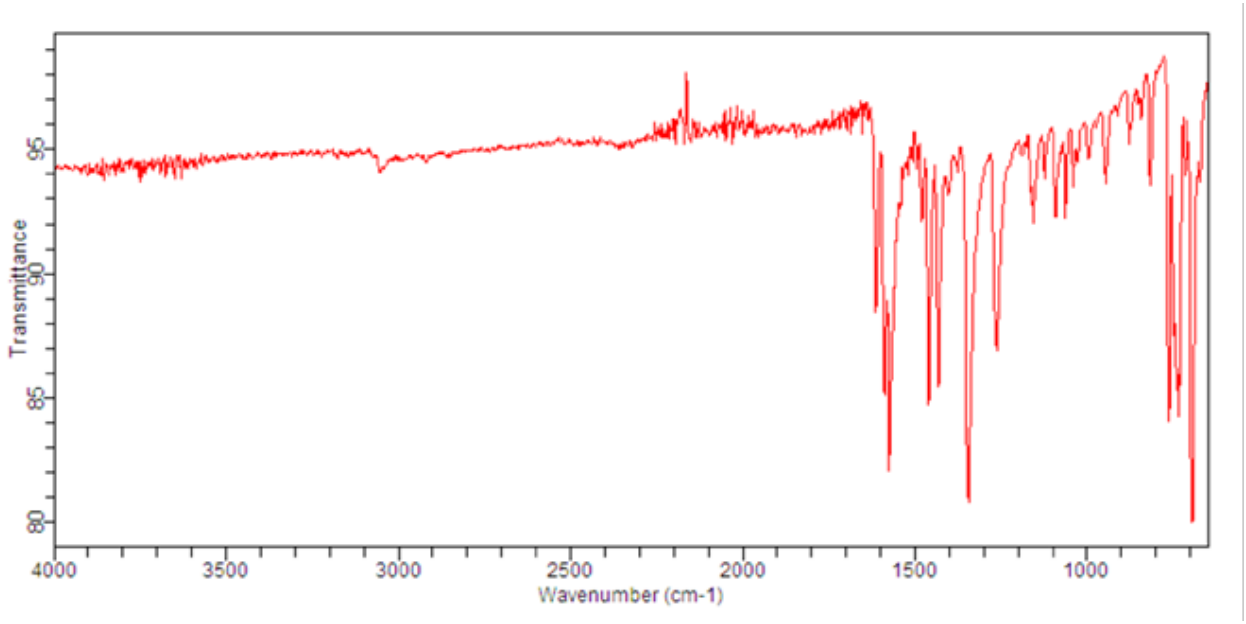

A.22: IR Spectrum of Cobalt (II) Complex

Mass Spectrometry & Proteomics Facility

Mass Spectrum SmartFormula Report

Analysis Info

Analysis Name	D:\Data\0621\NA56.d	Acquisition Date	6/21/2023 2:02:05 PM
Method	051523 tune low.m	Operator	BDAL@DE
Sample Name	NA56	Instrument / Ser#	micrOTOF II 8213750.10314
Comment	ACN/Water		

Acquisition Parameter

Source Type	ESI	Ion Polarity	Positive	Set Nebulizer	0.4 Bar
Focus	Not active	Set Capillary	4500 V	Set Dry Heater	180 °C
Scan Begin	50 m/z	Set End Plate Offset	-500 V	Set Dry Gas	4.0 l/min
Scan End	1650 m/z	n/a	n/a	Set Divert Valve	Waste

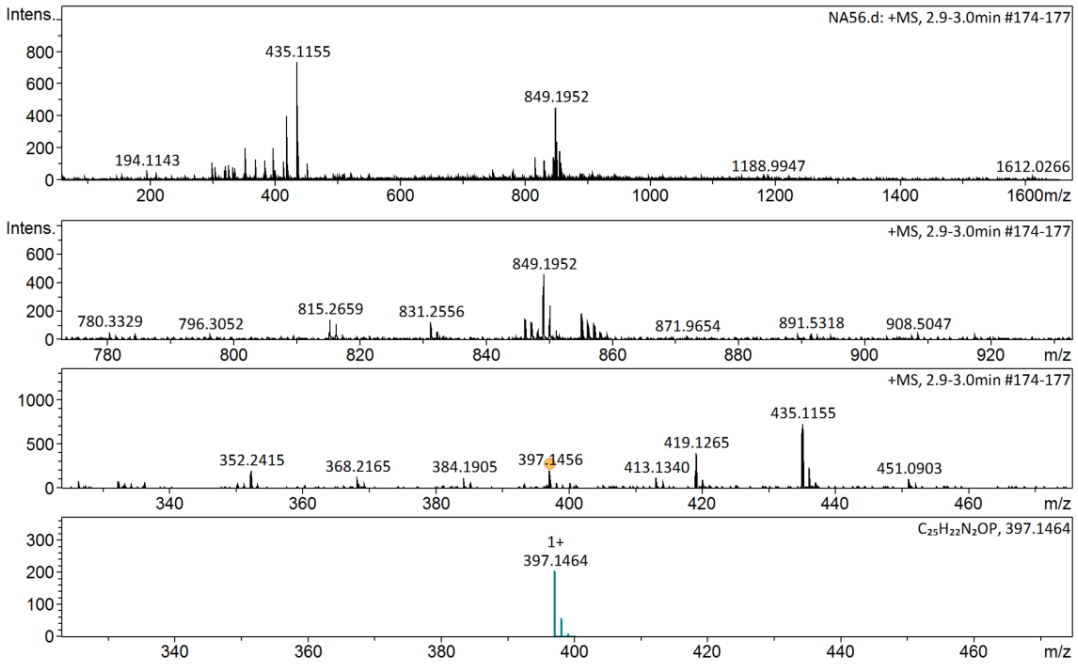

Meas. m/z	#	Ion Formula	m/z	err [ppm]	Mean err [ppm]	rdb	N-Rule	e⁻ Conf
397.145575	1	C25H22N2OP	397.146426	2.1	-3.5	16.5	ok	even

Bruker Compass DataAnalysis 4.2 printed: 6/21/2023 2:12:13 PM Page 1 of 1

This material is based upon work supported by the National Science Foundation under CHE-0741793

Report R.1: HRMS analysis report of L1**.**

Mass Spectrometry & Proteomics Facility

Mass Spectrum SmartFormula Report

Analysis Info

Analysis Name	D:\Data\0621\NA84.d	Acquisition Date	6/21/2023 11:41:45 AM
Method	051523 tune low.m	Operator	BDAL@DE
Sample Name	NA84	Instrument / Ser#	micrOTOF II 8213750.10314
Comment	ACN/Water		

Acquisition Parameter

Source Type	ESI	Ion Polarity	Positive	Set Nebulizer	0.4 Bar
Focus	Not active	Set Capillary	4500 V	Set Dry Heater	180 °C
Scan Begin	50 m/z	Set End Plate Offset	-500 V	Set Dry Gas	4.0 l/min
Scan End	1650 m/z	n/a	n/a	Set Divert Valve	Waste

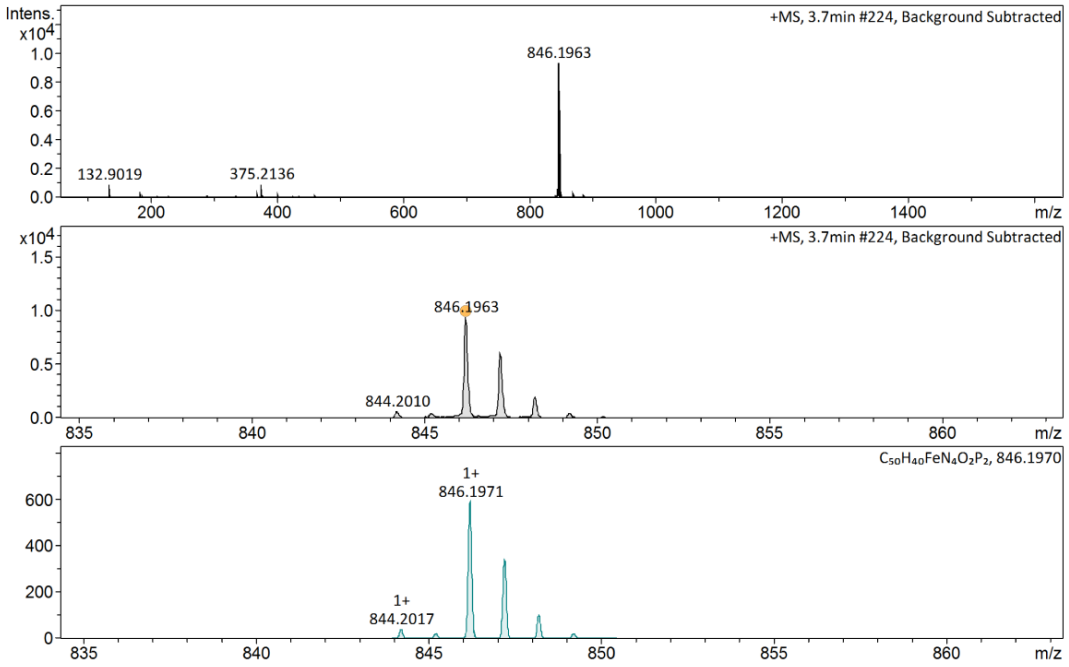

Meas. m/z	#	Ion Formula	m/z	err [ppm]	Mean err [ppm]	rdb	N-Rule	e⁻ Conf
846.196318	1	C50H40FeN4O2P2	846.197039	1.0	0.1	34.0	ok	odd

Bruker Compass DataAnalysis 4.2 printed: 6/21/2023 11:52:13 AM Page 1 of 1

This material is based upon work supported by the National Science Foundation under CHE-0741793

Report R.2: HRMS analysis report of iron (II) complex.

Mass Spectrometry & Proteomics Facility

Mass Spectrum SmartFormula Report

Analysis Info

Analysis Name	D:\Data\0621\NA85.d	Acquisition Date	6/21/2023 11:54:42 AM
Method	051523 tune low.m		
Sample Name	NA85	Operator	BDAL@DE
Comment	ACN/Water	Instrument / Ser#	micrOTOF II 8213750.10314

Acquisition Parameter

Source Type	ESI	Ion Polarity	Positive	Set Nebulizer	0.4 Bar
Focus	Not active	Set Capillary	4500 V	Set Dry Heater	180 °C
Scan Begin	50 m/z	Set End Plate Offset	-500 V	Set Dry Gas	4.0 l/min
Scan End	1650 m/z	n/a	n/a	Set Divert Valve	Waste

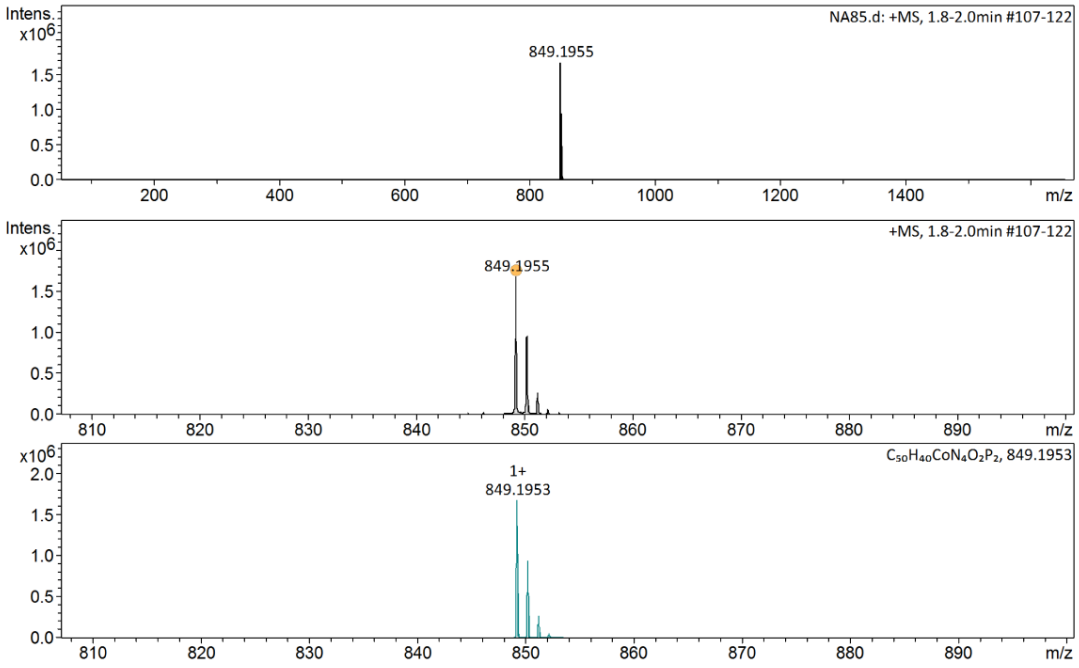

Meas. m/z	#	Ion Formula	m/z	err [ppm]	Mean err [ppm]	rdb	N-Rule	e¯ Conf
849.195515	1	C50H40CoN4O2P2	849.195296	-0.3	0.4	34.0	-	odd

Bruker Compass DataAnalysis 4.2 printed: 6/21/2023 11:59:29 AM Page 1 of 1

This material is based upon work supported by the National Science Foundation under CHE-0741793

Report R.3: HRMS analysis report of cobalt (II) complex.